Druitt, T.H., Kutterolf, S., Ronge, T.A., and the Expedition 398 Scientists
Proceedings of the International Ocean Discovery Program Volume 398
publications.iodp.org

Expedition 398 summary[1]

T.H. Druitt, S. Kutterolf, T.A. Ronge, S. Beethe, A. Bernard, C. Berthod, H. Chen, S. Chiyonobu, A. Clark, S. DeBari, T.I. Fernandez Perez, R. Gertisser, C. Hübscher, R.M. Johnston, C. Jones, K.B. Joshi, G. Kletetschka, O. Koukousioura, X. Li, M. Manga, M. McCanta, I. McIntosh, A. Morris, P. Nomikou, K. Pank, A. Peccia, P.N. Polymenakou, J. Preine, M. Tominaga, A. Woodhouse, and Y. Yamamoto[2]

[1] Druitt, T.H., Kutterolf, S., Ronge, T.A., Beethe, S., Bernard, A., Berthod, C., Chen, H., Chiyonobu, S., Clark, A., DeBari, S., Fernandez Perez, T.I., Gertisser, R., Hübscher, C., Johnston, R.M., Jones, C., Joshi, K.B., Kletetschka, G., Koukousioura, O., Li, X., Manga, M., McCanta, M., McIntosh, I., Morris, A., Nomikou, P., Pank, K., Peccia, A., Polymenakou, P.N., Preine, J., Tominaga, M., Woodhouse, A., and Yamamoto, Y., 2024. Expedition 398 summary. In Druitt, T.H., Kutterolf, S., Ronge, T.A., and the Expedition 398 Scientists, Hellenic Arc Volcanic Field. Proceedings of the International Ocean Discovery Program, 398: College Station, TX (International Ocean Discovery Program). https://doi.org/10.14379/iodp.proc.398.101.2024

[2] **Expedition 398 Scientists' affiliations.**

Contents

Keywords
International Ocean Discovery Program, IODP, R/V *JOIDES Resolution*, Expedition 398, Hellenic Arc Volcanic Field, Earth Connections, Earth in Motion, Biosphere Frontiers, Site U1589, Site U1590, Site U1591, Site U1592, Site U1593, Site U1594, Site U1595, Site U1596, Site U1597, Site U1598, Site U1599, Site U1600, Santorini caldera, Aegean Sea, Christiana-Santorini-Kolumbo volcanic field, subduction zone, shallow-marine volcanism

Core descriptions

Supplementary material

References (RIS)

MS 398-101
Published 30 July 2024

Funded by NSF OCE1326927, ECORD, and JAMSTEC

Abstract

The objectives of International Ocean Discovery Program Expedition 398, Hellenic Arc Volcanic Field (11 December 2022 to 10 February 2023), were to study the volcanic record of the central Hellenic island arc; document the links and feedbacks between volcanism/magmatism, crustal tectonics, and sea level; investigate the processes and products of shallow submarine eruptions of silicic magma; and groundtruth the seismic stratigraphy of Santorini caldera. Reconstructing the subsidence history of the southern Aegean Sea and searching for deep life inside and outside of Santorini caldera were additional objectives.

During the expedition, 10 primary and alternate sites that were originally proposed were drilled, in addition to 2 extra sites that were requested during the expedition. Outside of Santorini caldera, drilling penetrated the thick basin fills of the crustal rift system hosting the Christiana-Santorini-Kolumbo volcanic field, identifying numerous pumice and ash layers, some known from on land and others hitherto unknown, pushing back the onset of volcanism in the area into the Early Pleistocene or even Pliocene. Significant events of mass wasting into the basins, accompanied by very high sedimentation rates, were also documented. These basin sites served to groundtruth the seismic stratigraphy of the basins and open the way to unraveling relationships between volcanic activity and crustal rift pulses. Two sites of condensed sequences served to sample many volcanic layers within the detailed age-depth constraints provided mainly by biostratigraphy, as diagenetic effects complicated the magnetic reversal record significantly. Drilling penetrated the Alpine basement at three basin sites northeast of Santorini, whereas in the Christiana Basin to the southwest it penetrated a thick sequence of Messinian evaporites. Drilling inside Santorini caldera penetrated to ~120 meters below seafloor, less than planned due to hole instability issues but deep enough to groundtruth the seismic stratigraphy and sample the different layers. One intracaldera hole yielded a detailed tephra record of the history of the Kameni Islands, as well as possible evidence for deep bacterial colonies within the caldera. Despite variable recovery in the unstable pumice and ash deposits, the expedition was a significant success that may address almost all the scientific objectives once the laboratory work has been done.

Plain language summary

About 800 million people are threatened by volcanic eruptions around the globe: high plumes of ash, ground-hugging flows of hot ash and rock, earthquakes, and associated tsunamis. The Christiana-Santorini-Kolumbo volcanic group in the Aegean Sea of Greece is particularly hazardous because the volcanoes have produced many eruptions in the past, and some were highly explo-

sive. Santorini is an iconic volcano because of its well-known eruption in the Late Bronze Age, and it is a major tourist destination. Although much has been learned about the eruption history of the Aegean volcanoes on land, most of their volcanic products lie on the seafloor, requiring research to move offshore.

During International Ocean Discovery Program Expedition 398, we drilled the submarine sediment sequences, including the muds and volcanic products that fill the marine basins around the volcanoes and inside of Santorini caldera, at 12 sites. Outside of the caldera, we penetrated many layers of pumice and ash that represent eruptive products settled at the seafloor. Some of these layers represent hitherto unknown explosive eruptions whose products do not occur on land. The ages of the different layers were determined mainly from the assemblages of microfossils preserved in them. We also identified times in the past when large fault movements and earthquakes appear to have caused remobilization of previously deposited ash layers, causing them to pour into the actively deepening basins. In the Christiana Basin south of Santorini, we unexpectedly penetrated a thick sequence of evaporites formed 5.99–5.33 My ago during the so-called Messinian Salinity Crisis. Inside Santorini caldera, we drilled through sediments and volcanic products that have accumulated there since the Late Bronze Age eruption, offering a detailed record of the previously inaccessible prehistoric evolution of Kameni Volcano, inside the caldera. At two sites inside Santorini caldera and two others outside, we collected samples for microbiological and genetic analysis to identify and characterize any microbial life living in the muds below the sediment surface.

Despite variable recovery in the unstable pumice and ash deposits, the expedition was a great success that will enable us to address almost all of the original scientific objectives once detailed laboratory work has been done. Some particularly important aims will be to link the volcanic activity to ancient crustal tectonic processes, as well as to variations in sea level through time due to changes in Earth's climate, and see any governing feedbacks between these processes.

1. Introduction

Volcanic hazards and risks lie at the heart of global geoscience, with about 800 million people threatened by eruptions (Loughlin et al., 2015). Volcanoes in island arc settings impact humans and the environment through explosive eruptions (both subaerial and submarine), tephra fallout, pyroclastic flows, earthquakes, tsunamis, and ocean acidification. Some large eruptions, such as the Late Bronze Age (LBA) eruption of Santorini, may have destabilized entire civilizations (e.g., Bruins et al., 2008). On the other hand, volcanoes can host rich ecosystems and fertilize the oceans (Duggen et al., 2010; Christakis et al., 2018).

Better understanding of the processes governing arc volcanoes and their hazards is important as the twenty-first century unfolds (McGuire et al., 2017; National Academies of Sciences, Engineering, and Medicine, 2017; Cassidy and Mani, 2022). Crustal tectonics is one process that strongly influences volcanism, but it has rarely been studied at high spatial and temporal resolutions (e.g., Cembrano and Lara, 2009). Crustal thickness and thermal structure affect the production of magmas in the mantle and their subsequent evolution through crystal fractionation, crustal contamination, and magma mixing (e.g., Farner and Lee, 2017). Extensional crustal motions across many island arcs create space for magma ascent and influence the depths and sizes of magma storage regions (Acocella and Funiciello, 2010; Bachmann and Huber, 2016). Large earthquakes cause changes in crustal stresses sufficient to induce eruptions as far as several hundreds of kilometers away (e.g., Walter and Amelung, 2007). Changes in sea level driven by tectonics or climate modulate volcanic activity by loading or unloading the magma plumbing system (Kutterolf et al., 2013; Sternai et al., 2017; Satow et al., 2021).

The Christiana-Santorini-Kolumbo (CSK) volcanic field is an excellent region in which to address these fundamental questions (Nomikou et al., 2019). It is one of the most active in Europe, having produced more than 100 explosive eruptions in the last 360 ky (Druitt et al., 1999; Druitt and Vougioukalakis, 2019). Situated in a rift zone that cuts northeast–southwest across the island arc, the field includes the extinct Christiana Volcano, Santorini caldera with its intracaldera Kameni Vol-

cano, Kolumbo Volcano, and the 22 submarine cones of the Kolumbo volcanic chain (Figure **F1**) (Hooft et al., 2017; Hübscher et al., 2015; Nomikou et al., 2012, 2013, 2019), all of which have discharged their volcanic products into adjacent marine basins, creating a rich archive of past eruptions (Preine et al., 2022a). Santorini is one of the most explosive arc volcanoes in the world; its onland products have been mapped, dated, and chemically fingerprinted, and its historical eruptions are well documented (Druitt et al., 1999; Pyle and Elliott, 2006). Kolumbo Volcano has had at least five large explosive eruptions, the last in the year 1650 Common Era (CE) (Hübscher et al., 2015; Nomikou et al., 2016b).

Prior to Expedition 398 we had a record of Santorini volcanism going back to 650 ka, but it was only detailed since 360 ka (Druitt et al., 1999). Apart from the 1650 CE eruption, the past volcanism of Kolumbo Volcano was poorly documented and that of Christiana Volcano was largely unknown. Offshore drilling enabled us to use the thick volcano-sedimentary records of the rift basins and Santorini caldera as time capsules for reconstructing the volcanic and tectonic histories of the area since rift inception in the Pliocene (Nomikou et al., 2018; Heath et al., 2019; Preine et al., 2022c). Drilling allowed (1) groundtruthing of marine seismic profiles, (2) characterization and dating of seismic packages, (3) measurement of the physical properties of submarine strata, and (4) sampling for any subsurface ecosystems.

Hazards from the CSK rift zone include earthquakes, eruptions, and tsunamis (Cantner et al., 2014; Vougioukalakis et al., 2016). The level of seismicity is among the highest in Europe (Sachpazi et al., 2016), and the largest twentieth-century shallow earthquake in Europe (M 7.5) took place there in 1956 (Okal et al., 2009). The LBA eruption of Santorini in about 3.6 ka was one of the largest of the Holocene Epoch worldwide; it may have influenced the decline of the Minoan civilization on Crete and thus is an iconic event in both volcanology and archaeology (e.g., Bruins et al., 2008). The 1650 CE eruption of Kolumbo Volcano killed 70 people on Santorini through gas release and tsunami inundation (Fuller et al., 2018; Cantner et al., 2014). Santorini had an episode of bradyseismic unrest in 2011–2012 (Parks et al., 2015), raising awareness of the eruption threat at these islands, which are visited by 2 million tourists per year.

Drilling was carried out in the context of several new research initiatives in the marine environment of the volcanic field. A dense network of subseafloor seismic reflection profiles exists across the rift zones, giving high-resolution images of sedimentary fills and faults (Figure **F2**) (Hübscher et al., 2015; Nomikou et al., 2013, 2016a, 2018). Detailed correlations and interpretations of these profiles from northeast to southwest across the volcanic field previously led to a detailed seismic stratigraphic model (Preine et al., 2022c) that is now tested and refined by deep drilling. In 2015, an active seismic tomography experiment of the CSK system was carried out (Plumbing Reservoirs Of The Earth Under Santorini [PROTEUS]; Hooft et al., 2017). It identified an upper-crustal

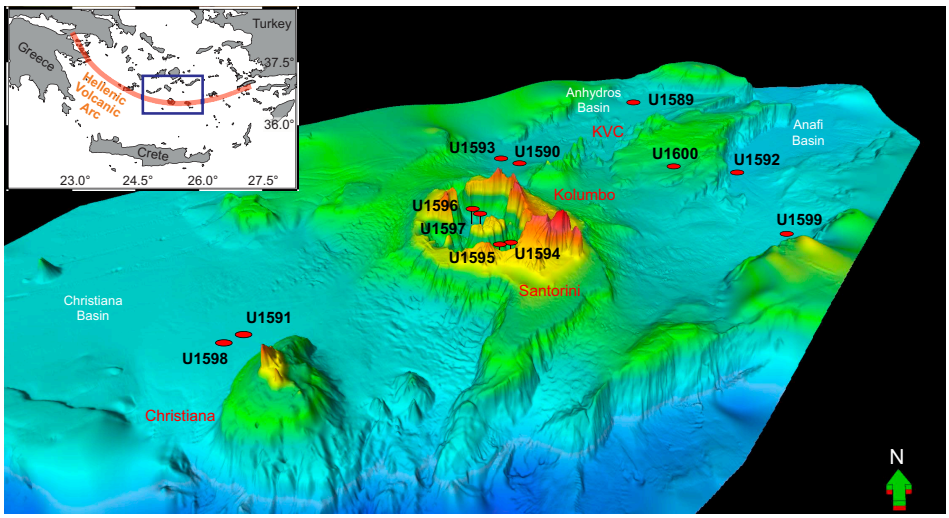

Figure F1. Three-dimensional view of the CSK volcanic field and its host rift basins, looking north. Locations of Sites U1589–U1600 are shown. KVC = Kolumbo Volcanic Chain.

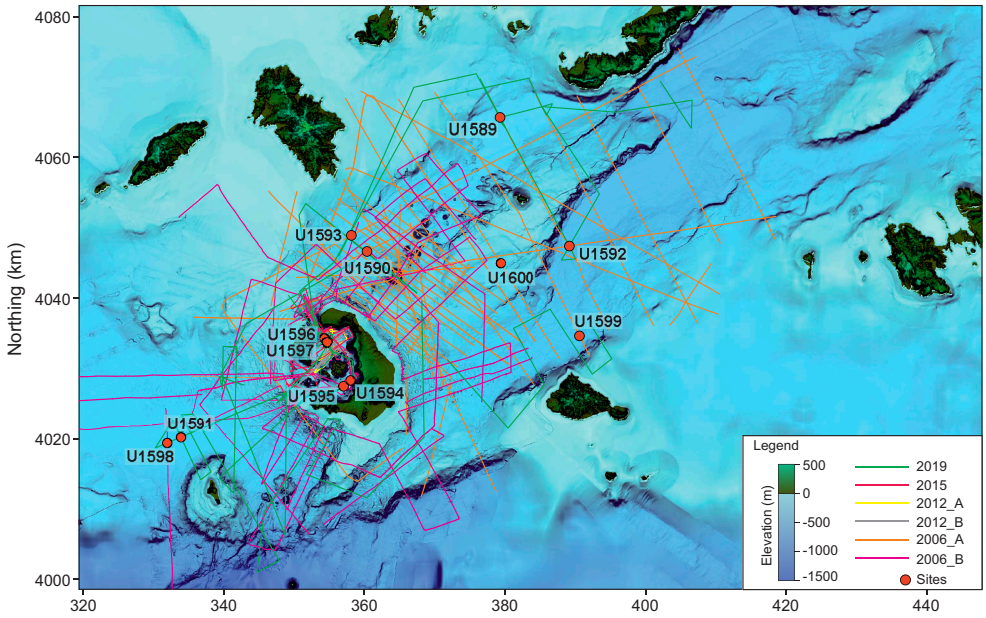

Figure F2. Seismic lines in and around the CSK volcanic field. Locations of Sites U1589–U1600 are shown.

magma reservoir beneath Santorini and extending northeastward toward Kolumbo Volcano (McVey et al., 2020). Multibeam bathymetric surveys imaged submarine volcanic edifices and calderas (Nomikou et al., 2012, 2013, 2016a). Seismic reflection profiles inside Santorini caldera previously allowed recognition of several intracaldera layers (Johnston et al., 2015) that were sampled now by drilling. Seafloor volcanic products, hydrothermal deposits, and bacterial mounds were previously sampled (Hanert, 2002; Camilli et al., 2015), and the surface biosphere was documented (Oulas et al., 2016; Polymenakou et al., 2021). Deep-sea ash layers were sampled by gravity coring across the Eastern Mediterranean, and many were correlated with onshore products. The resulting preexpedition marine ash stratigraphy that extended back to 200,000 ka included 12 ash deposits from CSK volcanoes and allowed estimation of the ages and masses of many of the tephra layers (Satow et al., 2015; Wulf et al., 2020; Kutterolf et al., 2021a, 2021b).

Expedition 398 started in Tarragona, Spain, on 11 December 2022 and ended in Heraklion, Greece, on 10 February 2023. Of the 12 drilled sites, 10 were primary or alternate sites proposed in the *Expedition 398 Scientific Prospectus* (Druitt et al., 2022); permission for the other two sites was granted during the expedition.

2. Geologic setting

The Hellenic volcanic arc owes its existence to subduction of the African plate beneath the European plate, which initiated in the Pliocene (Pe-Piper and Piper, 2005; Shaw and Jackson, 2010). The subducted slab descends at an angle of 10°–30°, and the back-arc Aegean region has been in extension since the Pliocene, a result of slab rollback (Jolivet et al., 2013; Papazachos, 2019). The convergence rate along the arc is 35 ± 8 mm/y, divided into 5–10 mm/y of relative motion between the Eastern Mediterranean and the Aegean and ~25 mm/y of slab rollback. Back-arc extension has thinned the Aegean continental crust, creating horsts and grabens (Le Pichon and Kreemer, 2010; Royden and Papanikolaou, 2011) (Figure **F1**). The Hellenic subduction system has one of the oldest (coolest) slabs and lowest convergence rates on Earth (Syracuse et al., 2010).

The island arc consists of five volcanic fields: Sousaki, Aegina-Poros-Methana, Milos, CSK, and Kos-Nisyros-Yali, from west to east. The CSK volcanic field lies in the center of the arc on 18–20 km of thinned continental crust (Makris et al., 2013). It is located in a rift zone 100 km long × 45 km wide with three main northeast-southwest–oriented marine basins and Pliocene–Quaternary sedimentary fills as thick as 1400 m (Piper and Perissoratis, 2003; Nomikou et al., 2016b, 2018;

Hooft et al., 2019; Preine et al., 2022a) (Figure **F1**). The Anhydros Basin contains the Kolumbo volcanic chain, whereas the Anafi Basin lacks volcanoes. The Anhydros and Anafi Basins each contain six seismic stratigraphic units (here named Seismic Units U1–U6, upward) separated by onlap surfaces (Preine et al., 2022a). Thickness variations of the units record initial symmetric rifting (Units U1–U3) followed by northwest-tilted, more asymmetric rifting (Units U4–U6). Prior to Expedition 398, rifting was believed to have begun 3.8–5.3 My ago in the Pliocene (Heath et al., 2019).

The Christiana Basin, a broad, fault-bounded basin at the southwest entrance of the rift zone (Figure **F1**), contains Pliocene–Quaternary sediments and volcaniclastics divided into six major units, Seismic Units U1–U6 (Preine et al., 2022a).

Santorini caldera is a complex 11 km × 7 km structure caused by at least four collapse events over the last ~200,000 y, the last of which was the LBA eruption (Druitt and Francaviglia, 1992). It has a northern basin 390 m deep, a southern basin 280 m deep, and is connected to the sea via three breaches (Nomikou et al., 2014). The caldera's volcano-sedimentary fill is about 1 km thick (Budetta et al., 1984). The Kameni Islands are the subaerial summit of a 470 m high intracaldera edifice formed since the LBA eruption.

Preexpedition onland studies suggested that volcanism at Santorini began 650,000 y ago with submarine, then subaerial, effusive activity and became highly explosive 360,000 y ago (Thera Pyroclastic Formation). There have since been about 12 Plinian eruptions (and ~100 less intense explosive eruptions), many of which generated high ash plumes and pyroclastic flows that entered the sea (Druitt et al., 1999). The LBA eruption of 3.6 ka (also called the Minoan eruption) discharged several tens of cubic kilometers of silicic magma as fallout and pyroclastic flows (Druitt, 2014), and the resulting subsidence deepened an already existing caldera (Athanassis et al., 2016). After the caldera collapsed, the sea broke through the northwest breach, carving out a 2 km wide submarine channel (Nomikou et al., 2016a). Kameni Volcano has had nine subaerial effusive eruptions between 197 Before Common Era (BCE) and 1950 (Pyle and Elliott, 2006; Nomikou et al., 2014).

Seismic profiles reveal four main units in the topmost caldera fill (here named Seismic Units S1–S4, downward), interpreted most recently as follows (Johnston et al., 2015; Nomikou et al., 2016a):

- S1: flat-lying sediments up to 40 m thick; mass wasting of the caldera cliffs.
- S2: sediments up to 100 m thick that merge into the clastic apron of Kameni edifice; tuffs and hyaloclastites from the submarine phase of Kameni.
- S3: down-faulted deposits as thick as 250 m; uppermost levels of LBA intracaldera tuffs and/or sediments related to posteruptive flooding of the caldera.
- S4: deposits lacking layering on seismic images and interpreted as LBA intercaldera tuffs.

The extinct Christiana Volcano produced lavas and tuffs of unknown ages (Aarbourg and Frechen, 1999), but an ignimbrite found on neighboring islands was tentatively dated at ~1 Ma (Keller et al., 2010). The eroded remains of the volcano form two main islands: Christiani and Askani. Geochemical and $^{40}Ar/^{39}Ar$ dating studies of onland Christiana volcanics are in progress (Vrije Universiteit, Amsterdam). Prior to Expedition 398, very little was known about the volcanic history of Christiana, but seismostratigraphic relations indicated an extended phase of eruptions occurring in the Late Pliocene to Early Pleistocene (Preine et al., 2022a).

Kolumbo Volcano rises 480 m above the surrounding seafloor, with a 1.7 km diameter summit crater formed in 1650 CE (Nomikou et al., 2012; Carey et al., 2013). Seismic profiles across it reveal five units interpreted as Kolumbo-derived volcaniclastics (Eruption Units K1–K5, from the base up); Unit K5 is the 1650 CE eruption (Hübscher et al., 2015). The submarine cones northeast of Kolumbo postdate Unit K2 on seismic profiles; they are much smaller than Santorini or Kolumbo, and their products are not expected to be prominent in our drill cores.

Based on the compiled seismic data set, Preine et al. (2022a) proposed that the entire CSK volcanic field evolved during four phases:

- Phase 1: initiated in the Pliocene with formation of the Christiana Volcano.

- Phase 2: formation of the current southwest-northeast–trending rift system associated with the evolution of two distinct volcanic centers, a proposed submarine Poseidon Center and the early Kolumbo Volcano.
- Phase 3: a period of widespread volcanic activity throughout the entire rift.
- Phase 4 (ongoing): confined to Santorini caldera and Kolumbo Volcano.

2.1. Seismic studies/site survey data

A dense network of multichannel and single-channel seismic reflection profiles (campaigns in 2006–2015; Figure **F2**) from collaborating groups and publications have been interpreted in detail in Santorini caldera (based on the volcanic history recorded on land; Johnston et al., 2015) and in the basins northeast of Santorini as well as to the southwest in the Christiana Basin (Hübscher et al., 2015; Nomikou et al., 2016a, 2016b, 2018; Tsampouraki-Kraounaki and Sakellariou, 2018). A further 620 km of new, high-quality multichannel seismic profiles was shot in October 2019 (Karstens et al., 2019). All profiles, which sum to 3350 km in length, were recorded with different sources and streamers and were merged into a homogeneous data set at the University of Hamburg (Preine et al., 2022a, 2022b, 2022c). All proposed primary drilling sites are situated at (or very close to) the intersections of multichannel seismic profiles. During the PROTEUS cruise in 2015 (Hooft et al., 2019), 3.5 kHz subbottom profiling and gravity and magnetic data were recorded.

In addition to the seismic survey and interpretations, fault distributions and throws have been mapped northeast of Santorini (Nomikou et al., 2016b; Hooft et al., 2017) and two-way traveltime (TWT) isopach maps have been constructed for each rift basin (Heath et al., 2019; Preine et al., 2022c). High-resolution multibeam bathymetry is available inside and outside of Santorini caldera (Nomikou et al., 2014, 2016a; Hooft et al., 2017).

Shallow sediments at or close to the drill sites provide initial sediment properties and tephrochronostratigraphic interpretations (Kutterolf et al., 2021a, 2021b). A large database of radiometric ages (K-Ar, $^{40}Ar/^{39}Ar$, and ^{14}C) and whole-rock chemical analyses exists for onland volcanic deposits from the CSK centers, particularly Santorini, along with glass major and trace element analyses for marine ash layers dating back to 200 ka (e.g., Druitt et al., 1999; Wulf et al., 2020; Kutterolf et al., 2021a, 2021b).

3. Scientific objectives

3.1. Objective 1: arc volcanism in an active rift environment

Analysis of preexpedition seismic profiles northeast and southwest of Santorini led to an interpretation of the development of the volcanic field in space and time (Preine et al., 2022a). This interpretation invoked (in chronological order) the development of Christiana Volcano (Late Pliocene), followed by Kolumbo Volcano Eruption Units K1 and K2 and an offshore submarine center (Poseidon; early Quaternary), a mass transport deposit of unknown origin, deposits from the Akrotiri and Peristeria Volcanoes, Kolumbo Volcano Eruption Unit K3 and Kolumbo submarine cones (0.65–0.36 Ma), and the post–0.36 Ma explosive products of Santorini (Thera Pyroclastic Formation) and Eruption Units K4/K5 of Kolumbo Volcano. We planned to test this hypothesis using cores from all sites to reconstruct a complete volcanic stratigraphy of the CSK volcanic field since rift inception in the Pliocene, consistent with both onshore and offshore constraints.

We anticipated that eruption products would be preserved in the rift basins not only as tephra fallout but also as turbidites channeled down the basin axes from volcanoes upslope (e.g., Schmincke and Sumita, 1998). Bed-to-bed and seismic unit-to-unit correlation between cores would use major and trace element compositions of juvenile blocks or lapilli, glasses, crystal-hosted glass inclusions (e.g., Lowe, 2011; Brandl et al., 2017; Freundt et al., 2021), and phenocrysts. Correlation of volcaniclastics to source volcanoes would exploit established chemical and mineralogical differences between the different volcanic centers, extending chemical correlation databases already developed for the <0.2 Ma tephra layers (Kutterolf et al., 2021a, 2021b). Tephra fall layers from other circum-Mediterranean volcanoes might serve as marker beds (Satow et al., 2015; Wulf et al., 2020). Absolute dates of cored volcanic layers based on (1) published onshore ages,

(2) published ages of marine tephra fall layers, and (3) new radiometric age determinations of suitably fresh drilled pyroclasts as well as biostratigraphic constraints would refine the volcanic chronostratigraphy.

3.2. Objective 2: the volcano-tectonic connection

Studies of Miocene plutons, fault patterns along the modern-day arc, and relationships between regional seismicity and caldera unrest at Santorini in 2011–2012 all hint at intimate relationships between Aegean volcanism and crustal tectonics (Kokkalas and Aydin, 2013; Feuillet, 2013; Rabillard et al., 2018; Heath et al., 2019; Preine et al., 2022c). We aimed to test this hypothesis by (1) reconstructing the histories of subsidence and tectonics of the Anhydros, Anafi, and Christiana Basins from our drill cores and seismic records; (2) integrating them with our volcanic chronostratigraphy; (3) seeking relationships between CSK volcanism and major crustal tectonic events; and finally (4) investigating how sea level may modulate volcanic activity.

We planned to reconstruct the sedimentary and subsidence histories of the basins using sediment-focused chronostratigraphic techniques: biostratigraphy, sapropel records, and magnetostratigraphy. Inclusion of the volcanic record would then build a detailed rift-wide stratigraphy with multiple independent age markers, enabling construction of a Bayesian age model for each basin. Benthic foraminifera would provide estimates of paleowater depths and, via integration with seismic profiles and chronologic data, time-integrated basin subsidence rates (Pallikarakis et al., 2018).

3.3. Objective 3: arc magmatism in a region of extending crust

Magmas of the CSK field have ascended through 18–20 km of rifted continental crust, which has influenced their chemical and isotopic evolution (e.g., Bailey et al., 2009; Elburg et al., 2014). Primitive basaltic melts rise into the crust, where they evolve to intermediate and silicic compositions through fractional crystallization, crustal melting/assimilation, and magma mixing (Cashman et al., 2017). It is likely that the structure of the rifted crust governs the polybaric ascent history of the CSK magmas, with faults, density interfaces, and rheological transitions (Jolivet et al., 2013) controlling levels of magma storage and differentiation (Flaherty et al., 2018), as observed in the exhumed Miocene magmatic complexes of the Aegean (Rabillard et al., 2018).

We aimed to investigate magma genesis and the links with rifting history using major, trace, and multi-isotopic data on suitably fresh rocks. Volatile contents of crystal-hosted melt inclusions and mineral-barometry techniques would be used to quantify magma storage depths during ascent prior to eruption. These data would constrain how mantle source characteristics and heterogeneity (Bailey et al., 2009; Klaver et al., 2016b), degree of magma contamination by the crust, and the role of lower crustal amphibole have varied in space and time since the Pliocene across the volcanic field.

3.4. Objective 4: unraveling an iconic caldera-forming eruption

The LBA eruption of Santorini has attracted attention for many decades (Friedrich, 2009), and the onland products have been studied in detail (Druitt, 2014). More recently, seismic studies have imaged the LBA products both outside (Karstens et al., 2023) and inside (Johnston et al., 2015) the caldera, although their firm identification on seismic profiles is problematic due to the many other eruptions and tuffs with which they can be confused.

LBA tuffs accumulated outside the caldera have been inferred from seismic profiles to be as thick as 50 m or more (Karstens et al., 2023). It was hoped that drilling would enable us to core the LBA deposits both outside and inside the caldera and to groundtruth the seismic profiles using downhole measurements of seismic velocities. Outside the caldera, drilling targeted the LBA submarine pyroclastic flows at Sites U1589–U1591, U1593, and U1598 to also test the published seismic interpretation.

Inside Santorini caldera, we planned to drill to 234 meters below seafloor (mbsf) in the northern caldera basin (Sites U1596 and U1597) and to 360 mbsf in the southern basin (Sites U1594 and

U1595). Our planned drilling targeted Seismic Unit S4, which is thought to be intracaldera LBA tuffs. By drilling into the LBA tuffs in the caldera, we would have been able to estimate their minimum volume, contributing to volume estimates for LBA deposits on- and offshore (outside of the caldera) to make a new, much more precise (minimum) estimate of the erupted volume.

3.5. Objective 5: volcanic hazards from submarine silicic eruptions

A potential future hazard at Santorini is a submarine eruption of the Kameni or Kolumbo Volcano, similar to that of 1650 CE. Better understanding of the dynamics of such eruptions would enable us to improve risk mitigation strategies in this densely populated and highly visited part of the Eastern Mediterranean (Vougioukalakis et al., 2016; Carey et al., 2018).

Studies of the products of the 1650 CE eruption of Kolumbo Volcano show that the eruption was driven mainly by primary degassing of the water-rich silicic magma, but with a component of phreatomagmatic fragmentation, and that the deposits were emplaced by a combination of subaerial plumes, submarine plumes, and density currents (Cantner et al., 2014). The planned drilling would enable us to traverse the products of at least three earlier explosive eruptions of Kolumbo Volcano (Eruption Units K1–K4). We would be able to compare these earlier submarine eruptions to that of 1650 CE, test the leading hypothesis, and arrive at a general model for this rarely accessible type of submarine volcanism.

Inside Santorini caldera, Seismic Unit S2 would provide access to a petrological time series of postcaldera volcanism that dates back to the birth of Kameni Volcano after the LBA eruption to its emergence in 197 BCE. Using similar methods as at Kolumbo Volcano, we could reconstruct the history of eruption styles over the growth of Kameni from 400 m water depth to the surface. It is rare to have a complete record of postcaldera volcanism at an arc caldera because the magmatic transition and the long subsequent evolution of the new intracaldera volcano are seldom both preserved.

3.6. Objective 6: transition from continental to marine environments in the southern Aegean

Drilling in the Christiana, Anhydros, and Anafi Basins will allow us to pierce the entire basin stratigraphy and reach the basement unconformity (presubsidence land surface). This provides the opportunity to reconstruct the environmental histories of the basins from continental to deep-marine stages, as well as the evolution of the Eastern Mediterranean paleoclimate since the Pliocene. Prior to Expedition 398, the subsidence history in the southern Aegean was poorly known due to the paucity of offshore studies. The plan was to build a high-resolution biostratigraphic framework for the recovered Expedition 398 cores and then extract a time series of paleoenvironmental data from the cores using assemblages of calcareous nannofossils, benthic and planktonic foraminifera, dinoflagellates, and pollen, refined by stable oxygen and carbon isotopes, total organic carbon (TOC), major and trace elements, and organic biomarkers for selected depth intervals.

3.7. Objective 7: biological systems reactions to volcanic eruptions and seawater acidification

The deep-marine biosphere hosts a large component of the world's microbial ecosystems, but little is known about them (Parkes et al., 2000; Schippers et al., 2005). Marine microbes have evolved to respond to environmental challenges, resulting in different survival mechanisms, growth strategies, and genetic adaptations. Knowing that Santorini caldera harbors highly diverse, metabolically complex microbial communities (Oulas et al., 2016; Christakis et al., 2018), we planned to use core material from inside the caldera (Sites U1594–U1597) and outside the caldera (Sites U1599 and U1600) to characterize the living and fossilized subseafloor biological communities present. This would enable us to document the sizes, genetic variabilities, and metabolic functions of subsurface ecosystems to 700 mbsf, as well as explore for past anoxic events in the subsurface, extant biological activity, and trace fossils of extinct seafloor life.

Study of drill cores and pore fluids would moreover investigate the relationship between extant, or fossilized, subseafloor microbial communities and subseafloor biogeochemical and mineralization processes, particularly the relative importance of Fe released from hydrothermal activity in sustaining subseafloor biomes (Templeton, 2011).

3.8. Connections to the 2050 Science Framework

Overall, the results of Expedition 398 will address five of the seven Strategic Objectives of the 2050 Science Framework (Habitability and Life on Earth, The Oceanic Life Cycle of Tectonic Plates, Earth's Climate System, Feedbacks in the Earth System, and Natural Hazards Impacting Society) and two of the Flagship Initiatives (Assessing Earthquake and Tsunami Hazards and Exploring Life and Its Origin).

4. Site summaries

In the following site summaries, penetration depths (all noted as meters below seafloor [mbsf]) are based on the drilling depth below seafloor (DSF) scale in Operations and on the core depth below seafloor, Method A (CSF-A), scale in Principal results. These scales may differ by up to a few meters in some cases.

4.1. Site U1589

4.1.1. Background and objectives

The principal aims at Site U1589 (proposed Site CSK-01A) were to drill through the sedimentary fill of the Anhydros Basin, reconstruct the evolution of the basin including its history of subsidence, document the presence of volcanic event layers in the basin sediments, and draw conclusions regarding the links between volcanism and crustal tectonics. The site is located about 10 km southwest of Amorgos Island at 484 mbsl. We received permission from the International Ocean Discovery Program (IODP) Environmental Protection and Safety Panel (EPSP) to touch Alpine basement using an advanced piston corer/extended core barrel/rotary core barrel (APC/XCB/RCB) drilling strategy.

The site was chosen because it is situated on a sediment distribution pathway that leads downstream from both Santorini and Kolumbo Volcanoes. It was therefore expected that the site would receive volcaniclastic material from both volcanic systems, both as turbidity currents directed by the basin bathymetry and as tephra fallout controlled by high-altitude wind patterns (Kutterolf et al., 2021a, 2021b). The aims of drilling at the site were to (1) fingerprint the volcaniclastic layers, (2) correlate them using chemical and mineralogical criteria with their source volcanoes, (3) establish a complete stratigraphy for Santorini and Kolumbo Volcanoes and how they interrelate, and (4) seek links between volcanic activity and the tectonic history of the Anhydros Basin as recorded on seismic profiles. Drilling was very successful, with good recovery in the cores from all three holes (U1589A–U1589C), and Hole U1589C touched limestone basement. The site transected all six seismic packages (Seismic Units U1–U6) of the Anhydros rift basin, as well as the onlap surfaces between them (Nomikou et al., 2016b, 2018; Preine et al., 2022a, 2022b).

4.1.2. Operations

We started our 1241 nmi voyage across the Mediterranean to Aegean Sea Site U1589 at 1254 h local time on 16 December 2022 in Tarragona, Spain, and completed the transit to Site U1589 on 21 December at 0715 h.

4.1.2.1. Hole U1589A

The bottom-hole assembly (BHA) and drill string were assembled and lowered to the seafloor at 484.3 mbsl. Using the APC, half-length APC (HLAPC), and XCB systems, Hole U1589A was cored to 446.7 mbsf, recovering 350.55 m of volcanic, tuffaceous, and nonvolcanic sediments (Table **T1**). The advanced piston corer temperature (APCT-3) tool was run on Cores 4H, 7H, 10H, and 13H.

4.1.2.2. Hole U1589B

Hole U1589B was spudded at 482.6 mbsl and recovered 331.46 m of volcaniclastic sediments, reaching a maximum depth of 359.4 mbsf. At the base of Core 70F, the Sediment Temperature 2 (SET2) probe was deployed at the bottom of Cores 54F and 70F to analyze the formation temperature.

4.1.2.3. Hole U1589C

The RCB BHA was assembled and tripped back down to the mudline, spudding Hole U1589C at 482.6 mbsl at 2304 h on 26 December 2022. The uppermost 360 m of Hole U1589C was drilled without recovery and continued to a depth 20 m above the base of Hole U1589B, recovering Cores 2R–28R. Beginning with Core 25R, we began to recover pebbles of limestone. Coring continued through Core 28R, and all cores contained limestone pebbles. The basement depth was determined at 589 mbsf. Following Core 28R, coring in Hole U1589C was ended. In total, Hole U1589C recovered 62.08 m of volcanic, tuffaceous, and nonvolcanic sediments and limestone basement, reaching a total depth of 621.9 mbsf. Core recovery was good in Holes U1589A (78%) and U1589B (87%) but poor in Hole U1589C (24%).

Table T1. Hole summary, Expedition 398. (Continued on next page.) **Download table in CSV format.**

Hole	Latitude	Longitude	Water depth (m)	Penetration DSF (m)	Cored interval (m)	Recovered length (m)	Recovery (%)	Drilled interval (m)	Drilled interval (no.)	Total cores (no.)	APC cores (no.)	HLAPC cores (no.)	XCB cores (no.)	RCB cores (no.)	Other cores (no.)
U1589A	36°43.7577′N	25°38.8915′E	484.3	446.7	446.7	350.55	78		0	75	15	49	11	0	1
U1589B	36°43.7574′N	25°38.9057′E	482.6	381.0	381.0	331.46	87		0	70	12	58	0	0	0
U1589C	36°43.7463′N	25°38.9046′E	482.6	621.9	261.9	62.08	24	360	1	27	0	0	0	27	0
		Site U1589 totals:		1449.6	1089.6	744.09		360	1	172	27	107	11	27	1
U1590A	36°33.2938′N	25°26.3888′E	397.1	99.3	99.3	60.87	61		0	11	11	0	0	0	0
U1590B	36°33.3129′N	25°26.3644′E	397.1	634.7	541.7	74.73	14	93	1	56	0	0	0	56	0
		Site U1590 totals:		734.0	641.0	135.60		93	1	67	11			56	
U1591A	36°18.7615′N	25°9.0057′E	514.6	98.8	98.8	64.76	66		0	11	11	0	0	0	0
U1591B	36°18.7621′N	25°9.0190′E	513.8	389.2	364.5	155.08	43	24.7	1	42	8	6	28	0	0
U1591C	36°18.7810′N	25°8.9962′E	513.8	902.9	668.6	384.47	58	234.3	2	69	0	0	0	69	0
		Site U1591 totals:		1390.9	1131.9	604.31		259	3	122	19	6	28	69	
U1592A	36°33.9358′N	25°45.6784′E	693.1	339.2	339.2	240.45	71		0	55	16	29	10	0	0
U1592B	36°33.9164′N	25°45.7027′E	693.1	527.8	234.8	117.04	50	293	1	25	0	0	0	25	0
		Site U1592 totals:		867.0	574.0	357.49		293	1	80	16	29	10	25	
U1593A	36°34.5103′N	25°24.8765′E	402.5	250.6	250.6	149.55	60		0	38	16	22	0	0	0
U1593B	36°34.4916′N	25°24.9000′E	404.0	232.8	232.8	156.78	67		0	39	11	28	0	0	0
U1593C	36°34.5060′N	25°24.8995′E	404.0	192.6	—	—	0	192.6	1	0	0	0	0	0	0
		Site U1593 totals:		676.0	483.4	306.33		192.6	1	77	27	50			
U1594A	36°23.3368′N	25°25.0290′E	291.0	51.7	51.7	47.94	93		0	6	6	0	0	0	0
		Site U1594 totals:		51.7	51.7	47.94				6	6				
U1595A	36°22.8955′N	25°24.3630′E	291.6	98.6	98.6	72.30	73		0	11	11	0	0	0	0
U1595B	36°22.8819′N	25°24.3358′E	291.4	127.1	127.1	74.02	58		0	15	13	2	0	0	0
U1595C	36°22.8674′N	25°24.3062′E	291.3	95.3	46.1	21.37	46	49.2	1	10	1	9	0	0	0
		Site U1595 totals:		321.0	271.8	167.69		49.2	1	36	25	11			
U1596A	36°26.5378′N	25°22.5130′E	382.1	41.9	41.9	38.00	91		0	5	5	0	0	0	0
U1596B	36°26.5568′N	25°22.4875′E	381.9	42.2	42.2	36.63	87		0	5	5	0	0	0	0
		Site U1596 totals:		84.1	84.1	74.63				10	10				
U1597A	36°26.2494′N	25°22.7326′E	382.4	43.6	43.6	40.84	94		0	5	5	0	0	0	0
		Site U1597 totals:		43.6	43.6	40.84				5	5				
U1598A	36°18.2937′N	25°7.7155′E	521.5	79.6	79.6	54.50	68		0	10	8	2	0	0	0
U1598B	36°18.2747′N	25°7.6929′E	521.5	98.8	23.5	7.91	34	75.3	1	5	0	5	0	0	0
		Site U1598 totals:		178.4	103.1	62.41		75.3	1	15	8	7			
U1599A	36°26.9592′N	25°46.8005′E	591.2	245.4	245.4	204.57	83		0	44	7	36	1	0	0
U1599B	36°26.9764′N	25°46.8237′E	592.7	241.0	241.0	199.13	83		0	40	10	29	1	0	0
U1599C	36°26.9389′N	25°46.7762′E	592.7	688.2	465.2	234.37	50	223	1	48	0	0	0	48	0
		Site U1599 totals:		1184.2	961.2	647.88		223	1	133	17	65	2	49	
U1600A	36°32.6277′N	25°39.0553′E	326.2	84.4	84.4	51.71	61		0	13	4	6	3	0	0
U1600B	36°32.6092′N	25°39.0311′E	326.3	91.4	91.4	68.67	75		0	19	1	18	0	0	0
U1600C	36°32.5890′N	25°39.0066′E	326.3	188.5	113.5	36.78	32	75	1	13	0	0	0	13	0
		Site U1600 totals:		364.3	289.3	157.16		75	1	45	5	24	3	13	
		Expedition 398 totals:		7344.8	5724.7	3346.37		1620.1	11	768	176	299	54	239	1

Hole U1589C was prepared for downhole logging using the triple combo tool string equipped with natural gamma radiation (HNGS), lithodensity (HLDS), electrical resistivity (HRLA), and magnetic susceptibility (MS) sensors. During logging Run 1, the tools encountered an obstruction at 544.9 mbsf that could not be passed. After a quick logging run up and down again, the tool got stuck at 227.7 mbsf. After tool recovery, the drill string was found to be stuck. The decision was made to sever the string during the evening on 30 December, and the line was successfully severed.

4.1.3. Principal results

Cores from the three consecutive holes (U1589A–U1589C) recovered a coherent stratigraphy from 0 to 612 mbsf. Hole U1589A extends 0–446 mbsf, Hole U1589B extends 0–360 mbsf, and Hole U1589C extends 372–612 mbsf. There is very good overlap between Holes U1589A and U1589B. Hole U1589C begins near the bottom of Holes U1589A and U1589B, and overlap is minimal with penetration to the basement.

The drilled interval fill is divided into five lithostratigraphic units (I–V) (Figure **F3**):

Table T1 (continued).

Hole	Date started	Time started UTC (h)	Date finished	Time finished UTC (h)	Time on hole (days)	Comments
U1589A	21 Dec 2022	0545	24 Dec 2022	0615	3.02	
U1589B	24 Dec 2022	0615	26 Dec 2022	1430	2.34	
U1589C	26 Dec 2022	1430	31 Dec 2022	1615	5.07	
U1590A	31 Dec 2022	1815	1 Jan 2023	1945	1.06	
U1590B	10 Jan 2023	1730	14 Jan 2023	0030	3.29	
U1591A	1 Jan 2023	2215	2 Jan 2023	1500	0.70	
U1591B	2 Jan 2023	1500	5 Jan 2023	0745	2.70	
U1591C	5 Jan 2023	0745	10 Jan 2023	1445	5.29	
U1592A	14 Jan 2023	0215	16 Jan 2023	0915	2.29	
U1592B	16 Jan 2023	0915	18 Jan 2023	1900	2.41	
U1593A	18 Jan 2023	2130	20 Jan 2023	0545	1.34	
U1593B	20 Jan 2023	0545	21 Jan 2023	1200	1.26	
U1593C	21 Jan 2023	1200	22 Jan 2023	1500	1.13	
U1594A	22 Jan 2023	1645	23 Jan 2023	0245	0.42	
U1595A	23 Jan 2023	0330	23 Jan 2023	2100	0.73	
U1595B	2 Feb 2023	0245	2 Feb 2023	2115	0.77	
U1595C	2 Feb 2023	2115	3 Feb 2023	1230	0.64	
U1596A	24 Jan 2023	0130	24 Jan 2023	0900	0.31	
U1596B	3 Feb 2023	1415	4 Feb 2023	0000	0.41	
U1597A	24 Jan 2023	0930	24 Jan 2023	1630	0.29	
U1598A	24 Jan 2023	1815	25 Jan 2023	0515	0.46	
U1598B	25 Jan 2023	0515	25 Jan 2023	1530	0.43	
U1599A	25 Jan 2023	1915	27 Jan 2023	1945	2.02	
U1599B	27 Jan 2023	1945	29 Jan 2023	0130	1.24	
U1599C	30 Jan 2023	1315	1 Feb 2023	2345	2.44	Reenter 2023-02-07 0230 h
U1600A	29 Jan 2023	0245	29 Jan 2023	1700	0.59	
U1600B	29 Jan 2023	1700	30 Jan 2023	1000	0.60	
U1600C	4 Feb 2023	0200	5 Feb 2023	0400	1.08	

- Unit I (~200 m thick) consists primarily of tuffaceous mud intercalated with intervals of ash, lapilli-ash, and lapilli, punctuated by less abundant nontuffaceous mud and ooze intervals. It is divided into Subunits Ia–Ic and is Holocene to Middle Pleistocene in age.
- Unit II (up to 173 m thick) primarily consists of muds and oozes interspersed with intermittent volcanic layers and organic-rich sapropelitic layers (Figures **F4**, **F5**). Five subunits of Unit II (IIa–IIe) are recognized. The unit is Middle Pleistocene to Early Pleistocene in age.
- Unit III (up to 14 m thick) is distinguished from Unit II by a gradual increase in both grain size and shell content. It consists primarily of sand with ash and shells interspersed with calcareous mud and sapropels. It is Early Pleistocene in age.
- Unit IV (up to ~190 m thick) consists of oxidized and carbonate-altered sands and conglomerates/breccias. Its age is uncertain.

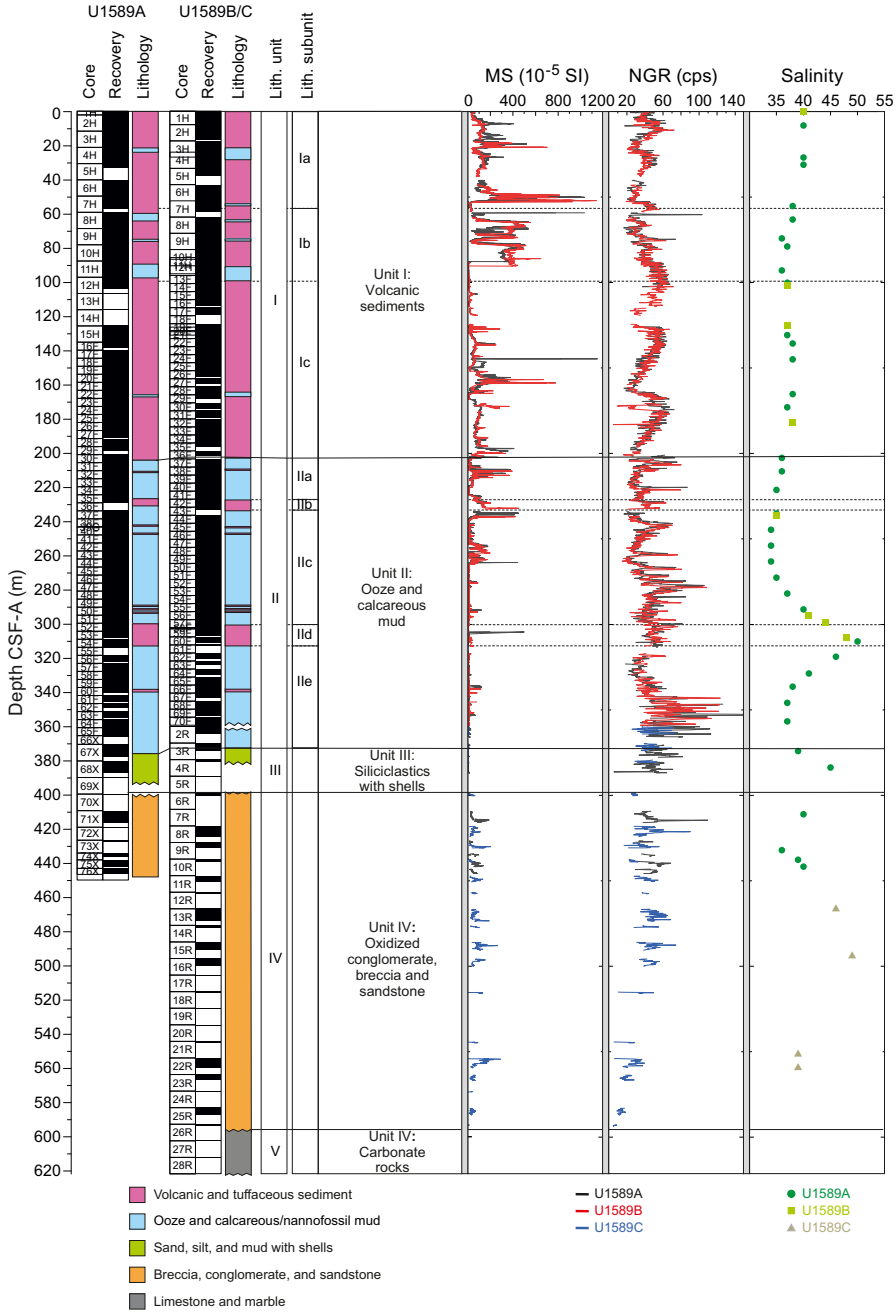

Figure F3. Simplified summary for Site U1589 in the Anhydros Basin. MS and NGR are whole-round measurements. Salinity measurements are from IW. cps = counts per second.

- Unit V (>20 m thick) is lithified limestone/marble that is the basement rock on which the above-lying sediments were deposited. The samples collected from Unit V consist of pluri-decimetric fragments of brecciated, carbonate-cemented, and nonbrecciated limestone/marble with large foraminifera (nummulites). This unit is of probable Middle Eocene to Cretaceous age.

The upper and lower boundaries of each lithostratigraphic unit are defined by lithologic changes that are usually accompanied by a change in physical properties (e.g., MS). Several types of core disturbance disrupt the lithostratigraphy at Site U1589: biscuiting, brecciation, fall-in, liquefaction to a soupy consistency, sediment flowage, sediment mixing, uparching, and core voids.

Structural measurements showed that the beds are horizontal to subhorizontal but that the dip decreases from the bottom to the top, with the median dip decreasing slightly from 5.0° in Unit IV

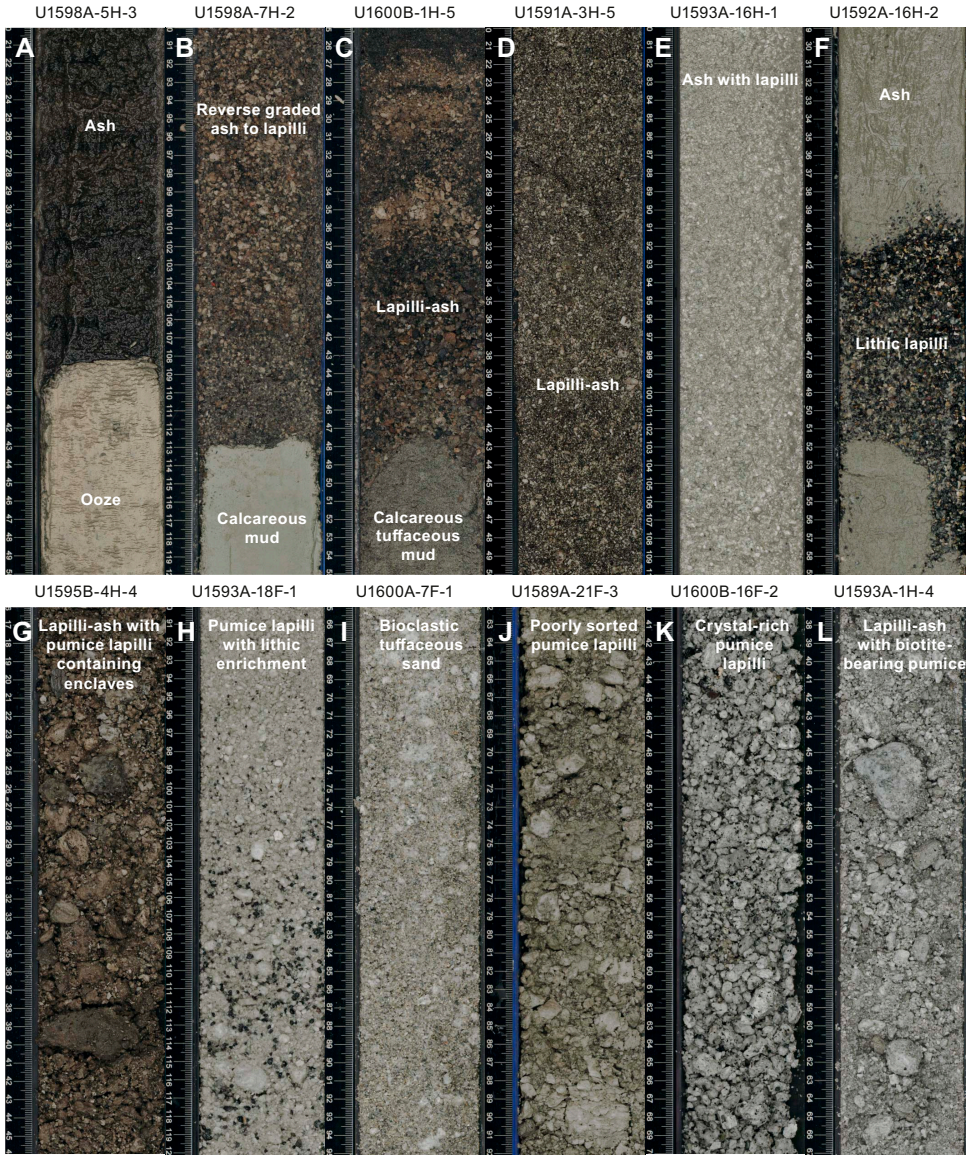

Figure F4. Volcanic lithologies, Expedition 398. Note variable strong core disturbances (e.g., uparching, sediment flowage, midcore flow, and fluidization) induced by the coring processes and seen in all cores. A. Coarse black ash with a sharp boundary to ooze. B. Reverse graded colorful lithic- and mineral-rich ash to fine lapilli with a sharp boundary to underlying calcareous mud. C. Multicolored lapilli-ash with variable thick horizons enriched in lapilli and ash. D. Black and white lapilli-ash. E. White ash with lapilli. F. Lithic lapilli layer embedded in fine white ash. G. Lapilli-ash layer with brown pumice containing mafic enclaves. H. Normally graded pumice lapilli to ash with basal enrichment of lithics. I. Bioclastic tuffaceous sand. J. Poorly sorted pumice lapilli layer. K. Crystal-rich lapilli layer with amphibole- and biotite-rich pumice. L. Lapilli-ash layer with biotite-bearing pumice.

to 4.2° in Unit I. The major change in the bedding dip was identified at the bottom of Unit II. Some core sections contain faults that correspond in orientation to the main basin structures.

Calcareous nannofossils, planktonic foraminifera, and benthic foraminifera recovered from core catcher samples and additional split core samples from Holes U1589A–U1589C were used to develop a shipboard biostratigraphic framework for Site U1589. Calcareous nannofossils and planktonic foraminifera provide good age resolution throughout the sediments. Ages provided by benthic foraminifera are consistent with those of calcareous nannofossils and planktonic foraminifera and show that the basin fill at Site U1589 ranges from the Holocene near the seafloor to the Early Pleistocene at ~400 mbsf (Figure **F6**). The data indicate highly variable sedimentation rates in different depth ranges of the basin fill, ranging from ~0.1 m/ky in Unit III to up to ~1 m/ky in Units II and I. Owing to high sedimentation rates through some of the cored section, semiquanti-

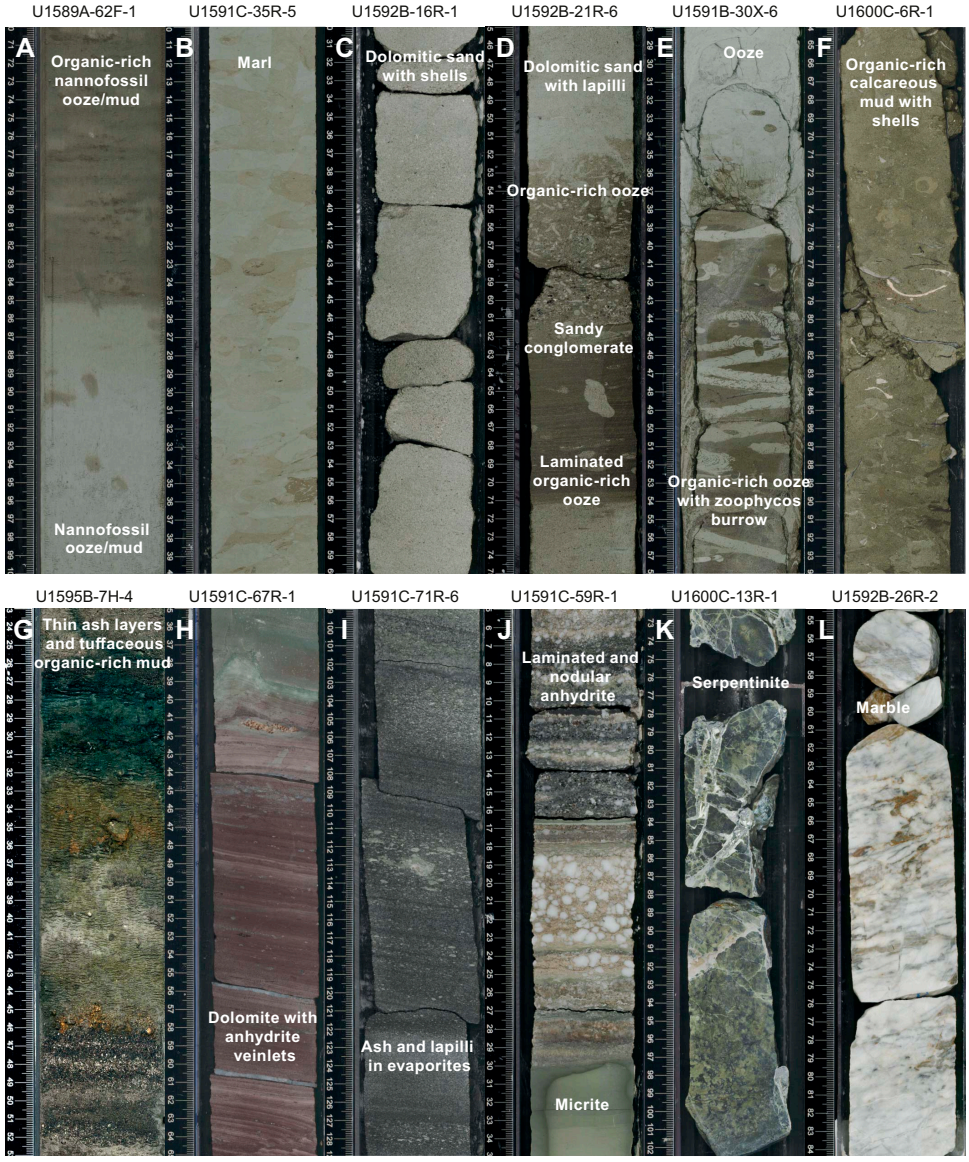

Figure F5. Nonvolcanic and mixed lithologies, Expedition 398. Note variable strong core disturbances (e.g., uparching, biscuiting, and brecciation) induced by the coring processes or bioturbation and seen in all cores. A. Nannofossil ooze/mud with and without organics. B. Bioturbated marl. C. Dolomictic sand with shells. D. Dolomictic sand with lapilli with an intercalated interval of laminated organic-rich ooze, sandy organic-rich conglomerate, and bioturbated organic-rich ooze. E. Bioturbated (*Zoophycos*) organic-rich ooze and overlying ooze. F. Organic-rich calcareous mud with shells. G. Thin ash layers intercalated in tuffaceous organic-rich mud. H. Laminated dolomite with anhydrite veinlets. I. Thinly bedded anhydrite and dolomite with horizons enriched in ash and lapilli. J. Laminated and nodular anhydrite above micrite. K. Serpentinite with veins filled with calcite and talc. L. Marble.

tative planktonic foraminiferal assemblage data were used in conjunction with calcareous nannofossil and planktonic foraminiferal biostratigraphic datums to tentatively recognize Marine Isotope Stages (MIS) 10 and 11. These were based primarily on fluctuations of the warm-water species *Globigerinoides ruber*, *Globigerinoides elongatus*, and *Globigerinoides pyramidalis*. Benthic foraminifera provided data on paleowater depths, which increase from 0 to 600–1000 m in Unit II and then stabilize at 200–600 m in Unit I. Oceanicity values (percent planktonic foraminifera) gave paleodepths similar to those provided by benthic foraminifer assemblages.

Holes U1589A and U1589B were analyzed for physical properties using the Whole-Round Multisensor Logger (WRMSL) for MS, gamma ray attenuation (GRA) density, and *P*-wave velocity; the Natural Gamma Radiation Logger (NGRL) for NGR intensity; and subsequently the Section-Half Multisensor Logger (SHMSL) for point magnetic susceptibility and color reflectance. Section halves were photographed after the cores were split into working and archive halves. In general, MS was recognized to be the most reliable physical parameter for correlations, whereas NGR and GRA density measurements were often significantly overprinted by the irregular distribution of core material in cores with low recovery and a high water content. MS also proved to be an excellent proxy for the presence of volcanic material in the cores (Figure **F3**). After the composite depth scale was established, selected sequences from Holes U1589A and U1589B were spliced and the additional (but scattered) parts of Hole U1589C were added to create the most complete and representative section possible.

Downhole variations in physical properties (Figure **F3**) arise from changes in lithology, compaction, and other diagenetic processes. Differences between volcanic and other lithologies are most prominent in MS because of the abundance of ferromagnetic minerals (e.g., magnetite) in volcanic (high) and nonvolcanic (low) sediments. Although density was expected to increase progressively with increasing depth due to compaction, low-density pumice deposits and unconsolidated ash layers between compacted biogenic ooze created a more complex porosity structure throughout the drilled formation. Similarly, shear strength and thermal conductivity both increase with depth but are often lower in volcaniclastic units relative to adjacent materials. In general, at this site volcaniclastic units have higher MS, lower *P*-wave velocity, and lower density than other sediments at the same depth. Physical property measurements could thus be used to interpret downhole logging data and to help identify thin ash and pumice layers in mostly biogenic, compacted sediment.

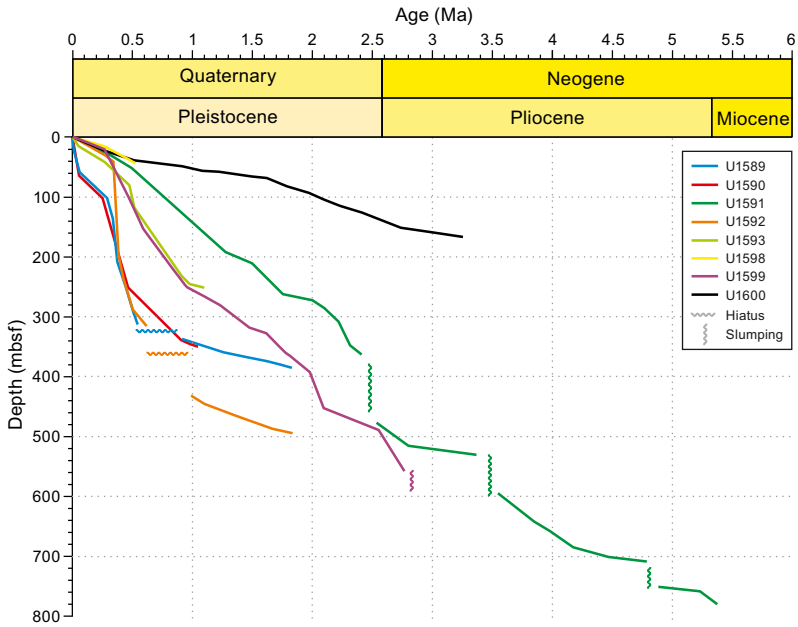

Figure F6. Early Pliocene to Holocene age-depth plot for Expedition 398 sites based on biochronologic events derived from foraminifera and nannofossils from Sites U1589–U1593 and U1598–U1600. Lines = interpolated sedimentation rates based on these datums. Unconformities in the form of assumed hiatuses and slumping events are indicated.

The triple combo tool string provided whole-hole in situ NGR, resistivity, density, and MS measurements at various sampling rates. NGR downhole logs (total counts) confirmed the whole-hole trend of NGR measurements on whole-round core sections acquired using the shipboard NGRL. Resistivity logs show a dichotomy in ranges of logged values between Lithostratigraphic Unit IV and the rest of the upper formation. Unit IV has the highest density values compared to the shallower formation, which is consistent with the trend observed by shipboard measurements.

To determine the geochemistry of the volcanic layers, 17 tephra samples were handpicked from various layers in Hole U1589A. Following cleaning, grinding, fusion, and dissolution, the volcaniclastic material was analyzed shipboard for major, minor, and trace elements using inductively coupled plasma–optical emission spectroscopy (ICP-OES) in atomic emission spectroscopy (AES) mode and are referred to as ICP-AES in this report. Of the volcaniclastic units sampled, two were classified as basaltic andesites or basaltic trachyandesites, four as andesites or trachyandesites, eight as dacites or trachydacites, and three as rhyolites. Trace element ratios were used to broadly discriminate between the volcanic centers of Kolumbo and Santorini using published trace element data for onland volcanics. These correlations were tentative because the analytical precision of certain trace elements such as Nb are not very good on the shipboard ICP-AES instrument, limiting our ability to discriminate between compositionally similar volcanic sources. Salinity of the interstitial waters (IWs) varies throughout the succession (Figure **F3**). IW concentrations of Ca, Mg, K, and SO_4^{2-} show downhole variations that strongly correlate with lithology. One layer exhibits a peak in Ba concentration at 246 mbsf in Lithostratigraphic Unit II that corresponds to the lowest SO_4^{2-} concentrations observed. Salinity, Cl^-, Br^-, SO_4^{2-}, Na^+, and K^+ all peak at ~320 mbsf in Unit II (Figure **F3**). Methane was the dominant hydrocarbon present at generally low concentrations (<4 ppmv). Ethane, propane, butane, and other heavier hydrocarbons were either low or below detection.

Natural remanent magnetism (NRM) intensities at Site U1589 are broadly normally distributed, but low-field susceptibilities display a bimodal distribution with peaks at ~10×10^{-5} SI and ~60×10^{-5} SI that suggest contributions from two distinct lithologic sources and/or magnetic minerals and/or magnetic grain sizes. When grouped into seven categories based on lithology, the data suggest the presence of two populations of magnetic grain assemblages demarcated by susceptibilities higher than and lower than ~20×10^{-5} SI. We suspected that the low-susceptibility group includes samples containing the diagenetic ferrimagnetic sulfide mineral greigite (Fe_3S_4) in lower intervals of the sampled section deeper than ~300 mbsf. The presence of greigite greatly complicated the use of the cores for creating a geomagnetic timescale. The core interval shallower than 300 mbsf could be confidently assigned to the Brunhes Chron, but recognition of the Brunhes/Matuyama reversal was problematic. Comparison with the biostratigraphic age-depth curve predicted that the Brunhes/Matuyama reversal should be seen at 330 mbsf and the Matuyama/Jaramillo reversal at 342 mbsf, but the reversals were obscured by the effects of spurious magnetizations carried by greigite.

The good recovery at Site U1589 led to the construction of a preliminary splice with few gaps. The age-depth model is very detailed, with a total of ~20 age constraints. Lithostratigraphic Unit V is Cretaceous–Eocene limestone that forms the Alpine basement. It is overlain by ~200 m of the intercalated brown to reddish sands and matrix-supported breccias of Unit IV, which is older than ~1.8 Ma and probably of terrestrial origin. Unit III is ~20 m thick and comprises a probable shoreline facies of 1.8–1.6 Ma age of sand with ash and shells interspersed with calcareous mud. It is overlain by the ~200 m thick Unit II, which is composed mainly of calcareous oozes with interleaved tuffaceous layers. It has an age of ~1.6–0.4 Ma, over which the water depth at Site U1589 increased from shoreline to as deep as 1000 m. At least one eruption laid down ash at this site during this period. Finally, Unit I is ~200 m thick and is dominated by volcanic and tuffaceous sediments with ooze intervals. It was laid down from ~0.4 Ma to present day. Water depth during this period ranged from <250 to 500–750 m or more. The lower limit of Unit I coincides approximately with the MIS 11/10 boundary. This unit contains several volcanic units derived from both Santorini and Kolumbo Volcanoes. Detailed core-seismic integration awaits further work.

4.2. Site U1590

4.2.1. Background and objectives

Site U1590 (proposed Site CSK-03A) is located 5 km northwest of the submarine Kolumbo crater on its flank in the Anhydros Basin at 397 mbsl.

The seismic profiles across the Kolumbo edifice reveal five units interpreted as Kolumbo-derived volcanics (Eruption Units K1–K5, from the base up), with Unit K5 representing the 1650 CE eruption (Hübscher et al., 2015; Preine et al., 2022c). The submarine cones northeast of Kolumbo postdate Unit K2 on seismic profiles, but their products were not expected to be prominent in our drill cores.

The aim of drilling on the flanks of Kolumbo Volcano was to penetrate the different seismically recognized volcanic eruption units from that volcano (K1–K5 or their thin, lateral equivalents), as well as many eruption units from Santorini and traces from the submarine cones northeast of Kolumbo Volcano. This would enable characterization of the products of the Kolumbo eruptions and construction of a coherent stratigraphy for Santorini and the submarine Kolumbo volcanic chain together. Site U1590 at the foot of the Kolumbo edifice allowed us to drill Seismic Units K1–K5 and therefore nearly the entire history of Kolumbo Volcano. Intercalated seismic units are believed to contain the products of Santorini eruptions, including potentially those of smaller magnitude than recorded at the more distal basin sites.

4.2.2. Operations

The transit to Site U1590 started at 1818 h on 31 December 2022. The vessel arrived on location and started lowering the thrusters at 1946 h.

4.2.2.1. Hole U1590A

At 0115 h on 1 January 2023, the trip in the hole started with the APC/XCB BHA. Hole U1590A was spudded with Core 1H from 403 meters below rig floor (mbrf) at 36°33.2938′N, 25°26.3888′E. Recovery was 4.3 m, giving a calculated seafloor depth of 397.1 mbsl. Coring continued to 89.8 mbsf. Various levels of overpull were observed on the core barrels to a maximum of 50,000 lb. The APCT-3 tool was run on Core 4H.

At 1200 h, the drill string took weight when trying to lower it, indicating ~8 m of fill had fallen into the hole. Core 11H was retrieved, and the sinker bars were pulled.

The severing tool was assembled and run into the hole to 4.6 mbsf. The BHA was severed at the top of the tapered drill collar at 1700 h. All thrusters were raised at 2136 h, and the sea passage to Site U1591 (proposed alternate Site CSK-20A) began at 2148 h, ending Hole U1590A.

4.2.2.2. Hole U1590B

Site U1590 was revisited on 10 January 2023 with the intention of coring an RCB hole to the target depth of 566 mbsf. At 1852 h, the vessel came onto location at Site U1590. Despite fairly significant hole trouble early on, through careful coring and the liberal use of mud sweeps the target of 566 mbsf was surpassed and went on to an EPSP-approved deepening to 634.7 mbsf (the EPSP approved drilling to 850 mbsf).

The vessel was offset 50 m northwest of Hole U1590A. An RCB BHA with bit was again assembled and run in the hole to 373.9 mbrf. Hole U1590B was spudded at 0030 h on 11 January and drilled down to 93.0 mbsf. High torque was observed at 26.4 and 83.8 mbsf.

At 0700 h, RCB coring started with Core 2R from 93.0 mbsf. As expected, the recovery was extremely low in the upper sections, but the decision to use the RCB system was made to reach the target depth. Coring continued through 12 January; recovery was mostly very poor.

On 13 January, RCB coring was completed with Core 57R to 634.7 mbsf, the final depth for Hole U1590B. Coring was terminated in favor of other objectives at the following sites. Overall, average core recovery was moderate in Hole U1590A (61%) but poor in Hole U1590B (14%).

4.2.3. Principal results

Cores from Hole U1590A recovered a coherent stratigraphy from 0 to 91 mbsf; a partial stratigraphy was recovered in Hole U1590B from 93 to 628 mbsf. Four types of disturbance affect the cores: fall-in, sediment mixing, biscuiting, and cracking and breaking. We identified two lithostratigraphic units (Figure F7):

- Unit I (91 m thick) is dominantly volcanic (ash and lapilli, including biotite-bearing pumices) with minor amounts of tuffaceous and nonvolcanic ooze/mud. Within Unit I, we identified three subunits (Ia–Ic) based on sharp changes in grain sizes within the predominantly volcanic succession. This unit is Holocene to Late Pleistocene in age.
- Unit II (>535 m thick) contains mixed nonvolcanic (oozes, muds, and calcareous sands), tuffaceous, and minor volcanic (ash/lapilli) intervals. Unit II was sampled in Hole U1590B, and four subunits (IIa–IId) were recognized. This unit is Late Pleistocene to Early Pleistocene in age.

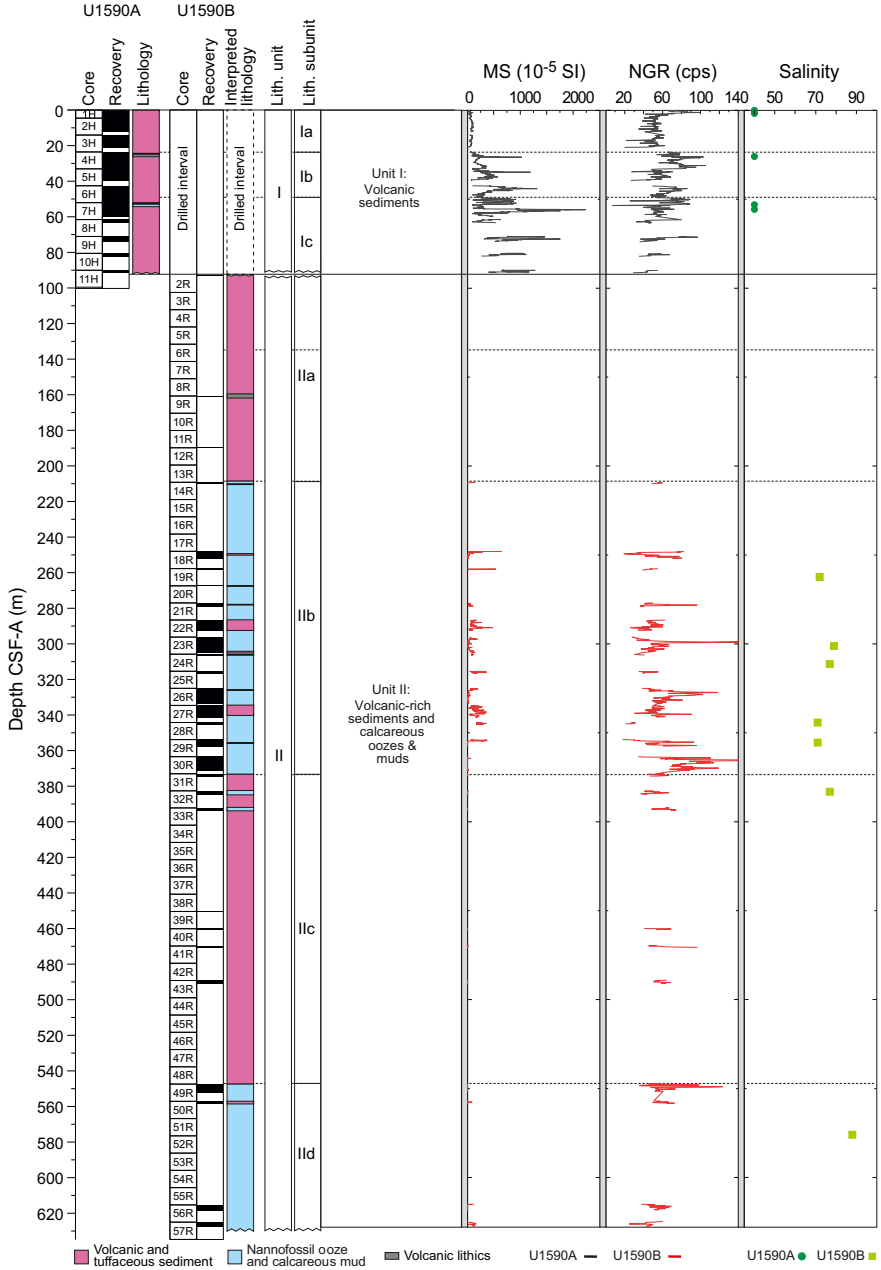

Figure F7. Simplified summary for Site U1590 at the slope of Kolumbo Volcano. MS and NGR are whole-round measurements. Salinity measurements are from IW. cps = counts per second.

Structural geology measurements showed that bedding planes are horizontal throughout the boreholes with dips ranging 0°–7°. Minor-scale slumps characterized by oblique foliation of sand-mud mixed layers were identified at 460 and 470 mbsf in Hole U1590B.

Calcareous nannofossils and planktonic and benthic foraminifera were used to develop a shipboard biostratigraphic framework for Site U1590. Additionally, planktonic and benthic foraminifera provided data on paleowater depths, downslope reworking, and possible dissolution. Calcareous nannofossils are rare to abundant in samples from the Holocene to Early Pleistocene sequence. Preservation is generally good to moderate with sporadically poor to very poor intervals throughout the sequence; however, there is significant reworking of older material in most of the Pleistocene samples. The assemblages are characterized by the occurrence of warm-water species such as *Rhabdosphaera clavigera* and *Umbilicosphaera sibogae* throughout the sequence at Site U1590. The oldest calcareous nannofossil datum found was the basal occurrence of *Reticulofenestra asanoi* (1.078 Ma) at 481 mbsf. Planktonic foraminifer assemblages from the Holocene to Pleistocene section of Site U1590 are mostly well preserved, where specimens are rarely broken or exhibit partially dissolved shell walls. Foraminiferal faunas are sufficiently common to biostratigraphically divide the Pleistocene sediments into three Mediterranean planktonic foraminiferal biostratigraphic zones: MPIe2b, MPIe2a, and MPIe1c.

The benthic foraminifer distributions indicate uppermost to upper bathyal (300–600 m) paleowater depths from 0 to 305 mbsf, mid to lower bathyal (600–1000 m) depths from 305 to 394 mbsf, and uppermost to upper bathyal (300–600 m) depths from 394 to 491 mbsf. Oceanicity values (percent planktonic foraminifera) are generally in agreement with the benthic foraminiferal paleowater depth indicators.

Because of the very low recovery in the uppermost 17 cores of Hole U1590B, no stratigraphic correlation was possible using physical properties. Poor recovery in both holes limited the ability to document continuous variations in physical properties measurements over more than several tens of meters. MS is highly variable within the volcaniclastic deposits at Site U1590, from $<100 \times 10^{-5}$ to $>1000 \times 10^{-5}$ SI. Mean *P*-wave velocity is 1.63 km/s (standard deviation = 0.15 km/s), and the largest value is 2.17 km/s. Moisture and density (MAD) measurements gave porosities of 39–73 vol%, bulk densities of 1.2–2.1 g/cm^3, and grain densities of 1.4–2.8 g/cm^3. Of a total of five thermal conductivity measurements, the mean value is 0.86 W/(m·K) (standard deviation = 0.20 W/[m·K]). A temperature of 15.67° ± 0.17°C was measured downhole using the APCT-3 tool at 33 mbsf.

Owing to potential hole instabilities in the ash- and pumice-rich lithologies, no wireline logging was possible at Site U1590.

Of 12 volcanic units sampled or analyzed using ICP-AES, 2 were classified as basaltic andesites or basaltic trachyandesites and 10 as trachydacites. Trace element ratios were used to broadly discriminate between the volcanic centers of Kolumbo and Santorini, showing that the products of both volcanoes are present at this site. IW salinity values in Hole U1590A are 40 in all samples, which is close to the current average Aegean salinity value of 39; those in Hole U1590B range 71–88 and show no correlation with depth (Figure **F7**). Values of alkalinity range 2.5–9.1 mM, and pH values range 7.1–7.9. Bromide, Cl^-, Na^+, B, Ca^{2+}, Mg^{2+}, and SO_4^{2-} all follow similar trends, with lower values in the uppermost 53 m and increased concentrations at depth. Analyses of TOC content identified one sapropel with TOC values >2.0 wt% and eight sapropelitic organic-rich layers for units with TOC values of 0.5–2.0 wt%. The data showed low methane concentrations in Hole U1590A (<3 ppmv); values were below detection limit at all depths in Hole U1590B. Ethane concentrations were below the detection limit for all samples measured in both Holes U1590A and U1590B.

Paleomagnetic analysis at Site U1590 focused on measurement and demagnetization of archive-half sections and 31 discrete samples to determine magnetostratigraphic age controls. The low overall recovery in Hole U1590B resulted in a restricted distribution of magnetic data downhole, and no reversal boundaries could be established. Nevertheless, by referring to biostratigraphic age constraints, it was possible to make the following correlations with the geomagnetic polarity timescale (GPTS): (1) the interval 0–393 mbsf correlates with the Brunhes Chron (C1n) and is

therefore <0.773 Ma in age, (2) the interval 470–491 mbsf corresponds to the Jaramillo Subchron (Chron C1r.1n) and was deposited within the period 1.008–1.076 Ma, and (3) the interval 617–628 mbsf carries a reversed magnetization that was acquired during Chron C1r.2r (1.076–1.189 Ma).

Owing to the poor recovery, particularly in Hole U1590B, any conclusions remain highly tentative. Detailed correlation of volcanic units by geochemical fingerprinting will be required to fully understand the stratigraphy. The volcanic layers of Lithostratigraphic Unit I are believed to include the pumice from the Kolumbo Volcano 1650 CE eruption (Eruption Unit K5) and the eruptions of the Thera Pyroclastic Formation of Santorini. Lithostratigraphic Unit II is believed to include Eruption Units K1–K4 from Kolumbo Volcano, although identification is not yet possible based on the available data. It is possible that the volcanic units cored from Lithostratigraphic Unit II come from Kolumbo, Santorini, or both volcanoes. The cores penetrated to 1.21 Ma, showing that volcanism has persisted in this part of the volcanic field since the mid-Pleistocene.

4.3. Site U1591

4.3.1. Background and scientific objectives

Prior to arrival on site, it was decided to replace the original primary site (proposed Site CSK-13A) with an alternate one (proposed Site CSK-20A); hence, the latter became Site U1591. This was done to pass through a slightly more complete suite of seismic reflectors in the 800–900 ms TWT interval.

Site U1591 is located ~8 km northwest of the Christiana Islands and ~20 km southwest of Santorini (Figure **F1**) at 514 mbsl. The drill site targeted the volcano-sedimentary fill of the Christiana Basin. This basin formed by subsidence along an ENE–WSW fault system before the changing tectonic regime activated the current northeast–southwest rift system in which the CSK volcanic field lies (Tsampouraki-Kraounaki and Sakellariou, 2018; Preine et al., 2022a, 2022c; Heath et al., 2019).

The Christiana Basin is deeper than the Anhydros and Anafi Basins; its volcano-sedimentary fill potentially records the earlier volcanic history of the CSK volcanic field (including the products of Christiana Volcano and early Santorini), as well as younger Santorini and possibly Milos Volcano to the west along the Hellenic volcanic arc. The now-extinct Christiana Volcano produced lavas and tuffs of unknown ages (Aarbourg and Frechen, 1999). An ignimbrite found on Christiani Island (one of the two small islands of Christiana Volcano), Santorini, and the nonvolcanic island of Anaphi, called the Christiani Ignimbrite, was identified (Keller et al., 2010).

Six seismic units were identified in the Christiana Basin in previous work (Preine et al., 2022b, 2022c). Site U1591 was chosen to pass through Seismic Units U1–U6, including volcaniclastics from both Santorini and Christiana, and to target the top few meters of prevolcanic basement below Seismic Unit U1. We received permission from the EPSP to drill to Alpine basement at this site in an APC/XCB/RCB drilling strategy involving three holes.

The aims of Site U1591 were to (1) better date the volcanic activity of Christiana using biostratigraphic and magnetostratigraphic means and determine whether the CSK volcanic field had Pliocene volcanism like Milos Volcano farther west, (2) relate Christiana volcanism to subsidence along the ENE–WSW fault sets and to the activation of the northeast–southwest fault sets, and (3) seek the submarine equivalent of the Christiani Ignimbrite. By using deeper coring (and seismic profiles) to reconstruct the volcanic, sedimentary, and tectonic histories of Christiana Volcano, and possibly Milos Volcano, we would complement the Santorini and Kolumbo volcanic records of Sites U1589 and U1590 and therefore access a near-continuous time series of volcanism of the CSK volcanic field since rift inception. Site U1591 addresses Scientific Objectives 1–4 and 6 of the *Expedition 398 Scientific Prospectus* (Druitt et al., 2022).

4.3.2. Operations

The operations at Site U1591 involved three holes but with heavier use of the XCB and RCB systems because of the seemingly poor hole conditions when piston coring.

4.3.2.1. Hole U1591A

At 0740 h on 2 January 2023, Hole U1591A was spudded at 36°18.7615′N, 025°09.0057′E, with a recovery of 3.8 m for Core 1H and a calculated seafloor at 514.6 mbsl. APC coring continued through Core 11H at 98.8 mbsf. The string was pulled out of the hole, and the bit cleared the rotary table at 1700 h, ending Hole U1591A.

4.3.2.2. Hole U1591B

Still on 2 January 2023, a reconfigured APC/XCB BHA was assembled using the same drill bit. Hole U1591B was spudded at 2150 h on 2 January at 36°18.7621′N, 025°09.0190′E. The recovery of 3.8 m indicated seafloor at 513.8 mbsl.

At 0245 h on the morning of 3 January, the APC system was pulled and an XCB center bit was dropped. The intention was to drill through a previously identified pumice section. The driller proceeded to drill from 74.1 to 98.8 mbsf. On 5 January, XCB coring finished with Core 43X at 389.2 mbsf, the final depth for Hole U1591B, after the XCB cutting shoe sheared off in the hole.

4.3.2.3. Hole U1591C

On 5 January 2023 at 1500 h, Hole U1591C was spudded at 36°18.7810′N, 025°08.9962′E, with an offset water depth of 524.9 mbrf. A drill-ahead section was completed to 149.3 mbsf. Coring began with the RCB system for Cores 2R–5R at 187.4 mbsf by midnight on 5 January. Coring continued through 10 January through Core 71R at 902.9 mbsf, the final depth for Hole U1591C. The decision was made to terminate coring in favor of other objectives. Average core recovery was similar in all three holes (U1591A = 66%; U1591B = 43%; U1591C = 58%).

4.3.3. Principal results

The material recovered at Site U1591 is sedimentary and unlithified throughout Holes U1591A and U1591B. A gradual transition to stiffer and more consolidated lithologies toward the bottom of Hole U1591B continues in Hole U1591C. Sediment in Hole U1591C in turn transitions gradually from consolidated sediment to sedimentary rock. The sedimentary succession in the uppermost ~770 m is characterized by both volcanic lithologies (ash/tuff, lapilli-ash, lapilli, and tuffaceous mud/sand/mudstone/sandstone) and nonvolcanic calcareous mud/mudstone and ooze/marl (Figure **F8**). At ~770 mbsf there is a sharp transition to anhydrite-bearing lithologies.

Three lithostratigraphic units are recognized (Figure **F8**):

- Unit I (153 m thick) is dominated by extensive volcanic intervals with lesser overall amounts of nonvolcanic material. This unit is divided into three subunits (Ia–Ic). Subunit Ic is a prominent layer rich in pumice lapilli and ash. This unit is Holocene to Middle Pleistocene in age.
- Unit II (614 m thick) is dominated by repeating packages of ooze/mud and organic-rich (sapropelic) ooze/mud with interspersed tuffaceous mud/sand, ash and lapilli-ash, and volcanic-dominated packages. It is divided into six subunits (IIa–IIf) and is Middle Pleistocene to Late Miocene (?) in age.
- Unit III (>130 m thick) is dominated by lithologies containing anhydrite (evaporite sequence), clearly showing a distinct change in depositional environment. Unit III is divided into two subunits (IIIa and IIIb). A transition to ash- and lapilli-bearing volcanic material containing anhydrite (Subunit IIIb) marks the end of Hole U1591C. This unit is of probable Miocene age.

Discrete samples from Unit III were analyzed using X-ray diffraction to characterize the evaporite sequences of Subunit IIIa. Anhydrite was identified as one of the major evaporite minerals, occurring as laminated and nodular varieties and as veins and veinlets.

Observed and measured structures in the cores of Site U1591 are bedding, faults, and deformation bands, mineral veins, and sediment veins. Bedding planes were measured mainly on thin sand beds/laminae, sapropels, micrites, and anhydrite boundaries. They exhibit horizontal to subhorizontal dips shallower than 350 mbsf. However, steeper inclinations develop below 350 mbsf, where dips range 5°–85°. Slump deposits were frequently identified as (1) block-in-matrix occurrences, (2) flow/disturbed mud, and (3) folding of sandy laminae/beds in muddy matrixes. Small-scale faults occur on split core surfaces with displacements from a few millimeters to a centimeter. Sed-

iment-filled veins and mineral veins were identified in specific intervals in the lower parts of Units II and III, respectively.

Planktonic foraminifera, benthic foraminifera, and calcareous nannofossils were used to develop a shipboard biostratigraphic framework for Site U1591 (Figure **F6**). Calcareous nannofossils and planktonic foraminifera provide good resolution in the Holocene through Early Pliocene sediments. Seawater depths for Unit I and Subunit IIa derived from benthic foraminifer assemblages range 300–1000 m and are consistent with oceanicity values (ratio of planktonic to benthic foraminifera).

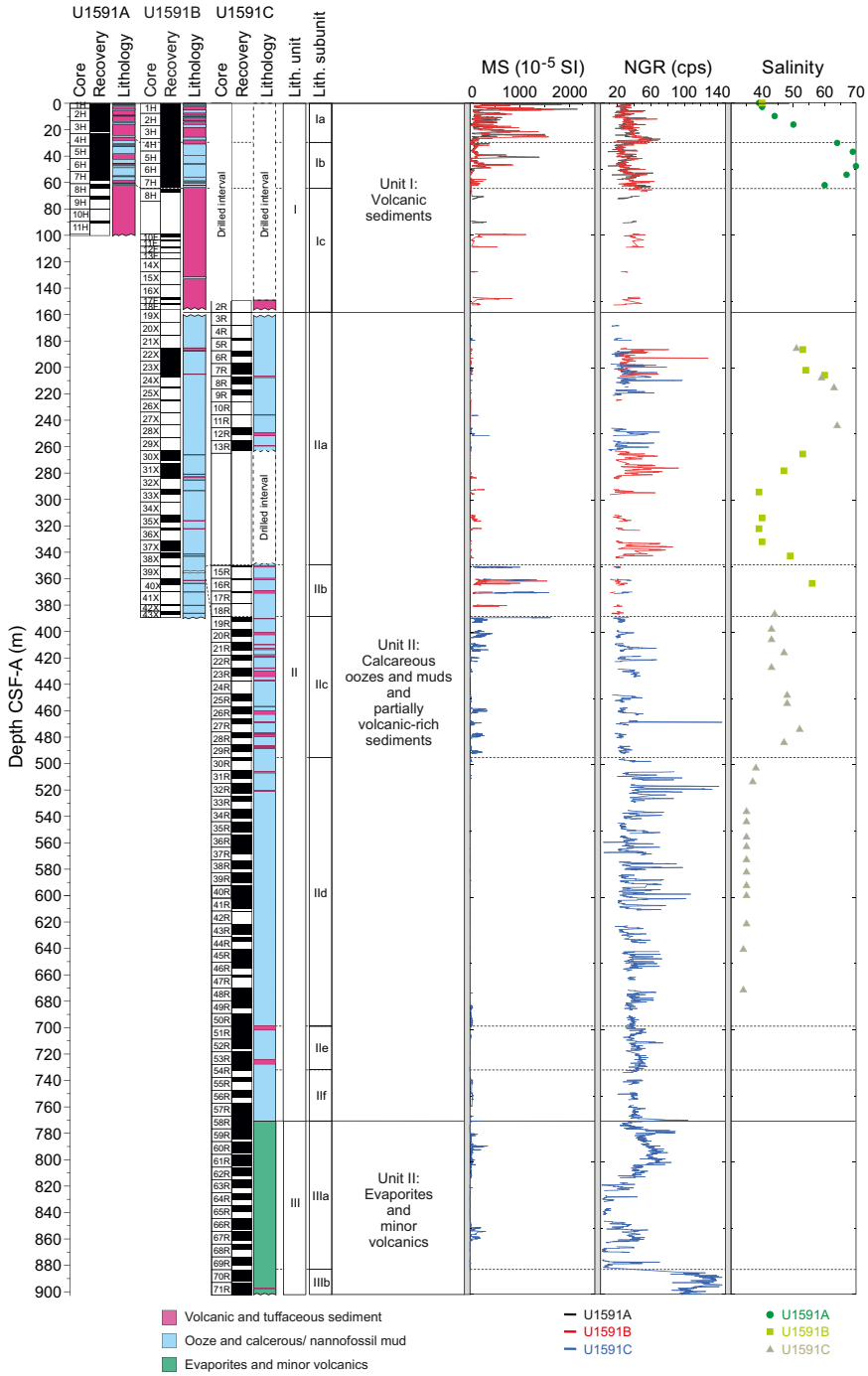

Figure F8. Simplified summary for Site U1591 in the Christiana Basin. MS and NGR are whole-round measurements. Salinity measurements are from IW. cps = counts per second.

Stratigraphic correlation mainly focused on the correlation of Holes U1591A and U1591B to identify coring gaps and create a first, tentative splice between holes. Following this, the focus shifted to correlation of the small overlap between the deeper parts of Hole U1591B and the uppermost cores of Hole U1591C. The majority of the work done by the stratigraphic correlation group, however, was on remodeling seismic velocities based on *P*-wave analyses from the physical properties group.

Physical properties at Site U1591 correlate well with lithology. Thick volcaniclastic layers in Unit I (ash, lapilli-ash, and lapilli) sometimes have low grain densities in coarse, pumice-rich subunits. Volcaniclastic deposits also exhibit large variations in MS and often have high MS compared to other sediments at this site. High-MS anomalies are most abundant and largest in amplitude at depths shallower than 490 mbsf (Figure **F8**). Unit II, which is dominated by nannofossil-rich oozes, often displays cyclic variations in NGR that correlate with organic-rich layers (Figure **F8**). Volcaniclastic materials in Unit I have *P*-wave velocities of 1.5–1.7 km/s. Typical *P*-wave velocities of the oozes in Unit II increase with depth from ~1.7 km/s at the top of Unit II to ~2.1 km/s at its base. Unit III has highly variable *P*-wave velocity; anhydrite-rich lithologies have velocities >5.0 km/s, whereas the background sediments have values similar to those of the overlying deposits of Unit II (2.1–2.8 km/s). The anhydrite-rich layers of Unit III also have higher thermal conductivity and bulk density and lower NGR than the surrounding sediments. Sediment porosity ranges 3–79 vol%, and bulk density ranges 1.2–2.9 g/cm^3. Some levels in Unit III have grain densities that exceed 2.9 g/cm^3, consistent with anhydrite-dominated lithologies.

Because of the instability of the formations encountered, downhole logging was not conducted at Site U1591.

Of the volcanic units sampled and analyzed using ICP-AES, 3 were classified as basaltic andesites or basaltic trachyandesite, 4 as andesites or trachyandesites, 13 as dacites or trachydacites, and 2 as rhyolites. Bulk chemistry values are less evolved than glass chemistry, as expected, due to bulk analyses including both minerals and glass. Trace element ratios were used to broadly discriminate between the volcanic centers of Kolumbo, Santorini, and Christiana, or indicate so-far unknown sources. The thick pumice-rich Subunit Ic shows chemical affinities to the Christiani Ignimbrite.

Salinities of IW samples range 35–70 throughout the hole (most values are 35–60) (Figure **F8**). Br^-, Cl^-, B, Na^+, K^+, Mg^{2+}, Ca^{2+}, and SO_4^{2-} trends all follow those of salinity. Lithium and strontium appear to be roughly correlated at depth. A total of 44 organic-rich units were identified; those with TOC values >2.0 wt% were identified as sapropels (22), and units with TOC values 0.5–2.0 wt% were identified as sapropelitic (37). Methane was the dominant headspace hydrocarbon present; the generally low concentrations locally reached as high as 883 ppmv, which is well within safe operational limits.

Paleomagnetic analysis at Site U1591 focused on measurement and demagnetization of archive-half sections to determine magnetostratigraphic age controls. The uppermost 63 m of Lithostratigraphic Unit I carries normal polarity remanences acquired during the Brunhes Chron. Scattered inclinations then prevented magnetostratigraphic correlations within Unit II from 185 to 480 mbsf; from 480 to 770 mbsf, however, the quality of data improved and eight reversal boundaries could be tied precisely to the GPTS (within the Pliocene), with a further four tentative correlations also possible. Data in the evaporite sequence of Unit III are less conclusive.

Correlation of the sequence with seismic stratigraphy must await full analysis. Overall, we can confirm that volcanic activity in the CSK volcanic field started in the Pliocene. Lithostratigraphic Unit III is an evaporite sequence dominated by anhydrite and is of Messinian age. Unit II consists of oozes with volcanic and tuffaceous horizons and ranges from Early Pliocene to Late Pleistocene in age; it contains several slumped horizons and layers of reworked benthic fauna. Unit I is dominated by volcanic and tuffaceous lithologies, including a thick pumice layer with chemical affinities to the Christiani Ignimbrite. Seawater depths during emplacement of Units II and I range 300–1000 m.

4.4. Site U1592

4.4.1. Background and scientific objectives

Site U1592 is located ~10 km southeast of Anhydros Island within the Anafi Basin at 693 mbsl. The aim at the site was to penetrate the entire volcano-sedimentary fill as far as the Alpine basement to reconstruct the evolution of the Anafi Basin: history of subsidence, the presence of volcanic event layers in the basin sediments, and links between volcanism and crustal tectonics.

The Anafi Basin potentially records the full volcanic history of Santorini (and any older centers) since rift inception but was envisaged to probably contain few eruptive products from Kolumbo Volcano. Drilling would enable reconstruction of the volcanic, sedimentary, and tectonic histories of the Anafi Basin, allowing us to compare its evolution with that of the Anhydros Basin. The site was also chosen to develop a core-log-seismic integration stratigraphy and compare it with the recently published seismic stratigraphy for the basin (Preine et al., 2022a, 2022b) and the paleotectonic reconstruction of the region (Nomikou et al., 2016b, 2018). The site transects the six seismic packages of the Anafi rift basin, as well as the onlap surfaces between them (Nomikou et al., 2016b, 2018; Preine et al., 2022a, 2022b).

The Anafi Basin is crossed by many seismic profiles obtained in campaigns between 2006 and 2019, many of them multichannel (Hübscher et al., 2015; Nomikou et al., 2016b, 2018). It is included within the area of the 2015 PROTEUS seismic tomography experiment, when subbottom profiling, gravity, and magnetic data were also recorded (Hooft et al., 2017). The basin bathymetry has been studied in several marine campaigns, and fault distributions and throws have been mapped (Nomikou et al., 2016b; Hooft et al., 2017).

Coring at Site U1592 in the Anafi Basin addressed Scientific Objectives 1–4 and 6 of the *Expedition 398 Scientific Prospectus* (Druitt et al., 2022). It is complemented by Site U1589 in the Anhydros Basin because each basin taps a different sediment distributary branch of the CSK volcanic system.

4.4.2. Operations

Operations at Site U1592 involved two holes with a switch to RCB coring for Hole U1592B, following slow progress using the XCB system. Hole U1592A was an APC/HLAPC/XCB advance to 339.2 mbsf. Hole U1592B was RCB cored to 527.8 mbsf after an initial 293.0 m drilled interval. Logging was not attempted because there were several sections of the same loose, unconsolidated layers that had been causing problems at earlier sites.

4.4.2.1. Hole U1592A

Hole U1592A was spudded on 14 January 2023 at 0830 h from 700 mbrf at 36°33.9358′N, 25°45.6784′E. The recovered core was 5.1 m long, giving a calculated seafloor depth of 693.1 mbsl. APC coring continued through Core 16H from 135.3 mbsf and switched to the HLAPC system for Core 17F.

HLAPC coring continued into 15 January with Core 45F to 273.8 mbsf, where the barrel became stuck. At 1330 h, an XCB barrel was dropped and coring reconvened with Core 46X from 273.8 mbsf. Coring continued on 16 January to Core 55X at 339.2 mbsf, the final depth for Hole U1592A. The rate of penetration for the XCB system was slowing to the 4 m/h range, so the decision was made to switch to the RCB system.

4.4.2.2. Hole U1592B

Hole U1592B was spudded at 1600 h at 36°33.9164′N, 25°45.7027′E. The seafloor depth was again 693.1 mbsl by offset. A drill-ahead finished at 293.0 mbsf. The driller started RCB coring with Core 2R from 293.0 mbsf. Cores 8R–13R were almost zero recovery and were assumed to be a pumice layer judging from the seismic profiles. Core 11R was a punch core, a 2 m advance with little to no rotation or pump, to try to recover some of the difficult pumice section. The recovery was still very poor but measurable because a handful of the pumice lapilli was recovered. Coring continued on 18 January 2023 until 1545 h with Core 26R to 527.8 mbsf, the final depth for Hole U1592B. Average core recoveries were 71% (Hole U1592A) and 50% (Hole U1592B).

4.4.3. Principal results

Five lithologic units are recognized at Site U1592 (Figure F9).

- Unit I (269 m thick) is a succession of volcanic layers (ash and lapilli) and tuffaceous or nonvolcanic layers, divided into four subunits (Ia–Id). It is Holocene to Middle Pleistocene in age.
- Unit II (135 m thick) is dominantly ooze and other nonvolcanic lithologies interspersed with minor volcanic and tuffaceous sediments. It is Middle Pleistocene to Early Pleistocene in age.
- Unit III (90 m thick) is composed of dolomitic muds and sands with shell fragments. It is Early Pleistocene in age.
- Unit IV (15 m thick) is a thin unit of bioclastic limestone of probable Early Pleistocene age.
- Unit V (>11 m thick) is limestone basement and marble. It is probably Early Pleistocene in age.

In the uppermost part of Unit V, near the boundary with the overlying bioclastic limestone of Unit IV, the limestones and marbles of Unit V are typically reddish yellow in color due to oxidation, but they transition downward to mainly nonoxidized, massive, white, and partly banded limestone and marble.

A distinguishing feature of the nonvolcanic sediments (sands and oozes) of Unit III, compared to Unit I and II lithologies, is the relatively high proportion of dolomite.

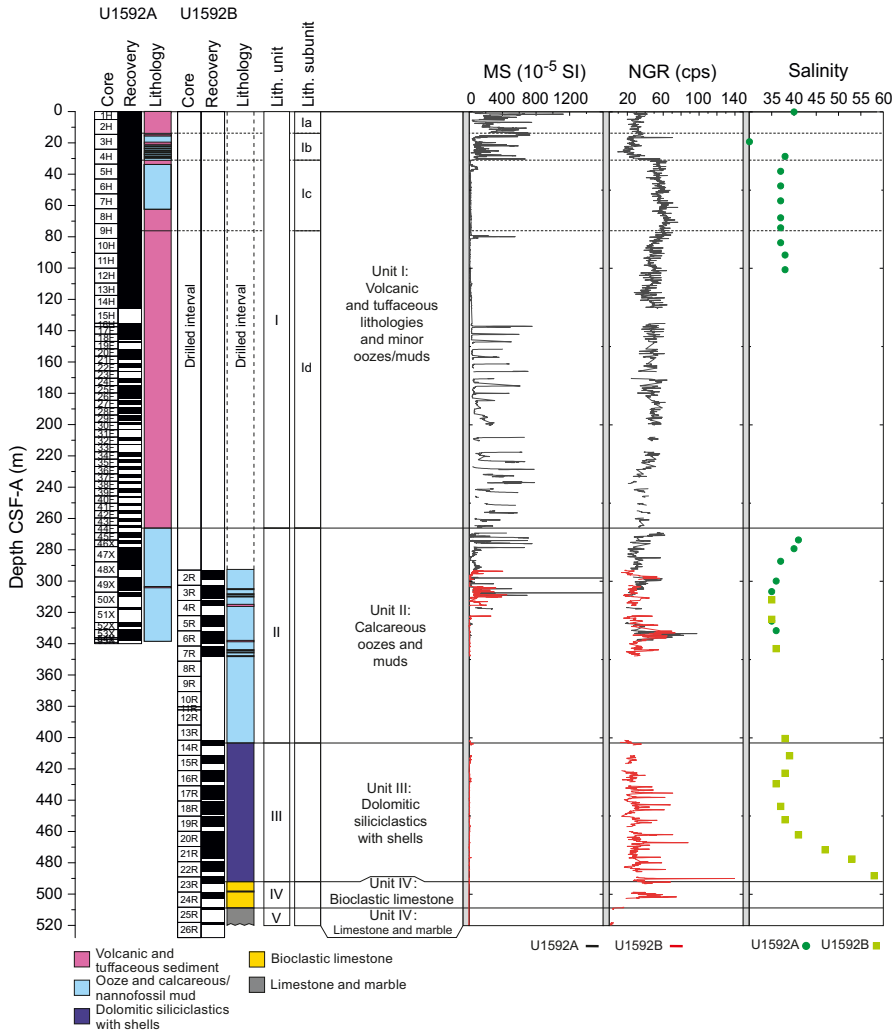

Figure F9. Simplified summary for Site U1592 in the Anafi Basin. MS and NGR are whole-round measurements. Salinity measurements are from IW. cps = counts per second.

Bedding planes at Site U1592 mostly exhibit horizontal to subhorizontal dips throughout the core. The bedding dip in Unit III (median dip = 7.0°) is greater than that in Unit II (median dip = 4.5°). The dip increases again from Unit II to Subunits Ib–Ic (4.5°–7.0°). One possibility is that the occurrence of volcanism triggered slumps in Subunits Ib–Ic and thus increased the median dip. A slump deposit was identified at the upper part (31–38 mbsf) of Unit I. A large population of normal faults and deformation bands occurs in the interval 300–350 mbsf, just above an ~50 m recovery gap from which a small amount of pumice was recovered.

Site U1592 recovered Holocene to Early Pleistocene sediments. Reworking of microfossils sourced from Pleistocene–Early Cretaceous sediments was observed throughout the entire cored interval, and reworked Eocene larger benthic foraminifera constitute a substantial bioclastic component of Unit IV. Seven nannofossil biostratigraphic datums were recognized at Site U1592, representing a continuous Middle to Late Pleistocene sedimentary sequence. Foraminiferal faunas are sufficiently common to divide the Pleistocene into six Mediterranean planktonic foraminiferal biostratigraphic zones: MPIe2b, MPIe2a, MPIe1c, MPIe1b, MPIe1a, and MPI6b.

Holocene to Pleistocene planktonic foraminifer faunas suggest large fluctuations in oceanicity (a proxy for relative paleowater depth) and highly variable planktonic abundances that range 5.5%–100%. Benthic foraminifer distributions are highly variable, indicating paleowater depths from inner shelf (<50 m) to lower bathyal (>1000 m).

Creation of a core composite depth below seafloor, Method A (CCSF-A), depth scale and construction of a splice for Holes U1592A and U1592B was not necessary because both holes had only a short overlap between 293 and 339 m (CSF-A scale). Within this overlapping interval, several correlations were established using MS and NGR measurements from WRMSL, as well as half core images.

Physical properties at Site U1592 were correlated with lithology and the respective units (Figure **F9**). The topmost volcaniclastic Lithostratigraphic Subunit Ia has low NGR counts and high MS relative to other volcaniclastic units. Volcaniclastic layers in Subunit Ic have lower MS and a factor of 2× higher NGR than Subunits Ia and Ib. Subunit Id exhibits large variations in MS and often has high MS compared to other sediments at this site. In Unit II, which is dominated by nannofossil-rich oozes, *P*-wave velocity increases with depth, NGR is low, and MS is low except where thin volcaniclastic layers have high MS. The dolomitic and siliciclastic layers of Unit III often display cyclic variations in NGR that correlate with organic-rich layers. Limestones and marbles in Units IV and V have higher *P*-wave velocity and lower NGR than Units I–III. Overall, porosities range 3–83 vol% and bulk densities range 1.2–2.7 g/cm^3. Bulk density increases with depth but is lowest in volcaniclastic materials. Grain densities range 1.9–2.8 g/cm^3, with the lowest values in volcaniclastic subunits in the upper 280 m. Thermal conductivity increases with depth, except in the uppermost 150 m, as expected from the compaction of sediments. The limestones and marbles in Units IV and V have higher thermal conductivities (>2 W/[m·K]) than other sediments at similar depths (1–2 W/[m·K]). Because of the instability of the formations encountered, downhole logging was not conducted.

Of the nine volcanic units analyzed for major and trace elements using ICP-AES, two were classified as basaltic andesites, two as trachyandesites, and five as dacites or trachydacites. IW salinity values range 30–58; the highest value of 58 was recorded near 490 mbsf (Figure **F9**). Values for alkalinity range 1.2–7.0 mM, and those of pH range 7.6–8.0. The concentrations of bromide, Cl^-, B, Na^+, and K^+ follow similar trends to salinity. Calcium, Mg^{2+}, and SO_4^{2-} correlate well with each other and show an increase in the lowermost 75 m as salinity also increases. Trends for Li, Sr, Mn, Ba, and Si do not follow salinity. Both carbonate and TOC decline from 19 to 101 mbsf; the highest carbonate values were noted below 283 mbsf, reaching 58 wt%. Six organic-rich units were identified as sapropelitic (TOC = 0.5–2.0 wt%). Methane, ethane, and propane concentrations were below the detection limit in headspace gases.

Paleomagnetic analysis at Site U1592 focused on measurement and demagnetization of archive-half sections to determine magnetostratigraphic age controls. The uppermost 82 m of the sequence sampled in Hole U1592A carries normal polarity remanences acquired during the Brunhes Chron. Below this interval, the cores recovered from Hole U1592A were unsuitable for paleo-

magnetic measurement. The interval ~270–348 mbsf in Hole U1592B is also normally magnetized and was assigned to the Brunhes Chron. The Brunhes–Matuyama transition (0.773 Ma) was not recovered, but the sequence from 400 to 457 mbsf exhibits changes in magnetic polarity, allowing three reversal boundaries to be tied precisely to the GPTS (corresponding to the start/end of the Jaramillo Subchron at 1.008/1.076 Ma and the start of the Cobb Mountain normal polarity subchron at 1.189 Ma in the Matuyama Chron). An additional tentative correlation to the base of the Cobb Mountain Subchron was also made by reference to a biostratigraphic marker. Samples below 460 mbsf exhibited mainly positive inclinations. However, this unit was dated biostratigraphically to the reversed polarity Matuyama Chron, suggesting that this interval was remagnetized during either the Jaramillo/Cobb Mountain Subchron or Brunhes Chron.

In summary, cores at Site U1592 in the Anafi Basin traversed a 1.8 My old basin fill sequence lying upon basement limestones. Lithostratigraphic Unit III consists of dolomitic sands aged 1.8 to <0.97 Ma and records the initial marine transgression into the basin. This was followed by a gap in our record that recovered only a small amount of pumice. Given that core loss commonly coincided with well-sorted pumice layers, it is possible that a thick pumice layer formed the base of Unit II. This is overlain by an interval with abundant faults and deformation bands. Following Unit II, Unit I consists of about 180 m of ash deposited with sedimentation rates exceeding ~1 m/ky, the origin of which is yet to be established. Finally, the top of Unit I contains volcaniclastic deposits from Santorini and Kolumbo Volcanoes. Correlation with the seismic stratigraphy of the Anafi Basin awaits detailed analysis of the data.

4.5. Site U1593

4.5.1. Background and scientific objectives

Site U1593 (alternate proposed Site CSK-04C) is located 8 km northwest of Kolumbo Volcano at 402 mbsl.

The seismic profiles across the Kolumbo edifice reveal five units interpreted as Kolumbo-derived volcaniclastics (K1–K5, from the base up), with Seismic Unit K5 representing the 1650 CE eruption (Hübscher et al., 2015; Preine et al., 2022a). The submarine cones northeast of Kolumbo postdate Unit K2 on seismic profiles, but their products were not expected to be prominent in our drill cores.

The aim of drilling on the flanks of Kolumbo Volcano was to penetrate the different seismically recognized volcanic eruption units from that volcano (K1–K3, K5, or their thin, lateral equivalents), as well as many eruption units from Santorini and traces from the submarine cones northeast of Kolumbo. This would enable characterization of the products of the Kolumbo eruptions as well as construction of a coherent stratigraphy for Santorini and the submarine Kolumbo volcanic chain together.

Site U1593 lies at the foot of the Kolumbo edifice, 3 km northwest of Site U1590. Owing to the poor recovery at the latter site, we decided to also drill at Site U1593, which lies on the other side (northwest) of the Kolumbo Fault to Site U1590. This had two advantages. First, we could measure the offset across the Kolumbo Fault by correlating key marker layers from one site to the other. Second, the sequence at Site U1593 was more condensed than that at U1590, offering us older recovery and potentially greater hole stability.

Like Site U1590, Site U1593 allowed us to drill Seismic Units K1–K3 and K5, and therefore nearly the entire history of Kolumbo Volcano, within the proposed drilling target depth of 581 mbsf. Intercalated seismic units were believed to contain the products of Santorini eruptions, including potentially those of smaller magnitude than recorded at the more distal basin sites.

4.5.2. Operations

4.5.2.1. Hole U1593A

Hole U1593A (36°34.5103′N, 25°24.8765′E) was spudded on 19 January 2023 at 0245 h from 409.0 mbrf. Recovery for Core 1H was 4.7 m, giving a calculated seafloor depth of 402.5 mbsl.

APC coring continued through Cores 2H–16H (4.7–147.2 mbsf). Indications of partial strokes on three consecutive cores plus high overpull on Core 16H led to a switch to the HLAPC system. HLAPC coring commenced with Core 17F and continued through Core 38F (250.6 mbsf), the final depth for Hole U1593A.

4.5.2.2. Hole U1593B

At 0940 h on 21 January, Hole U1593B (36°34.4916′N, 25°24.9000′E) was spudded from 412.0 mbrf. The recovery of 6.20 m gave a calculated seafloor depth of 404.0 mbsl. APC coring continued with Cores 2H–11H. HLAPC coring began with Core 12F at 101.2 mbsf and continued through Core 39F (232.8 mbsf), the final depth for Hole U1593B.

4.5.2.3. Hole U1593C

At 1445 h, the vessel was offset 25 m north. Hole U1593C (36°34.5060′N, 25°24.8995′E) was spudded at 1752 h with an RCB drill bit. The hole was advanced without recovery to 192.6 mbsf. At the 192 mbsf mark, the drill pipe started experiencing increasing torque. The drill string was severed at 37.0 mbsf at 1010 h on 22 January.

In total, we drilled to a maximum depth of 250.6 mbsf in three holes (U1593A, U1593B, and U1593C) with average core recoveries of 60%, 67%, and <1%, respectively.

4.5.3. Principal results

Cores from Site U1593 recovered a coherent stratigraphy from 0 to 251 mbsf (Figure **F10**). Hole U1593A consists of Sections 398-U1593A-1H-1 through 38F-CC (0–251 mbsf). Hole U1593B consists of Sections 398-U1593B-1H-1 through 39F-CC (0–232 mbsf). The recovered material is unlithified sediment, dominated by volcanic and tuffaceous sediments interspersed with minor amounts of nonvolcanic sediments in both holes. Site U1593 comprises two lithostratigraphic units:

- Unit I (235 m thick) is composed of volcanic (ash, lapilli, and lapilli-ash), tuffaceous, and minor nonvolcanic (oozes and muds) lithologies in four subunits (Ia–Id). It is Holocene to Early Pleistocene in age.
- Unit II (>16 m thick) consists mainly of nonvolcanic oozes or organic-rich oozes with intermittent intervals of tuffaceous ooze and ash and has no subunits. It is Early Pleistocene in age.

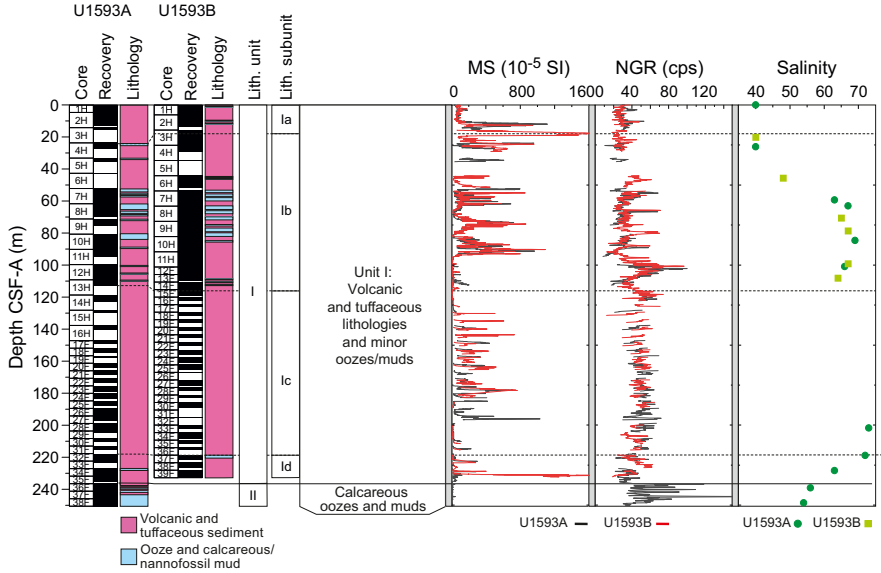

Figure F10. Simplified summary for Holes U1593A and U1593B at the distal Kolumbo Volcano site. MS and NGR are whole-round measurements. Salinity measurements are from IW. cps = counts per second.

Bedding planes are mostly horizontal to subhorizontal (median values = 3.6°–5.3°) throughout the core. Some slumps are documented in Subunits Ib and Id and in Unit II.

Site U1593 recovered Holocene to Early Pleistocene–aged sediments (1.078 Ma). Foraminiferal faunas are sufficiently common to biostratigraphically divide the Pleistocene sediments into three Mediterranean planktonic foraminiferal biostratigraphic zones: MPIe2b, MPIe2a, and MPIeIc.

Benthic foraminiferal assemblages are highly variable between abundant to reworked/transported specimens and totally barren samples. The low abundances or complete absence of benthic foraminiferal faunas in most of the samples are possibly correlated with rapid emplacement of volcaniclastic sediments and/or inhospitable environmental conditions. Benthic foraminifera yielded few useful paleodepth data. Relative paleowater depths based on oceanicity (percentage of planktonic foraminifera) range widely from 0 to 1000 m.

Coarse volcanic deposits at Site U1593 typically have low grain densities and thermal conductivities compared to other sediments at this site. MS is highly variable in the volcaniclastic layers (Figure **F10**), sometimes very high (>1500 × 10^{-5} SI), and helped, together with core images, to correlate, where possible, between Holes U1593A and U1593B. The typical increases of bulk density, *P*-wave velocity, and thermal conductivity with increasing depth are not clearly documented at this site. Porosity values range 36%–70%, bulk density ranges 1.1–2.1 g/cm^3, and grain density ranges 1.1–2.8 g/cm^3, with the lowest values in the volcaniclastic subunits. Compared to typical sediments in which thermal conductivity exceeds 1 W/(m·K) deeper than 100 mbsf, thermal conductivity is low in volcaniclastic sediments at Site U1593. Because of the instability of the formations encountered, downhole logging was not conducted.

Holes U1593A and U1593B have an overlap almost over the entire depth to 232.8 mbsf and allow stratigraphic correlation based mainly on the MS derived with the WRMSL. A preliminary splice was constructed that contained only minor gaps.

Of the volcanic units sampled, one was classified as a basalt, one as basaltic andesite, three as andesites or trachyandesites, seven as dacites or trachydacites, and one as a rhyolite. Trace element data suggest derivation from both Kolumbo and Santorini. IW salinity ranges 40–73, with most values 60–70 (Figure **F10**). Most values for IW alkalinity are 4–5.5 mM. Values for pH range 7.3–7.9 and generally decrease with depth. Br^-, Cl^-, B, Na^+, K^+, Mg^{2+}, Ca^{2+}, and SO_4^{2-} all follow trends similar to salinity. Trends for Sr, Mn, Ba, and Si do not follow salinity as strongly as the major cations and anions, although Li generally does. Methane, ethane, and propane concentrations were below the detection limit in all measured samples.

The uppermost 117 m of the sequence sampled in Hole U1592A carries normal polarity remanences acquired during Chron C1n (Brunhes). No cores suitable for paleomagnetic analysis were recovered in the 88 m below this interval (117–205 mbsf), but a 2 m interval with normal polarity at ~206 mbsf was also assigned to the Brunhes Chron. The Brunhes/Matuyama boundary (0.773 Ma) was assigned to the interval 207.5–218.0 mbsf and the interval displaying variable inclinations to Chron C1r.1r. The interval below 240 mbsf was assigned to Chron C1r.1n (Jaramillo).

In summary, Site U1593 recorded more than 1 My of rift fill and volcanism associated with Kolumbo and Santorini Volcanoes. The sequence is dominated by many volcanic and tuffaceous lithologies that will require a great deal of work to chemically fingerprint and to correlate across the study area. Water depths ranging 250–750 m appear to have been most common in this part of the rift system.

4.6. Site U1594

4.6.1. Background and scientific objectives

Site U1594 (proposed Site CSK-07B) is located in the southern basin of Santorini caldera. It lies at 291 mbsl. Site U1595 addresses the same drilling objectives and lies southwest of Site U1594. Two additional sites (U1596 and U1597) lie in the northern caldera basin.

The four intracaldera sites were planned to sample Seismic Units S1–S3; test the published correlations between the two caldera basins; penetrate below Unit S3 into Unit S4; and address Scientific Objectives 1, 4, 5, and 7 of the *Expedition 398 Scientific Prospectus* (Druitt et al., 2022). By drilling both caldera basins and exploiting our dense seismic reflection coverage, we would gain access to the 3D architecture of the entire caldera fill. We also targeted the question of why the northern basin is 100 m deeper than the southern one, with a thicker Unit S1 but a thinner Unit S3. Finally, we tested whether Unit S3 consisted of flood debris from the caldera-flooding event (Nomikou et al., 2016a) or was LBA intracaldera tuff (Johnston et al., 2015). The intracaldera sites were used for microbiological work regarding Objective 7.

4.6.2. Operations

On 22 January 2023 at 1830 h, the vessel arrived at Site U1594 in the southern end of Santorini caldera. The 15.0 nmi transit took 1.8 h at an average speed of 8.3 kt.

4.6.2.1. Hole U1594A

Hole U1594A (36°23.3368′N, 25°25.0290′E) was spudded on 22 January 2023 at 2310 h. The core was shot from 297.0 mbrf and recovered 4.2 m, establishing the seafloor at 291.0 mbsl.

APC coring continued on 23 January, with 94% recovery from Cores 2H (4.2 mbsf) through 6H and the bottom of the hole at 51.7 mbsf, the final depth for Hole U1594A. Excessive torque was observed, indicating a collapsing hole, and the drill string was pulled up.

The decision was made to offset to an alternate site in the southern caldera (proposed Site CSK-08B).

4.6.3. Principal results

One lithostratigraphic unit is recognized at this site (Figure **F11**). Unit I (>50 m thick) consists predominantly of volcanic lithologies, such as ash, lapilli-ash, and lapilli, with small amounts of tuffaceous and nonvolcanic sediments. Two subunits (Ia and Ib) are recognized. Unit I is Holocene in age.

Very rare planktonic and benthic foraminifera as well as rare calcareous nannofossils indicate an age of younger than 0.265 Ma for the sequence, which is consistent with the known intracaldera geology.

Physical properties measurements show a general trend of increasing *P*-wave velocity and MS (Figure **F11**) with increasing depth at the site. Porosity ranges 51–80 vol%, and bulk density ranges 1.2–1.6 g/cm^3. Bulk density does not obviously increase with depth. Grain density ranges 1.6–2.6 g/cm^3; more than 40% of discrete samples have grain densities <2.0 g/cm^3, and grain density decreases with increasing depth. Compared to typical sediments in which thermal conductivity is close to 1 W/(m·K) at these depths below seafloor, thermal conductivity is low in the volcaniclastic sediments. There is no apparent increase in thermal conductivity with increasing depth.

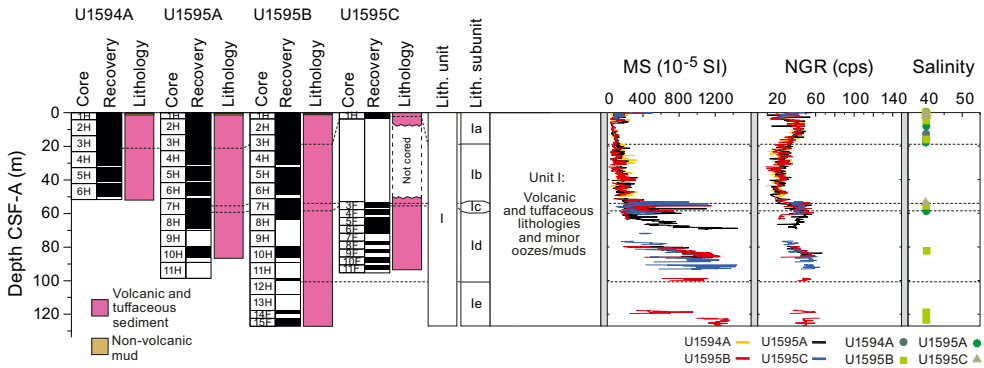

Figure F11. Combined simplified summary for Holes U1594A and U1595A–U1595C from the southern basin in Santorini caldera. MS and NGR are whole-round measurements. Salinity measurements are from IW. cps = counts per second.

Of the samples analyzed using ICP-AES, all are dacites or trachydacites of Santorini trace element affinity. IW salinity is 40 throughout the hole (Figure **F11**). There is a slight increase in alkalinity from the mudline (2.6 mM) to 13 mbsf (5.7 mM), followed by a slight decrease in total alkalinity with depth to the base of the hole at 15 mbsf. Values for pH range 7.8–7.9. There are small variations in boron and major cations and anions in the IW, except Br^-, which remains constant with depth. There are larger variations in Li, Sr, Mn, Ba, and Si than for cations and anions. Methane, ethane, and propane concentrations were below the detection limit throughout the hole.

Because there was only a single hole, no stratigraphic correlation was possible at Site U1594, and, due to the instability of the formations encountered, downhole logging was not conducted. None of the cores recovered were suitable for paleomagnetic analysis.

For Site U1594, six whole-round core samples were collected for microbial community composition analysis.

To briefly summarize our findings at Site U1594, Lithostratigraphic Subunit Ia corresponds approximately to Seismic Unit S1, which consists of muds and ashes. Lithostratigraphic Subunit Ib corresponds approximately to Seismic Unit S2 and is mostly volcanic in nature. The volcanic material in Subunit Ib appears to be of Kameni origin, but confirmation must await detailed geochemical characterization.

4.7. Site U1595

4.7.1. Background and scientific objectives

Site U1595 (formerly proposed alternate Site CSK-08B) is located in the southern basin of Santorini caldera at 291 mbsl. Site U1594 addresses the same drilling objectives and lies northeast of Site U1595. Two additional sites (U1596 and U1597) lie in the northern caldera basin.

The four intracaldera sites were planned to sample Seismic Units S1–S3; test the published correlations between the two caldera basins; penetrate below Unit S3 into Unit S4; and address Scientific Objectives 1, 4, 5, and 7 of the *Expedition 398 Scientific Prospectus* (Druitt et al., 2022). By drilling both caldera basins and exploiting our dense seismic reflection coverage, we would gain access to the 3D architecture of the entire caldera fill. We also targeted the question of why the northern basin is 100 m deeper than the southern one, with a thicker Unit S1 but a thinner Unit S3. Finally, we tested whether Unit S3 consisted of flood debris from the caldera-flooding event (Nomikou et al., 2016a) or was LBA intracaldera tuff (Johnston et al., 2015). The intracaldera sites were used for microbiological work regarding Objective 7.

4.7.2. Operations

4.7.2.1. Hole U1595A

Hole U1595A (36°22.8955′N, 25°24.3630′E) was spudded on 23 January 2023 at 0635 h. With a shot depth of 297.0 mbrf and a recovery of 3.6 m, the calculated seafloor depth was 291.6 mbsl.

APC coring continued through Core 11H at 98.6 mbsf, the final depth for Hole U1595A. At 1315 h, while preparing to shoot Core 11H, the hole packed off suddenly.

4.7.2.2. Hole U1595B

The ship returned to Site U1595, 50 m from Hole U1595A, at 0415 h on 2 February 2023. Hole U1595B was spudded at 1010 h with 3.7 m of recovery. The seafloor depth was calculated at 291.4 mbsl. APC coring continued for Cores 2H–13H. The change was made to the HLAPC system with Cores 14F and 15F to 127.1 mbsf, the final depth for Hole U1595B.

4.7.2.3. Hole U1595C

The vessel was again offset 50 m along the seismic line toward proposed Site CSK-18A. Hole U1595C (36°22.8674′N, 25°24.3062′E) was spudded at 0005 h on 3 February 2023, with Core 1H shot from 297.0 mbrf. The recovery of 3.8 m established the seafloor at 291.3 mbsl. With the drill-down completed to 53.0 mbsf, coring was picked up again with the HLAPC system for Cores 3F–11F to 95.3 mbsf.

After Core 11F, the plan was to drill ahead to 104 mbsf and resume coring. However, high torque led to the drill string stalling, and the decision was made to abandon the hole.

Overall, core recovery for Holes U1595A–U1595C was moderate (46%–73%).

4.7.3. Principal results

The material recovered from Site U1595 is grouped into a single lithostratigraphic unit (Figure **F11**). Lithostratigraphic Unit I (>127 m thick) consists predominantly of volcanic lithologies (such as ash, lapilli-ash, and lapilli), with small amounts of tuffaceous and nonvolcanic sediments. Five subunits (Ia–Ie) are identified. The unit is Holocene in age.

No calcareous nannofossils or planktonic foraminifera were found at Site U1595; very rare benthic foraminifera and ostracods were insufficient to permit paleoenvironmental analyses.

There is a general trend of increasing bulk density and MS with increasing depth at the site (Figure **F11**). Porosity ranges 21–77 vol%, and bulk density ranges 1.3–2.3 g/cm^3. Bulk density does not obviously increase with depth. Grain density ranges 1.6–2.7 g/cm^3; one-fifth of discrete samples have grain densities <2.0 g/cm^3. Compared to typical sediments in which thermal conductivity is close to 1 W/(m·K) at these depths below seafloor, thermal conductivity is low in the volcaniclastic sediments. Because of the instability of the formations encountered, downhole logging was not conducted.

To establish the CCSF-A depth scale, Holes U1595A–U1595C were analyzed for physical properties using the WRMSL for MS and GRA density and the NGRL for NGR intensity, as well as section-half photos once the cores were split into working and archive halves. Correlation was very challenging at this site, and only the MS data allow several reliable correlations, whereas NGR and GRA density measurements are strongly overprinted by the irregular distribution of core material in cores with low recovery and a high content of water.

Only five core sections from two cores recovered at Site U1595 were suitable for paleomagnetic analysis using the superconducting rock magnetometer (SRM). The interval analyzed was assigned to the Brunhes Chron, consistent with the age of Santorini caldera.

Of six volcanic units sampled, two were classified as andesites or trachyandesites and four as dacites or trachydacites of Santorini affinity. IW salinity is 40–41 throughout the hole (Figure **F11**), total alkalinity is 2.5–9.7 mM, and pH is 6.9–7.8. Bromide, Cl^-, Na^+, Mg^{2+}, and SO_4^{2-} increase with depth. Methane, ethane, and propane concentrations were below the detection limit throughout Hole U1595A.

In total, 97 subsamples were collected for microbiological analysis from 14 whole-round core samples.

Lithostratigraphic Subunit Ia corresponds approximately to Seismic Unit S1, which consists of muds and ashes. Lithostratigraphic Subunit Ib corresponds approximately to Seismic Unit S2 and is mostly volcanic in nature. The volcanic material in Subunit Ib appears to be of Kameni origin, as proposed by Johnston et al. (2015), but confirmation must await detailed geochemical characterization. Lithostratigraphic Subunits 1c and 1d correspond approximately to Seismic Unit S3. This shows that Seismic Unit S3 is composed of lithic-pumice sands and gravels rather than intracaldera tuff from the LBA eruption.

4.8. Site U1596

4.8.1. Background and scientific objectives

Site U1596 (alternate proposed Site CSK-06B) is located in the northern basin of Santorini caldera at 382 mbsl. Site U1597 addresses the same drilling objectives and lies southeast of Site U1596. Two additional sites (U1594 and U1595) lie in the southern caldera basin.

The four intracaldera sites were planned to sample Seismic Units S1–S3; test the published correlations between the two caldera basins; penetrate below Unit S3 into Unit S4; and address Scientific Objectives 1, 4, 5, and 7 of the *Expedition 398 Scientific Prospectus* (Druitt et al., 2022).

By drilling both caldera basins and exploiting our dense seismic reflection coverage, we would gain access to the 3D architecture of the entire caldera fill. We also targeted the question of why the northern basin is 100 m deeper than the southern one, with a thicker Unit S1 but a thinner Unit S3. Finally, we tested whether Unit S3 consisted of flood debris from the caldera-flooding event (Nomikou et al., 2016a) or was LBA intracaldera tuff (Johnston et al., 2015). The intracaldera sites were used for microbiological work regarding Objective 7.

4.8.2. Operations

4.8.2.1. Hole U1596A

Hole U1596A (36°26.5378′N, 25°22.5130′E) was spudded on 24 January 2023 at 0650 h. The recovery of 3.9 m gave a calculated seafloor depth of 382.0 mbsl. Using the APC system, coring continued through Core 5H at 41.9 mbsf, the final depth for Hole U1596A. Excessive torque was encountered before shooting Core 6H. The decision was made to pull out and offset to the primary site, proposed Site CSK-05C.

4.8.2.2. Hole U1596B

On 3 February 2023 at 1615 h, the ship revisited Site U1596 at a location 50 m northwest of Hole U1596A. Hole U1596B (36°26.5568′N, 25°22.4875′E) was spudded at 1915 h. A recovery of 4.2 m gave a calculated mudline as 381.9 mbsl. APC coring continued through Core 5H at 42.2 mbsf, the final depth for the hole. Core recovery for the two holes (U1596A and U1596B) was 87%–91%.

4.8.3. Principal results

Cores from Site U1596 recovered a coherent stratigraphy from 0 to 41 mbsf. This site consists of two holes (U1596A and U1596B). The sequence is classified as a single lithostratigraphic unit (Figure **F12**). Unit I (>41 m thick) consists of a massive, fine-grained, dark gray volcanic ash in the uppermost ~10 m, transitioning into a slightly lighter colored, brownish gray ash with lapilli. This is followed downhole by a lapilli-ash and lapilli interval that continues for the remainder of the hole. Three intervals of tuffaceous mud and one interval of mud are observed within the upper section. Two subunits are recognized (Ia and Ib) that contain layers with bedding dips of 1°–4° (average = 2.4°). The unit is Holocene in age.

No calcareous nannofossils or planktonic foraminifera were found at Site U1596; the very rare benthic foraminifera and ostracods abundances were insufficient to permit paleoenvironmental analyses.

There is a general trend of increasing *P*-wave velocity and MS and decreasing NGR with increasing depth at the site (Figure **F12**). Porosity ranges 52–74 vol%, and bulk density ranges 1.2–1.6 g/cm^3. Bulk density does not obviously increase with depth. Grain density ranges 1.6–2.5 g/cm^3; more than 70% of discrete samples have grain densities <2.0 g/cm^3. Compared to typical sediments in which thermal conductivity is close to 1 W/(m·K) at these depths below seafloor, the mean value of 0.83 W/(m·K) is low in the volcaniclastic sediments.

Similar to Site U1595, correlation was very challenging at this site, and only the MS data allowed several reliable correlations, whereas NGR and GRA density measurements are strongly overprinted by the irregular distribution of core material in cores. A preliminary CCSF-A depth scale was constructed but must await further refinement during onshore analysis. Because of the insta-

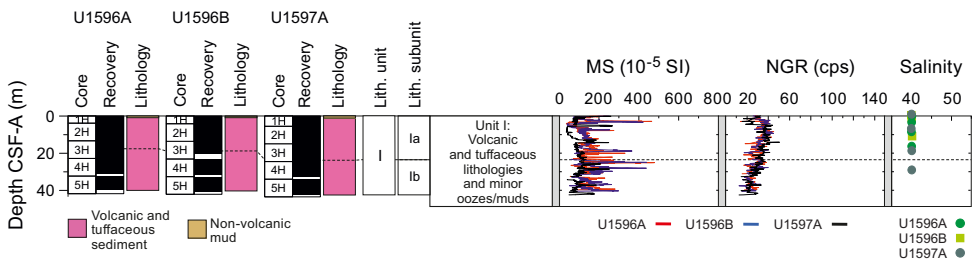

Figure F12. Combined simplified summary for Holes U1596A, U1596B, and U1597A from the northern basin in Santorini caldera. MS and NGR are whole-round measurements. Salinity measurements are from IW. cps = counts per second.

bility of formations encountered, downhole logging was not conducted. None of the cores recovered at this site were suitable for paleomagnetic analysis.

IW salinity is 40 throughout both holes (Figure **F12**). Total alkalinity (2.5–4.3 mM) increases with depth to 8.4 mbsf before decreasing to the base of the hole. Values for pH show variation within the sampled depths, ranging 7.6–7.9, with the highest value recorded in the mudline sample. Only small variations in Br^-, Cl^-, B, Na^+, and Ca^+ were detected. Lithium, Sr, Fe, Mn, Ba, and Si all increase with depth, reaching maxima at either 2.9 mbsf (Sr, Mn, and Ba) or 8.4 mbsf (Li, Fe, and Si). Methane, ethane, and propane concentrations were below the detection limit. Concentrations of heavier hydrocarbons (*iso*-butane, *n*-butane, and *n*-pentane, and so on) were also below the detection limit throughout the hole.

In total, 14 subsamples were collected for microbiological analysis from two whole-round core samples, and 11 samples were collected from the mudline of Core 398-U1596B-1H for microbial community composition analysis.

The upper part of Site U1596 was drilled to assess any potential technical problems in drilling deeper. It was partly a reconnaissance exercise. It enabled us to discover that Lithostratigraphic Subunits Ia and Ib, which correspond approximately to Seismic Units S1 and S2, were the same in the northern caldera basin as in the southern one. The two upper seismic units in the northern and southern basins therefore correlate.

4.9. Site U1597

4.9.1. Background and scientific objectives

Site U1597 (proposed Site CSK-05C) is located in the northern basin of Santorini caldera at 382 mbsl. Site U1596 addresses the same drilling objectives and lies northwest of Site U1597. Two additional sites (U1594 and U1595) lie in the southern caldera basin.

The four intracaldera sites were planned to sample Seismic Units S1–S3; test the published correlations between the two caldera basins; penetrate below Unit S3 into Unit S4; and address Scientific Objectives 1, 4, 5, and 7 of the *Expedition 398 Scientific Prospectus* (Druitt et al., 2022). By drilling both caldera basins and exploiting our dense seismic reflection coverage, we would gain access to the 3D architecture of the entire caldera fill. We also targeted the question of why the northern basin is 100 m deeper than the southern one, with a thicker Unit S1 but a thinner Unit S3. Finally, we tested whether Unit S3 consisted of flood debris from the caldera-flooding event (Nomikou et al., 2016a) or was LBA intracaldera tuff (Johnston et al., 2015).

4.9.2. Operations

The revised plan was to be very conservative, while learning the nature of the formation to aid in planning the future caldera work. The immediate foreseen work was limited to 1–2 holes, 40–50 mbsf each.

4.9.2.1. Hole U1597A

Hole U1597A (36°26.2494′N, 05°22.7326′E) was spudded on 24 January 2023 at 1240 h. With a recovery of 5.6 m, the depth of the seafloor was calculated as 382.3 mbsl. APC coring continued through Core 5H, a final depth of 43.6 mbsf, and core recovery of 94%. Again, excessive torque started building. The drill string was tripped up with the top drive, and the bit cleared the seafloor at 1547 h.

4.9.3. Principal results

A single hole (U1597A) was drilled at this site to 42 mbsf. The recovered material is unlithified sediment, dominated by volcanic material. A single lithostratigraphic unit was identified (Figure **F12**). Unit I (>43 m thick) consists of a fine- to coarse-grained dark gray ash interval in the uppermost ~10 m, partly accompanied by lapilli-sized clasts, and a slightly lighter colored ash and lapilli-ash interval that continues for the remainder of the hole. Subunits Ia and Ib are defined by changes in grain size, color, and componentry. The unit is Holocene in age.

No sedimentary structures were identified at Site U1597. Although there are some bedding planes, core-induced disturbance prevented measurements.

No calcareous nannofossils or benthic foraminifera were found at this site. Very rare planktonic foraminifera and ostracods occur but are of insufficient quantity to permit paleoenvironmental analyses.

Physical properties measurements show a layer at 1–5 mbsf with distinctly higher *P*-wave velocity and lower bulk density than volcaniclastic deposits at shallower and greater depths. Overall, there is a general trend of decreasing NGR with increasing depth (Figure **F12**). Porosity ranges 58–70 vol%, and bulk density ranges 1.3–1.6 g/cm^3. Bulk density does not obviously increase with depth. Grain density ranges 1.7–2.5 g/cm^3; more than 20% of discrete samples have grain densities <2.0 g/cm^3. Compared to typical sediments in which thermal conductivity is close to 1 W/(m·K) at these depths below seafloor, the mean value of 0.81 W/(m·K) is low in volcaniclastic sediments at Site U1597.

Because there is only a single hole, no stratigraphic correlation was possible at Site U1596, and due to the instability of the formations encountered, downhole logging was not conducted. None of the cores recovered were suitable for paleomagnetic analysis.

All three volcaniclastic units sampled were classified as dacites or trachydacites. IW salinity is 40 throughout the hole, and no significant variations were recorded (Figure **F12**). Total alkalinity (2.4–6.6 mM) increases with depth to 18.1 mbsf before decreasing to the base of the hole. Values for pH show variation within the sampled depths, ranging 7.6–7.7, with values increasing with depth. Bromide, Cl^-, Na^+, and Mg^{2+} all increase with depth, whereas B decreases. Potassium and Ca^{2+} are inversely correlated, with K^+ decreasing to a minimum of 5.7 mM at 18.1 mbsf and Ca^{2+} increasing to a maximum of 15 mM at the same depth. IW values of Li are inversely correlated with Sr, Mn, and Ba, whereas Fe and Si both increase with depth to their maxima at 18.1 mbsf before slightly decreasing downhole. Methane, ethane, and propane concentrations were below the detection limit throughout the hole. Concentrations of heavier hydrocarbons (*iso*-butane, *n*-butane, and *n*-pentane) were also below the detection limit.

The upper part of Site U1597 was drilled to assess any potential technical problems in drilling deeper. It enabled us to discover that Lithostratigraphic Subunits Ia and Ib, which correspond approximately to Seismic Units S1 and S2, were the same in the northern caldera basin as in the southern one. The upper two seismic units in the northern and southern basins therefore correlate.

4.10. Site U1598

4.10.1. Background and scientific objectives

Site U1598 (alternate proposed Site 14A) is located ~8 km northwest of Christiana Island and ~20 km southwest of Santorini at 521 mbsl. The drill site targeted the volcano-sedimentary fill of the Christiana Basin in two holes.

Christiana Basin formed by subsidence along an ENE–WSW fault system before the changing tectonic regime activated the current northeast–southwest rift system in which the CSK volcanic field lies (Tsampouraki-Kraounaki and Sakellariou, 2018; Preine et al., 2022b, 2022c). Christiana Basin is deeper than the Anhydros and Anafi Basins; its volcano-sedimentary fill potentially records the earlier volcanic history of the CSK volcanic field (including the products of Christiana and early Santorini), as well as younger Santorini and possibly Milos Volcano to the west along the Aegean volcanic arc. The now-extinct Christiana Volcano produced lavas and tuffs of unknown ages (Aarbourg and Frechen, 1999). An ignimbrite found on Christiani Island (one of the two small islands of Christiana Volcano), Santorini, and the nonvolcanic island of Anaphi, called the Christiani Ignimbrite, was identified (Keller et al., 2010).

Site U1598 was chosen to complement the previously drilled Site U1591. The aim was to retarget a thick pumice layer found at Site U1591 (Lithostratigraphic Subunit Ic), for which we had insuffi-

cient recovery for our scientific aims. The site addresses Scientific Objectives 1–4 and 6 of the *Expedition 398 Scientific Prospectus* (Druitt et al., 2022).

4.10.2. Operations

4.10.2.1. Hole U1598A

Hole U1598A (36°18.2937′N, 25°7.7155′E) was spudded at 2350 h on 24 January 2023 from 527.0 mbrf with the APC coring system. Core 1H recovered 3.7 m, establishing the seafloor at 521.5 mbsl. Coring continued on 25 January through Core 8H from 60.7 mbsf. The switch was made to the HLAPC system for Cores 9F–10F to 79.6 mbsf. High torque was observed when drilling, and the decision was made to pull out of the hole.

4.10.2.2. Hole U1598B

The vessel was offset 50 m southwest of Hole U1598A. Hole U1598B (36°18.2747′N, 25°7.6929′E) was spudded at 0805 h, using the offset water depth of 532.8 mbrf. A drill-ahead section was completed to 75.6 mbsf. At 1015 h on 25 January 2023, coring commenced with the HLAPC system for Cores 2H–6F at 98.8 mbsf, the final depth for Hole U1598B. Excessive torque was again observed, and the decision was made to abandon the hole. Core recoveries for Holes U1598A and U1598B were 69% and 34%, respectively.

4.10.3. Principal results

The recovered material at Site U1598 is unlithified in Holes U1598A and U1598B and is characterized by predominantly volcanic lithologies comprising a single lithostratigraphic unit, as at Site U1591 (Figure **F13**). Unit I (>96 m thick) consists primarily of intercalated volcanic (lapilli-ash, ash, and lapilli) and tuffaceous lithologies, punctuated by intervals of calcareous mud and ooze. As at Site U1591, Unit I is divided into three subunits (Ia–Ic). Subunit Ic is the same as at Site U1591 and composed mainly of pumice lapilli and ash. Unit I is Holocene to Middle Pleistocene in age.

Bedding planes throughout the sequence dip at 1°–12° (mean = 5°); however, steeper inclinations (22°–33°) developed in slumps at the bottom of Lithostratigraphic Subunit Ia.

Two nannofossil biostratigraphic datums were recognized at Site U1598, representing a continuous Pleistocene sedimentary sequence. The presence of *Emiliania huxleyi* indicates a Middle Pleistocene to Holocene age (≤0.265 Ma) within Zones MNN21a and 21b; the last appearance datum of *Pseudoemiliania lacunosa* defines the NN19/20 boundary. Foraminiferal faunas biostratigraphically divide the Pleistocene into two Mediterranean planktonic foraminiferal biostratigraphic zones, MPIe2b and MPIe2a.

The oceanicity data for Site U1598 generally indicate fluctuations from extraneritic to oceanic conditions (100 to >1000 mbsl) through the study section; benthic foraminifer distributions indicate an uppermost to upper bathyal (300–700 m) paleowater depths in the <42 mbsf range.

Because of the instability of formations encountered downhole, logging was not conducted.

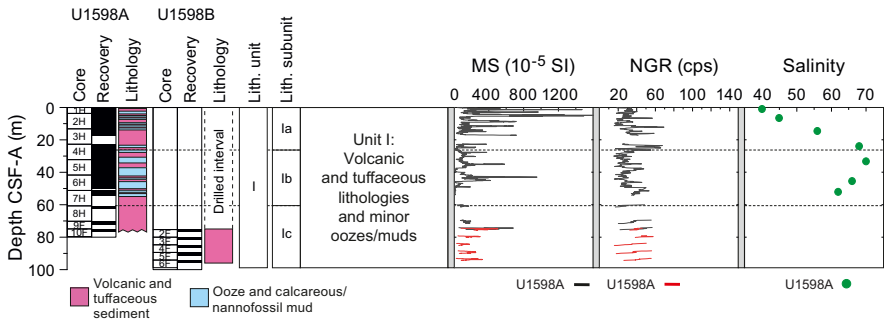

Figure F13. Simplified summary for Site U1598 from the western Christiana Basin. MS and NGR are whole-round measurements. Salinity measurements are from IW. cps = counts per second.

Physical properties measurements reveal that MS is highly variable within the volcaniclastic deposits at this site and could exceed 2500 × 10^{-5} SI in some volcaniclastic layers (Figure **F13**). There is no clear systematic increase in *P*-wave velocity with increasing depth in the whole-round measurements. Discrete sample *P*-wave velocities range 1.50–2.45 km/s (mean = 1.61 km/s). Sample porosities range 50–74 vol%, bulk densities range 1.05–1.79 g/cm^3, and grain densities range 1.10–2.79 g/cm^3; most of the low grain densities are found in lapilli layers deeper than 60 mbsf. The mean thermal conductivity is 1.06 W/(m·K), and there is no apparent increase with depth.

The one volcaniclastic unit sampled was classified as a dacite. IW salinity ranges 40–70, with the maximum occurring at 34 mbsf before salinity decreases to the base of the hole (Figure **F13**). Total alkalinity is 2.5–6.8 mM, and values for pH range 7.3–7.8, with the highest value at the mudline. Similar to other sites, Br^-, Cl^-, B, Na^+, K^+, Mg^{2+}, Ca^{2+}, and SO_4^{2-} trends resemble those of salinity, but not Li, Sr, Mn, Ba, or Si. Sediment carbonate contents range 21–42 wt%; three organic-rich sediment layers were identified as sapropelitic and one as a sapropel. Headspace methane, ethane, and propane concentrations were below the detection limit throughout Hole U1598A. A single volcaniclastic unit analyzed using ICP-AES was classified as dacite.

No paleomagnetic reversals are present in the data set; the sampled interval was therefore assigned to the Brunhes Chron (C1n, <0.773 Ma), which is compatible with available biostratigraphic age constraints.

Site U1598, corresponding to the shallow levels of Site U1591, resembles the uppermost ~100 m of the latter site and provides no particular extra conclusions. However, it succeeded in its objective to provide better sampling of Lithostratigraphic Subunit Ic. This pumice layer, tentatively correlated with the Christiani Ignimbrite onland, is now well sampled in the Christiana Basin.

4.11. Site U1599

4.11.1. Background and scientific objectives

Site U1599 is located ~6 km north of Anafi Island within the upper reaches of the Anafi Basin at 592 mbsl. Permission to drill there was granted by the EPSP during the expedition.

Site U1592 is situated on the axis of the Anafi Basin and penetrated a thick basin fill including mass transported material, and Site U1599 is located on the southeast margin of the basin. It was chosen to offer a relatively condensed sequence of tephra without quantities of mass wasting debris. As such, it provides a complete stratigraphy of volcanic tephra from Santorini and Kolumbo. The same six seismic units (U1–U6, from the bottom up; Preine et al., 2022a, 2022b) present at Site U1592 are present at Site U1599.

Drilling at Site U1599 enabled us to reconstruct a near-complete volcanic stratigraphy consistent with both onshore and offshore constraints and pinned by chronological markers from biostratigraphy, magnetostratigraphy, and sapropel records. Benthic foraminifera from fine-grained sediments provided estimates of paleowater depths and, via integration with seismic profiles and chronologic data, of time-integrated basin subsidence rates. Drilling in the Anafi Basin addresses Scientific Objectives 1–4 and 6 of the *Expedition 398 Scientific Prospectus* (Druitt et al., 2022). It is complemented by Site U1589 in the Anhydros Basin because each basin tapped a different sediment distributary branch of the CSK volcanic system.

Although not anticipated in the expedition proposal, biological samples were collected from Hole U1599C. Drilling addresses Scientific Objectives 1–4, 6, and 7 of the *Expedition 398 Scientific Prospectus* (Druitt et al., 2022).

4.11.2. Operations

4.11.2.1. Hole U1599A

The crew made up the APC/XCB BHA with a bit. The BHA was run in to 585.7 mbrf. On 26 January 2023, at 1315 h, the APC system was fired for Core 1H from 599.0 mbrf. Once retrieved, it was discovered the core barrel had parted at the midconnection. The switch was made to the HLAPC system for Core 2F from 9.7 mbsf. The 97% recovery showed the material was suitable for piston coring. Coring was switched to the APC system for Cores 3H–9H at 71.4 mbsf. The forma-

tion stiffened up quickly, forcing the change to HLAPC coring at Core 10F and all the way to Core 44F to 245.4 mbsf, the final depth for Hole U1599A.

4.11.2.2. Hole U1599B

The vessel was offset 50 m northeast of Hole U1599A. The seafloor was tagged at 604.0 mbsf. Hole U1599B (36°26.9764′N, 25°46.8237′E) was spudded at 2330 h on 27 January 2023 with the XCB coring system, and Core 1X was recovered to 9.7 mbsf. Coring was switched to the APC system for Cores 2H–11H at 95.2 mbsf. Coring was again switched, this time to the HLAPC system, for Cores 12F–40F from 104.7 to 241.0 mbsf, the final depth for Hole U1599B.

4.11.2.3. Hole U1599C

Hole U1599C (36°26.9389′N, 25°46.7762′E) was spudded on 30 January 2023 at 1925 h. A seafloor depth of 604.0 mbrf was used by offset. A drill-ahead without recovery progressed to 223.0 mbsf at 0445 h. RCB coring commenced on 30 January with Core 2R and continued on 1 February through Core 25R to 455.5 mbsf. The drill string was tripped from 455.5 to 404.9 mbsf. The top drive was racked back, and the pipe trip up continued to 55.6 mbsf. Next, the rig crew pulled the upper guide horn in preparation for launching a free fall funnel (FFF). The FFF was assembled and welded in the moonpool and then launched at 2005 h. The vessel was switched to bridge control at 0130 h on 2 January. All thrusters were up and secure with the start of the sea passage to Site U1595 at 0142 h, ending Site U1599 for the time being. At 1840 h on 6 February, the ship started the dynamic positioning move back over Hole U1599C, following 39.75 h of waiting on weather. At 1300 h on 7 February, RCB coring commenced with Core 26R from 455.5 mbsf and continued on 9 February through Core 50R at 697.8 mbsf, the final depth for Hole U1599C.

4.11.3. Principal results

The recovered material in Holes U1599A and U1599B is divided into four lithostratigraphic units (Figure **F14**).

- Unit I (up to 213 m thick) is nonlithified sediment with mixed volcanic (ash, lapilli, and lapilli-ash), tuffaceous, and nonvolcanic material (oozes). Four subunits (Ia–Id) are recognized. The unit is Holocene to Middle Pleistocene in age.
- Unit II (up to 28 m thick) is composed mainly of oozes interspersed with minor volcanic and tuffaceous sediments. The unit is Middle Pleistocene to Early Pleistocene in age.
- Unit III (305 m thick) consists of dolomitic marl with organic-rich intervals, with three subnits (IIIa–IIIc). The unit is Early Pleistocene to Pliocene in age.
- Unit IV (>145 m thick) consists of micrite and calcareous sandstones. It begins with calcareous mudstone with interbedded sandstone layers and a few tuffs and then transitions downhole into a micrite-dominated succession with interbedded calcareous sandstone. Some sandstone intervals contain ash. This unit is Early to Middle Miocene in age.

Bedding dips at the site are mostly <30°, except in Unit IV and Subunit IIIa, where they reach up to 70°. Sand dikes, faults, and sediment-filled veins are also common in Unit IV and Subunit IIIa.

Calcareous nannofossils and planktonic foraminifera provide good resolution in the Holocene through Upper Pliocene sediments at Site U1599. Ages provided by benthic foraminifera are also consistent with those of planktonic foraminifera and calcareous nannofossils. Ten nannofossil biostratigraphic datum planes and two calcareous nannofossil zones were recognized, representing a discontinuous Pleistocene–Miocene sedimentary sequence. Unit IV was assigned to the Non-Distinctive Zone (Miocene?) or older due to the absence of normal marine planktonic foraminiferal assemblages and, where present, faunas are dwarfed and exhibit very poor preservation. The microfossil component within this section is primarily composed of rare, moderately preserved Ostracoda. There is a significant quantity of carbonaceous plant matter and charcoal present within this interval.

Benthic foraminiferal distributions are variable, indicating paleowater depths from uppermost bathyal (200–400 m) to lower bathyal (>1000 m). Oceanicity (percent planktonic foraminifera) values are generally in agreement with benthic foraminiferal paleowater depth indicators in intervals where reworking is low or absent.

To establish the CCSF-A depth scale, Holes U1599A–U1599C were analyzed for physical properties using the WRMSL for MS and GRA density, and images were taken once the cores were split. The MS data are the most reliable physical parameter for correlations.

Physical properties whole-round measurements show that MS is highly variable within the volcaniclastic deposits of Unit I and could be very high, exceeding 2500 × 10^{-5} SI. High values of MS correspond to volcaniclastic layers. MS in Unit III is much lower than that of Units I and II and lower than in Unit IV. NGR is more variable in Unit III than in volcaniclastic-dominated Units I and II and the micrites of Unit IV. There is no systematic increase in whole-round GRA bulk density and *P*-wave velocity with increasing depth in Unit I. Discrete measurement porosities range 30–78 vol%, density ranges 1.25–2.18 g/cm^3, and grain density ranges 1.74–2.81 g/cm^3. Most of the low grain densities are found in lapilli layers between 120 and 230 mbsf. Overall, there is a general trend of decreasing porosity and increasing bulk density with increasing depth. Because of hole instability issues, no wireline logging was possible at this site.

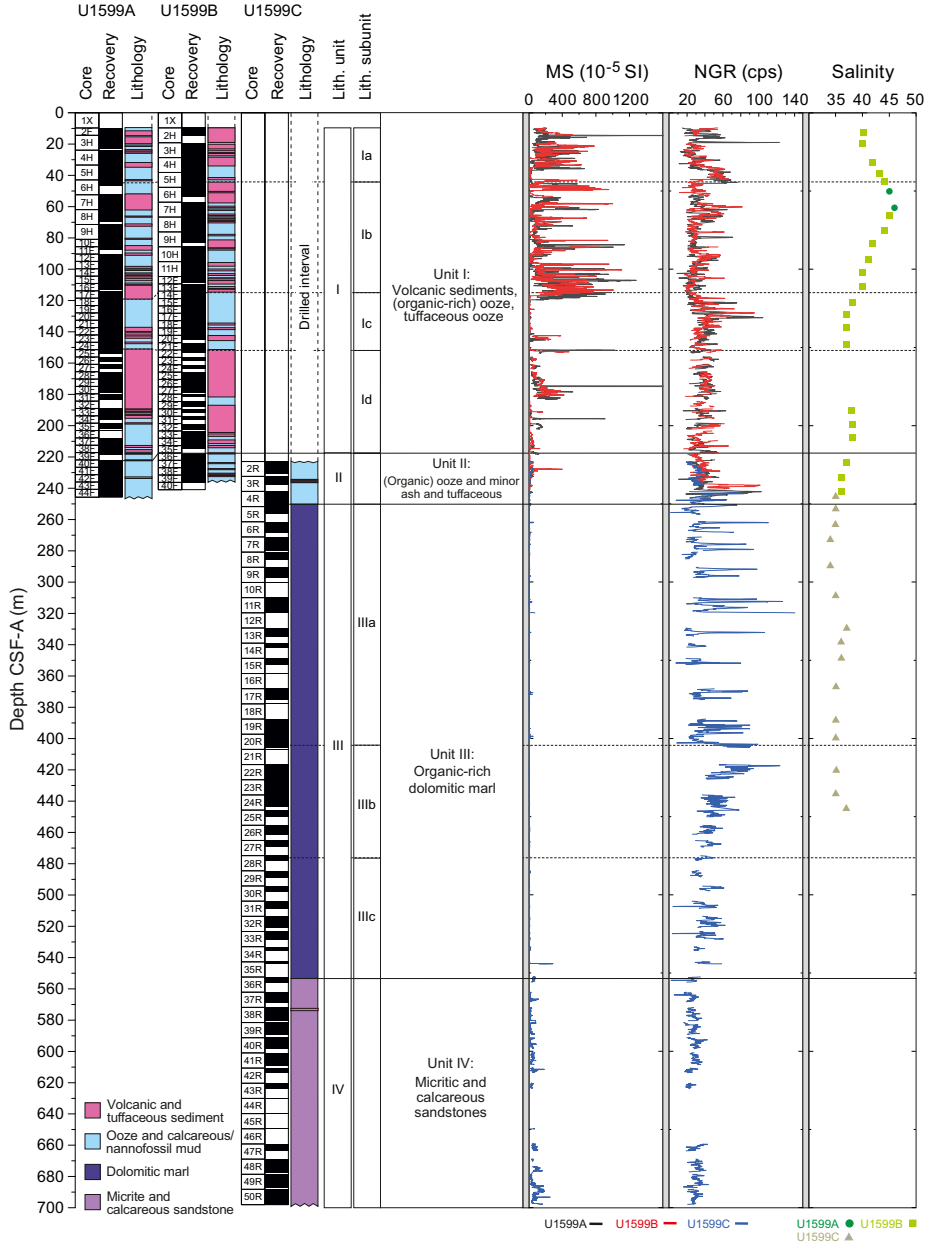

Figure F14. Simplified summary for Site U1599 drilled close to Anafi Island. MS and NGR are whole-round measurements. Salinity measurements are from IW. cps = counts per second.

Of nine volcanic units analyzed using ICP-AES for major and trace elements, one was classified as a basalt and eight as dacites. IW salinity ranges 34–46 throughout Holes U1599A–U1599C, with the highest value at 61.6 mbsf. Alkalinity values range 1.3–7.9 mM, and pH ranges 7.5–8.2. Ca, Mg, K, Li, and SO_4 follow similar trends and have similar local maxima as salinity, but Br, Cl, B, Na, Sr, Mn, Ba, and Si do not. A total of 19 organic-rich sediment units were identified as sapropelitic from TOC measurements, and 11 were identified as sapropels. Headspace methane concentrations in Hole U1599C increased between 266 and 311 mbsf, reaching a maximum of 816.3 ppmv at 275.7 mbsf. Methane, ethane, and propane concentrations were below the detection limit in all other samples.

Paleomagnetic analysis at Site U1599 focused on measurement and demagnetization of archive-half sections to determine magnetostratigraphic age controls. Three reversal boundaries could be tied with confidence to the GPTS as follows: (1) the Brunhes–Matuyama transition (0.773 Ma) occurs at 228.3 mbsf (CCSF scale), (2) the top of the Jaramillo Subchron (C1r.1n; 1.008 Ma) is observed at 250.0 mbsf, and (3) the base of the Jaramillo Subchron (1.076 Ma) occurs at 260.5 mbsf. No magnetostratigraphic correlations were possible deeper than 260.5 mbsf (CCSF scale) due to a combination of degradation of the record by diagenetic alteration and lack of available independent biostratigraphic markers to aid correlation.

A total of 35 whole-round core samples were collected for microbiological study from Hole U1599C.

In summary, Site U1599 proved to be an excellent choice for accessing a condensed (sedimentation rate ~20 cm/ky prior to 0.5 Ma; ~50 cm/ky since 0.5 Ma) succession containing tephra layers from Santorini, Kolumbo, and possibly Christiana. Totals of 21 biostratigraphic datums and 3 magnetostratigraphic datums allowed construction of a detailed age-depth model that will ultimately allow fine-scale dating of the many tephra layers observed. The site provides an excellent complement to the adjacent basin sites (U1589 and U1592).

4.12. Site U1600

4.12.1. Background and scientific objectives

Site U1600 is located 10 km south of Anhydros Island within a small graben atop the Anhydros Horst at 326 mbsl. The Anhydros Horst separates the Anhydros Basin to the west from the Anafi Basin to the east (Nomikou et al., 2018; Hooft et al., 2017). Permission to drill there was requested as proposed Site CSK-24A and granted by the EPSP during the expedition. Three holes were drilled (U1600A–U1600C).

The site was chosen because of its situation on the Anhydros Horst immediately east of the Kolumbo chain of volcanoes and for the well-stratified nature of the graben fill on seismic profiles. It seemed a likely site at which to drill a condensed sequence of muds and tephra for chronology, sheltered from the large-scale mass wasting of the main basins.

Drilling at Site U1600 would enable us to reconstruct a near-complete volcanic stratigraphy consistent with both onshore and offshore constraints and pinned by chronological markers from biostratigraphy and magnetostratigraphy. Benthic foraminifera from fine-grained sediments could provide estimates of ancient water depths and, through integration with seismic profiles and chronologic data, of time-integrated basin subsidence rates. Although not anticipated in the expedition proposal, biological samples were collected from Hole U1600C. Drilling on the Anhydros Horst addresses Scientific Objectives 1–4, 6, and 7 of the *Expedition 398 Scientific Prospectus* (Druitt et al., 2022).

4.12.2. Operations

4.12.2.1. Hole U1600A

Hole U1600A (proposed Site CSK-24A; 36°32.6277′N, 25°39.0553′E) was spudded with Core 1H on 29 January 2023 at 0710 h. The recovery of 4.0 m gave a calculated seafloor of 326.2 mbsl. APC coring continued with Cores 2H–4H. The switch was made to the HLAPC system with Cores 5F–10F at 60.7 mbsf. Coring continued with the XCB system for Cores 11X–13X at 84.4 mbsf, the final

depth for Hole U1600A. The recovery for the XCB system was extremely poor, and the decision was made to repeat the piston section with Hole U1600B.

4.12.2.2. Hole U1600B

The ship was positioned 50 m southwest of Hole U1599A. Hole U1600B (36°32.6092′N, 25°39.0311′E) was spudded with Core 1H on 29 January 2023 at 2005 h using the APC coring system. Recovery of 6.8 m established the water depth at 326.3 mbsl. Coring was switched to the HLAPC system for Cores 2F–19F at 91.4 mbsf, the final depth for Hole U1600B.

4.12.2.3. Hole U1600C

The vessel returned to Site U1600 on 4 February 2023. Hole U1600C (36°32.5890′N, 25°39.0067′E) was spudded at 0655 h. A drill-ahead was done to 75.0 mbsf. RCB coring was initiated with Core 2R from 75.0 mbsf through Core 14R at 188.5 mbsf on 5 February, the final depth for Hole U1600C. Holes U1600A–U1600C achieved a total penetration of 188.5 mbsf, with average hole core recoveries between 37% and 69%.

4.12.3. Principal results

The recovered material from Site U1600 is unlithified in Holes U1600A and U1600B, with a gradual transition to more consolidated material toward the bottom of Hole U1600B (Figure **F15**). Hole U1600C consists of more consolidated sediments; however, the change from sediment to sedimentary rock was clearly identified at ~166 mbsf. Lithostratigraphic units are described below.

- Unit I (74 m thick) is dominated by volcanic and tuffaceous lithologies with minor intermittent intervals of nonvolcanic muds and sands. All cores are rich in bioclasts (shells and shell fragments), including the volcanic intervals. Four subunits (Ia–Id) are recognized. This unit is Holocene to Early Pleistocene in age.
- Unit II (92 m thick) is a continuation of the calcareous muds and sands present in Unit I but with two important distinctions: (1) these sediments are nearly devoid of any volcanic and tuffaceous intervals and show only rare ash pods, whereas Unit I has abundant volcanic and tuffaceous intervals; and (2) the sediments are almost entirely organic rich. This unit is Early Pleistocene to Pliocene in age.
- Unit III (>12 m thick), defined after a sharp discontinuity at 172 mbsf, is composed of moderately to completely serpentinized peridotites. Its age is unknown.

Bedding measurements mostly exhibit horizontal to subhorizontal dips ranging 1°–15° (mean = 4°). Major increases in the bedding dip were identified (upward) from Unit II to Subunit Id, with median dips increasing from 4° to 11°. In contrast, from Subunit Id to Subunit Ia, the median dip decreases from 11° to 2°. Mineral veins are abundant in Unit III.

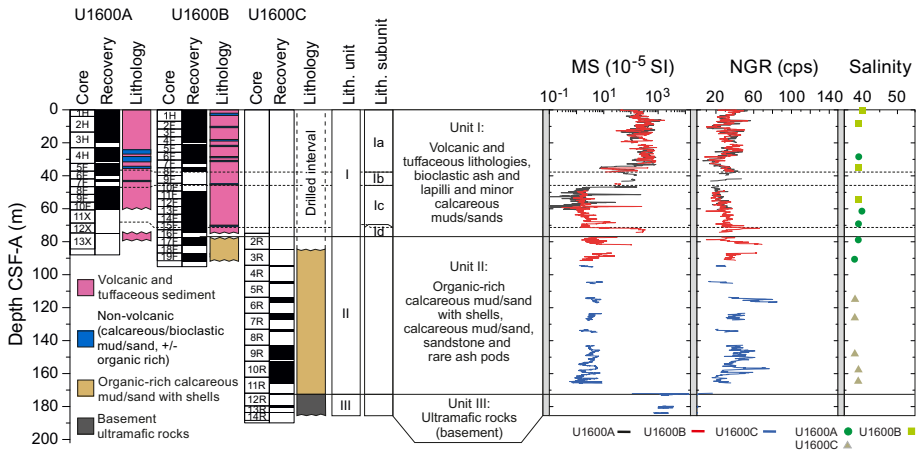

Figure F15. Simplified summary for Site U1600 drilled on the Anhydros Horst structure. MS and NGR are whole-round measurements. Salinity measurements are from IW. cps = counts per second.

Seven nannofossil biostratigraphic datums were recognized at Site U1600, representing a continuous Middle–Late Pleistocene sedimentary sequence (CN Zones MNN21b-21a, MNN20-19, MNN18-16b, and MNN16a). Foraminiferal faunas are sufficiently common to biostratigraphically divide the Pleistocene into the majority of Pleistocene Mediterranean planktonic foraminiferal biostratigraphic zones determined via both primary and secondary marker species: MPle2b, MPle2a, MPle1c, MPle1b-a, MPl6b, MPl6, and MPl5b.

Planktonic foraminifer abundances are highly variable, ranging 0%–94%. Benthic foraminiferal distributions are also variable, indicating paleowater depths from 200 to >1000 m.

To establish the CCSF-A depth scale, we analyzed Holes U1600A and U1600B for physical properties using the WRMSL for MS and GRA density and the NGRL for NGR intensity, as well as photos once the cores were split into working and archive halves. The MS data proved to be the most reliable physical parameter for correlations. Because Hole U1600C has no overlap with Holes U1600A and U1600B, no correlation was possible.

Whole-round physical properties measurements show that MS is high and variable in the volcaniclastic deposits and exceptionally high in the basement (>10,000 × 10^{-5} SI) (Figure **F15**). Two high *P*-wave velocity layers, around 17 and 71 mbsf, correspond to lapilli-ash layers; overall, there is no clear systematic increase of *P*-wave velocity with increasing depth. Discrete measurements of *P*-wave velocity on working-half core sections show similar downhole variations as those measured on whole-round cores. In basement rocks deeper than 166 mbsf, *P*-wave velocity ranges 3.37–5.29 km/s. Above the basement in the uppermost 166 m, porosity ranges 40–83 vol%, bulk density ranges 1.24–2.00 g/cm^3, grain density ranges 1.82–2.77 g/cm^3 (with the lowest values in volcaniclastic subunits), and mean thermal conductivity is 1.16 W/(m·K). The two basement samples from Unit III have thermal conductivities markedly higher at 3.1 and 2.2 W/(m·K). Because of the instability of formations encountered downhole, logging was not conducted.

Of the volcaniclastic units analyzed using ICP-AES, one was classified as a basalt, one as basaltic andesite, two as trachyandesites, and two as dacites or trachydacites. IW salinity values range 38–40, with the highest recorded value of 40 at the mudline and at 61.5 mbsf (Figure **F15**). Alkalinity ranges 2.53–3.3 mM and pH 7.5–7.9. IW concentrations of Br^-, Cl^-, and Na^+ show mutually similar trends and generally decrease with depth. Other elements exhibit more complex variations with depth. Carbonate values in sediment samples are highest in Unit I, peaking at 82 wt% at 54 mbsf, which is characterized by volcanic and tuffaceous material but contains calcareous oozes. Carbonate values decrease and TOC increases in Unit II, which is characterized by organic-rich calcareous mud/sand. Four organic-rich layers were identified as sapropels, and seven were identified as sapropelitic. Methane, ethane, and propane concentrations were below the detection limit in all measured headspace samples.

The uppermost 40 m of the sequence at Site U1600 carried normal polarity remanences acquired during Chron C1n (Brunhes). We assigned the Brunhes/Matuyama boundary (0.773 Ma) to the interval 40.0–55.3 mbsf where no data are available, and this interval must also span Chrons C1r.1r and C1r.1n. Several reversals were recognized by reference to biostratigraphic markers below this level. Very limited data are available below 165.8 mbsf.

Microbiological analysis was conducted on three whole-round samples from Site U1600. The whole-round samples were split into 21 subsamples. Most of the microbiological analyses will be conducted on shore, but first culturing experiments indicate the presence of an iron-oxidizing bacterium, most probably *Mariprofundus ferroxydans*.

In summary, Site U1600 proved to be an excellent choice with which to access a condensed (sedimentation rate ~5 cm/ky) succession containing tephra layers from Santorini, Kolumbo, and possibly Christiana. A total of 20 biostratigraphic datums, combined with magnetostratigraphic controls, allowed construction of a detailed age-depth model that will ultimately allow fine-scale dating of the many tephra layers observed. This includes some pumice layers older than a million years that offer access to the ancestral roots of the CSK volcanoes. The site provides an excellent complement to the adjacent basin sequences (Sites U1589, U1592, and U1599).

5. Preliminary scientific assessment

5.1. Drilling summary

In total, Expedition 398 drilled 7.34 km, cored an interval of 5.72 km, and recovered 3.35 km of sediments and basement rock.

Despite a number of technical problems, the expedition went a long way toward achieving its objectives. One obstacle was the unstable nature of some of the drilled formations that caused holes to be prematurely abandoned. The most problematic lithologies were thick pumice layers and thick ash layers. The pumice layers had low strength and appeared to avalanche into the hole, causing the drill string to jam. However, it was judged that the worst offender was the fine-grained ash layers, some of them many meters thick. These ashes appeared to liquefy when drilled, allowing them in some cases to close the hole and jam the drill bit. The combination of these two lithologies restricted the depths to which we could drill at several sites. At Site U1589, the hole collapsed during wireline logging, and at Sites U1590, U1593, and U1595, collapse occurred during drilling. At three sites in the caldera (U1594, U1596, and U1597), we were unable to penetrate deeper than 40–50 m without problems. As a result of hole instability, we were unable to wireline log at any site except Site U1589, where only one rapid pass was made, and attempts to carry out thermal measurements at all sites except Sites U1589 and U1590 were not possible. At several sites, we were forced to pull out prematurely when the drill bit began to stick.

Owing to a combination of these issues, we found ourselves with extra time. We therefore requested permission from the EPSP and Greek Foreign Ministry to drill at two new sites (U1599 and U1600), which was granted during the expedition. These two sites were chosen to be situated within condensed sequences on the edges of the basins, where complete successions could be expected and a greater abundance of mud would stabilize the holes.

The final total of 12 drilling sites provided an excellent combination of successions with which to address the expedition objectives (Druitt et al., 2022). Basin Sites U1589 and U1591–U1593 provided the opportunity to groundtruth the basin seismic stratigraphy and to link volcanism and tectonics and possibly also sea level. These sites suffered, however, from multiple hiatuses and abundant mass wasting. Therefore, Sites U1599 and U1600 at the basin edges were drilled to provide a most complete and continuous sequence and complement the basin sites to achieve a most complete time series for sediments and eruptive events. Sites U1590 and U1593 both drilled through proximal sequences of Kolumbo pumice layers, allowing us to characterize them, and because they straddle the Kolumbo Fault, these sites enabled us to determine the displacement across the fault using biostratigraphic datums. Finally, we drilled at all four caldera sites (U1594–U1597), giving us a thorough coverage of the intracaldera fill. Unfortunately, the inability to wireline log all but one site (U1589) limited our ability to do real-time core-seismic integration, which must now await detailed analysis of volcanic stratigraphy and chronology.

5.2. Meeting the objectives of the expedition

5.2.1. Objective 1

Objective 1 (arc volcanism in an active rift environment) was to reconstruct the volcanic history of the CSK volcanic field and its development in space and time. The recovered cores provided us with the volcanic material we need to achieve this goal.

- We successfully drilled through the different units of the Anhydros (Site U1589) and Anafi (Site U1592) Basins as seen on seismic profiles, including many units from Santorini and Kolumbo Volcanoes.
- We drilled on the flanks of Kolumbo Volcano (Sites U1590 and U1593) and traversed several thick pumice layers, although the lack of detailed wireline logging and detailed core-seismic integration have so far limited our ability to correlate the layers in detail to the seismic stratigraphy of Kolumbo.

- Basin margin Sites U1599 and U1600 provided condensed sequences in calmer depositional environments, with preservation of large numbers of tephra ranging from mafic to felsic in composition, ideal for reconstructing a complete record of volcanism of the CSK volcanic field.
- Christiana Basin Site U1591 provided a succession from the Miocene to recent with many visible tephra layers, as well as tephra preserved in burrows, offering samples of the earliest stages of the CSK volcanic field and of Milos Volcano to the west.
- Within the caldera at Site U1595, we penetrated a 125 m sequence of tephra and pumice layers that records the history of Kameni Volcano since close to its inception following the LBA eruption 3600 y ago.

Pyroclastic deposits occur in the cores both as fallout tephra and as volcaniclastic turbidites. MS turned out to be a good proxy for certain types of volcaniclastic layers but not all. For example, the deposits of the Thera Pyroclastic Formation of Santorini were recognized by their high MS, although some ash layers have lower MS signals. Liquefaction of ash-rich intervals during core retrieval commonly caused homogenization, blurring the stratigraphic record and destroying sedimentary structures.

Preliminary findings related to Objective 1 include the discovery of a large mid-Pleistocene eruption (possibly the Christiani Ignimbrite of Keller et al., 2010), either from ancestral Santorini or from an unknown center between Santorini and Christiana Volcanoes. The main phase of construction of Christiana Volcano itself has been shown to be Late Pliocene to Middle Pleistocene. Both Santorini and Kolumbo have unexpectedly long volcanic histories, stretching back over a million years. Owing to poor recovery, we were unable to directly sample the oldest eruptive units of Kolumbo Volcano (K1 and K2), and we will have to rely on basin margin Sites U1599 and U1600 for this. The cores could confirm the seismostratigraphic correlations of Preine et al. (2022a, 2022b, 2022c) between the Christiana Basin, Anafi Basin, and western Anhydros Basin. However, correlations to the eastern Anhydros Basin have now been disproven. An unexpected feature of all the tephra in our cores was their fresh nature; this will allow glass major and trace element chemical fingerprinting to be done at all levels of all our cores, simplifying the task of tephra correlation.

The volcanic record was chronologically pinned by large numbers of biostratigraphic datums from foraminifer and nannofossil assemblages. Magnetostratigraphy was less useful in our sequences due to the widespread diagenetic sulfide phase, greigite, which significantly complicated the recognition of magnetic reversals. Large numbers of sapropels offer the potential of using astronomically tuned markers to provide a timeline for some drilled intervals with particularly good recovery.

In-depth postcruise work of the shipboard and shore-based scientists will now (1) chemically fingerprint (major and trace element compositions) the main tephra and pumice layers from all cores, using pilot samples taken onboard and those to be collected at the postcruise sampling party, and use established trace element ratios to correlate packages of tephra and major pumice layers across the volcanic field (e.g., Kutterolf et al., 2021a, 2021b; Flaherty et al., 2022); (2) radiometrically date key volcanic layers using $^{40}Ar/^{39}Ar$ on biotite, amphibole, and plagioclase, and/or U-Pb, U-Th, or (U-Th)/He on zircon, to provide absolute ages of volcanic layers, building on the existing biostratigraphic and magnetostratigraphic constraints from the expedition; (3) seek well-dated marker tephra in our cores, such as the 0.39 Ma Campanian eruption. X-ray fluorescence scanning of archive-half sections at the IODP Gulf Coast Repository in the summer of 2023 will aid in identification of cryptotephra, as will planned scanning using a visible/near-infrared spectrometer at the IODP Bremen Repository (Bremen, Germany) in May 2023. Another postcruise objective is to perform a detailed velocity analysis that will allow a more precise core-(log)-seismic integration to more reliably integrate core data with the seismostratigraphic framework.

5.2.2. Objective 2

Objective 2 (the volcano-tectonic connection) aimed, once Objective 1 had been largely achieved, to carry out core-seismic integration and to establish links between volcanism and rift pulses in the Anhydros and Anafi Basins. This would test published interpretations based on seismic data (Preine et al., 2022a, 2022b) and feed into modeling of causal relationships and feedbacks. So far, the expedition has provided certain observations relevant to Objective 2:

- The fault west of Kolumbo Volcano has a larger offset than previously known, suggesting that it may be a major structure of the volcanic field and might exert strong control on magmatism at Santorini and Kolumbo.
- There is clear evidence for an association between ash-rich layers and major rift pulses inferred from seismic profiles, notably the presence of volcanic and tuffaceous units on onlap surfaces. However, whether these relate to eruptions, mass wasting of previously deposited pyroclastics, or both has to be established by detailed laboratory analysis of glass and mineral populations in the volcanic layers. Structural observations also identified numerous intervals of slumping and debris flows. The cores and biostratigraphic age constraints support a previously published idea that a major rift pulse in the Anafi Basin preceded the Thera Pyroclastic Formation (Preine et al., 2022a), although with some details modified.

The cores also provide the opportunity to study the possible relationships between volcanism and sea level (e.g., McGuire et al., 1997; Satow et al., 2021). Some cores such as those of Sites U1591 and U1599 contain thick intervals with well-preserved ash layers, sapropels, and sets of biostratigraphic and magnetostratigraphic datums. Such levels will form the basis for detailed tephra chemical fingerprinting, cryptotephra detection, sapropel chronology, and oxygen isotope chronology to tease out relationships between volcanic activity and sea level.

5.2.3. Objective 3

Objective 3 (arc magmatism in a region of extending crust) aims, once Objectives 1 and 2 have been achieved, to use glass major elements, trace elements, and radiogenic isotopes to track different magma batches of the volcanic field in space and time, linking to previous work (Klaver et al., 2016a, 2016b). The cores have provided us with ample samples to achieve this goal. This work will enable us to discover to what extent crustal rift pulses cause tapping of different melt batches stored in the crust and mantle, as well as to explore the extent to which rifting lowers the pressure on the mantle wedge sufficiently to cause decompression melting, diluting the existing flux melting component of primary magma generation (Bailey et al., 2009; Sternai et al., 2017; Flaherty et al., 2022).

5.2.4. Objective 4

Objective 4 (unraveling an iconic caldera-forming eruption) aimed to groundtruth the seismic stratigraphy to identify the products of the LBA eruption, thereby allowing much more precise calculation of eruptive volume for this iconic event. We drilled through the LBA deposits outside of the caldera at several sites (U1589–U1593 and U1598–U1600); once chemical analysis has confirmed identification of the LBA deposits in these cores, we can proceed with this objective. A preliminary observation is that the LBA deposits are thinner than envisaged by some previous authors, leading toward lower estimates of erupted volume (Pyle, 1990; Karstens et al., 2023). The cores also provide many sections through the offshore continuations of LBA pyroclastic flows, allowing distinction between fallout and turbidite facies and establishment of facies models for these kinds of deposits through detailed sedimentological and textural work. We discovered that lithic clasts in the LBA turbidites are typically centimeter sized, ruling out the thermal remanent magnetism approach proposed by Druitt et al. (2022). Inside the caldera, we failed to reach the level of LBA intracaldera tuff due to hole instability issues. However, we confirmed that Seismic Unit S1 consists mostly of mud/ash and that Unit S2 consists of material derived from the submarine phase of Kameni, as proposed by Johnston et al. (2015). We also discovered that Unit S3 is not intracaldera tuff but consists of sands and gravels related either to marine currents or to the caldera-flooding event proposed by Nomikou et al. (2016a). By penetrating through Unit S1 to Unit S2 in both the northern and southern caldera basins, we confirmed the intracaldera stratigraphy of Johnston et al. (2015) is the same across the entire caldera.

5.2.5. Objective 5

Objective 5 (volcanic hazards from submarine silicic eruptions) addresses the submarine silicic eruptions of the CSK volcanoes and the implications of hazards related to such eruptions. Many of the main discoveries made during Expedition 398 related to this objective.

- We discovered a thick and extensive submarine pumice layer related to a mid-Pleistocene explosive eruption from ancestral Santorini-Christiana.
- We cored at least four pumice deposits from Kolumbo Volcano, tracing the history of this volcano back at least a million years.
- We cored into the intracaldera fill of Santorini caldera, showing that Seismic Unit S2 does indeed come from the Kameni Volcano, as previously postulated (Johnston et al., 2015). This unit therefore provides a time series record of the volcanic and magmatic history of Kameni Volcano since its submarine inception 3600 years ago. Recovery of vegetation traces and calcareous microfossils within these deposits may permit ^{14}C dating of the eruptive layers. Detailed sedimentological, textural, and petrological studies of these different submarine tuffs are planned (e.g., Rotella et al., 2015; Carey et al., 2018).

5.2.6. Objective 6

Objective 6 (transition from continental to marine environments in the southern Aegean) benefited from a wealth of new observations and data. In the Anhydros (Site U1589) and Anafi (Site U1592) Basins, we penetrated the basin fills to basement limestones/marbles of Eocene age. In so doing, we passed through sequences of siliciclastics overlying the basement, including dolomitic ones in Anafi, and recovered benthic foraminifer assemblages recording the early basin flooding and subsequent seawater depths as each basin evolved through successive rift pulses. These two basins turned out to be Late Pleistocene in age rather than Pliocene as previously envisaged (Nomikou et al., 2018). An unexpected feature of these basins was the very high sedimentation rates recorded in some intervals (up to 1 m/ky or more), probably due to large mass wasting events accompanying and following rift pulses. This is consistent with the low measured temperature gradient, steep vertical gradients in pore water chemistry, and fresh glassy tephra in the Anhydros Basin. On the horst separating the Anhydros and Anafi Basins (Site U1600), we bottomed out in serpentinites, which shows that the basement geology of the CSK rift-horst system is very complex. In the Christiana Basin, we penetrated the Pliocene–Quaternary basin fill and bottomed out in 120 m of anhydrite-bearing Miocene sediments, providing a valuable example of a marginal Messinian sequence for the general geological community. In drilling the basins, we encountered and documented many sapropel sequences (e.g., De Lange et al., 2008); this opens up the possibility of studying the influence of ash-derived nutrients on sapropel formation.

The cores from these three basins offer excellent opportunities for detailed studies of basin development in the southern Aegean using paleoenvironmental indicators and subsidence modeling and supported by dense age-depth curves from biostratigraphy, magnetostratigraphy, and, in the future, radiometric dating of volcanic minerals. Use of astronomically tuned sapropel records may further refine the age-depth curves (Rohling et al., 2015; Grant et al., 2016).

5.2.7. Objective 7

Objective 7 (biological systems reaction to volcanic eruptions and seawater acidification) focused on two intracaldera sites (U1595 and U1596), one site in the Anafi Basin (Site U1599), and one site on the Anhydros Horst (Site U1600) where multiple thin iron-rich layers and one thicker such layer may reflect the presence of bacteria (possibly the iron-oxidizing bacterium *M. ferroxydans*) and were sampled for culture-based analysis, genetic characterization of microorganisms present, and metagenomic analysis. These samples provide a potentially rich source of information on deep ecosystems, both inside and outside of the caldera. Laboratory-based biochemical and genetic and metagenomic characterization of these layers is now planned.

References

Aarburg, S., and Frechen, M., 1999. Die pyroklastischen Abfolgen der Christiana-lnseln (Süd-Ägäis, Griechenland). In Becker-Haumann, R., and Frechen, M. (Eds.) Terrestrische Quartargeologie. 260–276.

Acocella, V., and Funiciello, F., 2010. Kinematic setting and structural control of arc volcanism. Earth and Planetary Science Letters, 289(1–2):43–53. **https://doi.org/10.1016/j.epsl.2009.10.027**

Athanassas, C.D., Bourlès, D.L., Braucher, R., Druitt, T.H., Nomikou, P., and Léanni, L., 2016. Evidence from cosmic ray exposure (CRE) dating for the existence of a pre-Minoan caldera on Santorini, Greece. Bulletin of Volcanology, 78(5):35. **https://doi.org/10.1007/s00445-016-1026-3**

Bachmann, O., and Huber, C., 2016. Silicic magma reservoirs in the Earth's crust. American Mineralogist, 101(11):2377–2404. **https://doi.org/10.2138/am-2016-5675**

Bailey, J.C., Jensen, E.S., Hansen, A., Kann, A.D.J., and Kann, K., 2009. Formation of heterogeneous magmatic series beneath north Santorini, South Aegean island arc. Lithos, 110(1):20–36. **https://doi.org/10.1016/j.lithos.2008.12.002**

Brandl, P.A., Hamada, M., Arculus, R.J., Johnson, K., Marsaglia, K.M., Savov, I.P., Ishizuka, O., and Li, H., 2017. The arc arises: the links between volcanic output, arc evolution and melt composition. Earth and Planetary Science Letters, 461:73–84. **https://doi.org/10.1016/j.epsl.2016.12.027**

Bruins, H.J., MacGillivray, J.A., Synolakis, C.E., Benjamini, C., Keller, J., Kisch, H.J., Klügel, A., and van der Plicht, J., 2008. Geoarchaeological tsunami deposits at Palaikastro (Crete) and the late Minoan IA eruption of Santorini. Journal of Archaeological Science, 35(1):191–212. **https://doi.org/10.1016/j.jas.2007.08.017**

Budetta, G., Condarelli, D., Fytikas, M., Kolios, N., Pascale, G., Rapolla, A., and Pinna, E., 1984. Geophysical prospecting on the Santorini Islands. Bulletin Volcanologique, 47(3):447–466. **https://doi.org/10.1007/BF01961218**

Camilli, R., Nomikou, P., Escartín, J., Ridao, P., Mallios, A., Kilias, S.P., Argyraki, A., Andreani, M., Ballu, V., Campos, R., Deplus, C., Gabsi, T., Garcia, R., Gracias, N., Hurtós, N., Magí, L., Mével, C., Moreira, M., Palomeras, N., Pot, O., Ribas, D., Ruzié, L., Sakellariou, D., and the Caldera Science Team, 2015. The Kallisti Limnes, carbon dioxide-accumulating subsea pools. Scientific Reports, 5(1):12152. **https://doi.org/10.1038/srep12152**

Cantner, K., Carey, S., and Nomikou, P., 2014. Integrated volcanologic and petrologic analysis of the 1650AD eruption of Kolumbo submarine volcano, Greece. Journal of Volcanology and Geothermal Research, 269:28–43. **https://doi.org/10.1016/j.jvolgeores.2013.10.004**

Carey, R., Soule, S.A., Manga, M., White, J.D.L., McPhie, J., Wysoczanski, R., Jutzeler, M., Tani, K., Yoerger, D., Fornari, D., Caratori-Tontini, F., Houghton, B., Mitchell, S., Ikegami, F., Conway, C., Murch, A., Fauria, K., Jones, M., Cahalan, R., and McKenzie, W., 2018. The largest deep-ocean silicic volcanic eruption of the past century. Science Advances, 4(1):e1701121. **https://doi.org/10.1126/sciadv.1701121**

Carey, S., Nomikou, P., Bell, K.C., Lilley, M., Lupton, J., Roman, C., Stathopoulou, E., Bejelou, K., and Ballard, R., 2013. CO_2 degassing from hydrothermal vents at Kolumbo submarine volcano, Greece, and the accumulation of acidic crater water. Geology, 41(9):1035–1038. **https://doi.org/10.1130/G34286.1**

Cashman, K.V., Sparks, R.S.J., and Blundy, J.D., 2017. Vertically extensive and unstable magmatic systems: a unified view of igneous processes. Science, 355(6331):eaag3055. **https://doi.org/10.1126/science.aag3055**

Cassidy, M., and Mani, L., 2022. Huge volcanic eruptions: time to prepare. Nature, 608:469–471. **https://doi.org/10.1038/d41586-022-02177-x**

Cembrano, J., and Lara, L., 2009. The link between volcanism and tectonics in the southern volcanic zone of the Chilean Andes: a review. Tectonophysics, 471(1–2):96–113. **https://doi.org/10.1016/j.tecto.2009.02.038**

Christakis, C.A., Polymenakou, P.N., Mandalakis, M., Nomikou, P., Kristoffersen, J.B., Lampridou, D., Kotoulas, G., and Magoulas, A., 2018. Microbial community differentiation between active and inactive sulfide chimneys of the Kolumbo submarine volcano, Hellenic Volcanic Arc. Extremophiles, 22(1):13–27. **https://doi.org/10.1007/s00792-017-0971-x**

De Lange, G.J., Thomson, J., Reitz, A., Slomp, C.P., Speranza Principato, M., Erba, E., and Corselli, C., 2008. Synchronous basin-wide formation and redox-controlled preservation of a Mediterranean sapropel. Nature Geoscience, 1(9):606–610. **https://doi.org/10.1038/ngeo283**

Druitt, T., Kutterolf, S., and Höfig, T.W., 2022. Expedition 398 Scientific Prospectus: Hellenic Arc Volcanic Field. International Ocean Discovery Program. **https://doi.org/10.14379/iodp.sp.398.2022**

Druitt, T.H., 2014. New insights into the initiation and venting of the Bronze-Age eruption of Santorini (Greece), from component analysis. Bulletin of Volcanology, 76(2):794. **https://doi.org/10.1007/s00445-014-0794-x**

Druitt, T.H., Edwards, L., Mellors, R.M., Pyle, D.M., Sparks, R.S.J., Lanphere, M., Davies, M., and Barreirio, B., 1999. Santorini Volcano. Memoir - Geological Society of London, 19. **http://pubs.er.usgs.gov/publication/70094778**

Druitt, T.H., and Francaviglia, V., 1992. Caldera formation on Santorini and the physiography of the islands in the late Bronze Age. Bulletin of Volcanology, 54(6):484–493. **https://doi.org/10.1007/BF00301394**

Druitt, T.H., and Vougioukalakis, G.E. (Eds.), 2019. South Aegean Volcanic Arc. Elements, 15(3). **https://www.elementsmagazine.org/south-aegean-volcanic-arc/**

Duggen, S., Olgun, N., Croot, P., Hoffmann, L., Dietze, H., Delmelle, P., and Teschner, C., 2010. The role of airborne volcanic ash for the surface ocean biogeochemical iron-cycle: a review. Biogeosciences, 7(3):827–844. **https://doi.org/10.5194/bg-7-827-2010**

Elburg, M.A., Smet, I., and De Pelsmaeker, E., 2014. Influence of source materials and fractionating assemblage on magmatism along the Aegean arc, and implications for crustal growth. Geological Society Special Publication, 385(1):137–160. **https://doi.org/10.1144/SP385.1**

Farner, M.J., and Lee, C.-T.A., 2017. Effects of crustal thickness on magmatic differentiation in subduction zone volcanism: a global study. Earth and Planetary Science Letters, 470:96–107. **https://doi.org/10.1016/j.epsl.2017.04.025**

Feuillet, N., 2013. The 2011–2012 unrest at Santorini rift: stress interaction between active faulting and volcanism. Geophysical Research Letters, 40(14):3532–3537. **https://doi.org/10.1002/grl.50516**

Flaherty, T., Druitt, T.H., Francalanci, L., Schiano, P., and Sigmarsson, O., 2022. Temporal variations in the diversity of primitive melts supplied to the Santorini silicic magmatic system and links to lithospheric stresses. Contributions to Mineralogy and Petrology, 177(8):79. **https://doi.org/10.1007/s00410-022-01941-6**

Flaherty, T., Druitt, T.H., Tuffen, H., Higgins, M.D., Costa, F., and Cadoux, A., 2018. Multiple timescale constraints for high-flux magma chamber assembly prior to the Late Bronze Age eruption of Santorini (Greece). Contributions to Mineralogy and Petrology, 173(9):75. **https://doi.org/10.1007/s00410-018-1490-1**

Freundt, A., Schindlbeck-Belo, J.C., Kutterolf, S., and Hopkins, J.L., 2021. Tephra layers in the marine environment: a review of properties and emplacement processes. In Di Capua, A., De Rosa, R., Kereszturi, G., Le Pera, E., Rosi, M.,

and Watt, S.F.L. (Eds.), Volcanic Processes in the Sedimentary Record: When Volcanoes Meet the Environment. Geological Society Special Publication, 520. **https://doi.org/10.1144/SP520-2021-50**

Friedrich, W.L., 2009. Santorini: Volcano, Natural History, Mythology: Aarhus, Denmark (Aarhus University Press).

Fuller, S., Carey, S., and Nomikou, P., 2018. Distribution of fine-grained tephra from the 1650?CE submarine eruption of Kolumbo volcano, Greece. Journal of Volcanology and Geothermal Research, 352:10–25. **https://doi.org/10.1016/j.jvolgeores.2018.01.004**

Grant, K.M., Grimm, R., Mikolajewicz, U., Marino, G., Ziegler, M., and Rohling, E.J., 2016. The timing of Mediterranean sapropel deposition relative to insolation, sea-level and African monsoon changes. Quaternary Science Reviews, 140:125–141. **https://doi.org/10.1016/j.quascirev.2016.03.026**

Hanert, H.H., 2002. Bacterial and chemical iron oxide deposition in a shallow bay on Palaea Kameni, Santorini, Greece: microscopy, electron probe microanalysis, and photometry of in situ experiments. Geomicrobiology Journal, 19(3):317–342. **https://doi.org/10.1080/01490450290098405**

Heath, B.A., Hooft, E.E.E., Toomey, D.R., Papazachos, C.B., Nomikou, P., Paulatto, M., Morgan, J.V., and Warner, M.R., 2019. Tectonism and its relation to magmatism around Santorini Volcano from upper crustal P wave velocity. Journal of Geophysical Research: Solid Earth, 124(10):10610–10629. **https://doi.org/10.1029/2019JB017699**

Hooft, E.E.E., Heath, B.A., Toomey, D.R., Paulatto, M., Papazachos, C.B., Nomikou, P., Morgan, J.V., and Warner, M.R., 2019. Seismic imaging of Santorini: subsurface constraints on caldera collapse and present-day magma recharge. Earth and Planetary Science Letters, 514:48–61. **https://doi.org/10.1016/j.epsl.2019.02.033**

Hooft, E.E.E., Nomikou, P., Toomey, D.R., Lampridou, D., Getz, C., Christopoulou, M.-E., O'Hara, D., Arnoux, G.M., Bodmer, M., Gray, M., Heath, B.A., and VanderBeek, B.P., 2017. Backarc tectonism, volcanism, and mass wasting shape seafloor morphology in the Santorini-Christiana-Amorgos region of the Hellenic Volcanic Arc. Tectonophysics, 712–713:396–414. **https://doi.org/10.1016/j.tecto.2017.06.005**

Hübscher, C., Ruhnau, M., and Nomikou, P., 2015. Volcano-tectonic evolution of the polygenetic Kolumbo submarine volcano/Santorini (Aegean Sea). Journal of Volcanology and Geothermal Research, 291:101–111. **https://doi.org/10.1016/j.jvolgeores.2014.12.020**

Johnston, E.N., Sparks, R.S.J., Nomikou, P., Livanos, I., Carey, S., Phillips, J.C., and Sigurdsson, H., 2015. Stratigraphic relations of Santorini's intracaldera fill and implications for the rate of post-caldera volcanism. Journal of the Geological Society (London, UK), 172(3):323–335. **https://doi.org/10.1144/jgs2013-114**

Jolivet, L., Faccenna, C., Huet, B., Labrousse, L., Le Pourhiet, L., Lacombe, O., Lecomte, E., Burov, E., Denèle, Y., Brun, J.-P., Philippon, M., Paul, A., Salaün, G., Karabulut, H., Piromallo, C., Monié, P., Gueydan, F., Okay, A.I., Oberhänsli, R., Pourteau, A., Augier, R., Gadenne, L., and Driussi, O., 2013. Aegean tectonics: strain localisation, slab tearing and trench retreat. Tectonophysics, 597–598:1–33. **https://doi.org/10.1016/j.tecto.2012.06.011**

Karstens, J., Crutchley, G., Elger, J., Kühn, M., Schmid, F., Dalla Valle, G., Preine, J., and Nomikou, P., 2019. R/V Poseidon Cruise Report 538: THESEUS Tsunami hazard of explosive submarine eruptions: Kiel, Germany (GEOMAR Helmholtz Centre for Ocean Research Kiel). **https://doi.org/10.3289/cr_pos538**

Karstens, J., Preine, J., Crutchley, G.J., Kutterolf, S., van der Bilt, W.G.M., Hooft, E.E.E., Druitt, T.H., Schmid, F., Cederstrøm, J.M., Hübscher, C., Nomikou, P., Carey, S., Kühn, M., Elger, J., and Berndt, C., 2023. Revised Minoan eruption volume as benchmark for large volcanic eruptions. Nature Communications, 14(1):2497. **https://doi.org/10.1038/s41467-023-38176-3**

Keller, J., Dietrich, V., Reusser, E., Gertisser, R., and Aarburg, S., 2010. Recognition of a major ignimbrite in the early evolution of the Santorini Group: the Christiani Ignimbrite. Presented at the Cities on Volcanoes Conference, Tenerife, Spain, January 2010.

Klaver, M., Carey, S., Nomikou, P., Smet, I., Godelitsas, A., and Vroon, P., 2016a. A distinct source and differentiation history for Kolumbo submarine volcano, Santorini volcanic field, Aegean arc. Geochemistry, Geophysics, Geosystems, 17(8):3254–3273. **https://doi.org/10.1002/2016GC006398**

Klaver, M., Davies, G.R., and Vroon, P.Z., 2016b. Subslab mantle of African provenance infiltrating the Aegean mantle wedge. Geology, 44(5):367–370. **https://doi.org/10.1130/G37627.1**

Kokkalas, S., and Aydin, A., 2013. Is there a link between faulting and magmatism in the south-central Aegean Sea? Geological Magazine, 150(2):193–224. **https://doi.org/10.1017/S0016756812000453**

Kutterolf, S., Freundt, A., Druitt, T.H., McPhie, J., Nomikou, P., Pank, K., Schindlbeck-Belo, J.C., Hansteen, T.H., and Allen, S., 2021a. The medial offshore record of explosive volcanism along the central to eastern Aegean Volcanic Arc, part 2: Tephra ages and volumes, eruption magnitudes and marine sedimentation rate variations. Geochemistry, Geophysics, Geosystems, 22(12):e2021GC010011. **https://doi.org/10.1029/2021GC010011**

Kutterolf, S., Freundt, A., Hansteen, T.H., Dettbarn, R., Hampel, F., Sievers, C., Wittig, C., Allen, S.R., Druitt, T.H., McPhie, J., Nomikou, P., Pank, K., Schindlbeck-Belo, J.C., Wang, K.-L., Lee, H.-Y., and Friedrichs, B., 2021b. The medial offshore record of explosive volcanism along the central to eastern Aegean Volcanic Arc: 1. tephrostratigraphic correlations. Geochemistry, Geophysics, Geosystems, 22(12):e2021GC010010. **https://doi.org/10.1029/2021GC010010**

Kutterolf, S., Jegen, M., Mitrovica, J.X., Kwasnitschka, T., Freundt, A., and Huybers, P.J., 2013. A detection of Milankovitch frequencies in global volcanic activity. Geology, 41(2):227–230. **https://doi.org/10.1130/G33419.1**

Le Pichon, X., and Kreemer, C., 2010. The Miocene-to-Present kinematic evolution of the eastern Mediterranean and Middle East and its implications for dynamics. Annual Review of Earth and Planetary Sciences, 38(1):323–351. **https://doi.org/10.1146/annurev-earth-040809-152419**

Loughlin, S.C., Sparks, S., Brown, S.K., Jenkins, S.F., and Vye-Brown, C. (Eds.), 2015. Global Volcanic Hazards and Risk: Cambridge, UK (Cambridge University Press). **https://doi.org/10.1017/CBO9781316276273**

Lowe, D.J., 2011. Tephrochronology and its application: a review. Quaternary Geochronology, 6(2):107–153. **https://doi.org/10.1016/j.quageo.2010.08.003**

Makris, J., Papoulia, J., and Yegorova, T., 2013. A 3-D density model of Greece constrained by gravity and seismic data. Geophysical Journal International, 194(1):1–17. **https://doi.org/10.1093/gji/ggt059**

McGuire, J., Plank, T., Barrientos, S., Becker, T., Brodsky, E., Cottrell, E., French, M., Fulton, P., Gomberg, J., Gulick, S., Haney, M., Melgar, D., Penniston-Dorland, S., Roman, D., Skemer, P., Tobin, H., Wada, I., and Wiens, D., 2017. The SZ4D initiative: understanding the processes that underlie subduction zone hazards in 4D. Vision document submitted to the National Science Foundation. The IRIS Consortium. **http://www-udc.ig.utexas.edu/external/becker/sz4dmcs/ftp/sz4d.pdf**

McGuire, W.J., Howarth, R.J., Firth, C.R., Solow, A.R., Pullen, A.D., Saunders, S.J., Stewart, I.S., and Vita-Finzi, C., 1997. Correlation between rate of sea-level change and frequency of explosive volcanism in the Mediterranean. Nature, 389(6650):473–476. **https://doi.org/10.1038/38998**

McVey, B.G., Hooft, E.E.E., Heath, B.A., Toomey, D.R., Paulatto, M., Morgan, J.V., Nomikou, P., and Papazachos, C.B., 2020. Magma accumulation beneath Santorini volcano, Greece, from P-wave tomography. Geology, 48(3):231–235. **https://doi.org/10.1130/G47127.1**

National Academies of Sciences, Engineering, and Medicine, 2017. Volcanic Eruptions and Their Repose, Unrest, Precursors, and Timing: Washington, DC (The National Academies Press). **https://doi.org/10.17226/24650**

Nomikou, P., Carey, S., Papanikolaou, D., Croff Bell, K., Sakellariou, D., Alexandri, M., and Bejelou, K., 2012. Submarine volcanoes of the Kolumbo volcanic zone NE of Santorini caldera, Greece. Global and Planetary Change, 90–91:135–151. **https://doi.org/10.1016/j.gloplacha.2012.01.001**

Nomikou, P., Druitt, T.H., Hübscher, C., Mather, T.A., Paulatto, M., Kalnins, L.M., Kelfoun, K., Papanikolaou, D., Bejelou, K., Lampridou, D., Pyle, D.M., Carey, S., Watts, A.B., Weiß, B., and Parks, M.M., 2016a. Post-eruptive flooding of Santorini caldera and implications for tsunami generation. Nature Communications, 7(1):13332. **https://doi.org/10.1038/ncomms13332**

Nomikou, P., Hübscher, C., and Carey, S., 2019. The Christiana–Santorini–Kolumbo volcanic field. Elements, 15(3):171–176. **https://doi.org/10.2138/gselements.15.3.171**

Nomikou, P., Hübscher, C., Papanikolaou, D., Farangitakis, G.P., Ruhnau, M., and Lampridou, D., 2018. Expanding extension, subsidence and lateral segmentation within the Santorini - Amorgos basins during Quaternary: implications for the 1956 Amorgos events, central - south Aegean Sea, Greece. Tectonophysics, 722:138–153. **https://doi.org/10.1016/j.tecto.2017.10.016**

Nomikou, P., Hübscher, C., Ruhnau, M., and Bejelou, K., 2016b. Tectono-stratigraphic evolution through successive extensional events of the Anydros Basin, hosting Kolumbo volcanic field at the Aegean Sea, Greece. Tectonophysics, 671:202–217. **https://doi.org/10.1016/j.tecto.2016.01.021**

Nomikou, P., Papanikolaou, D., Alexandri, M., Sakellariou, D., and Rousakis, G., 2013. Submarine volcanoes along the Aegean volcanic arc. Tectonophysics, 597–598:123–146. **https://doi.org/10.1016/j.tecto.2012.10.001**

Nomikou, P., Parks, M.M., Papanikolaou, D., Pyle, D.M., Mather, T.A., Carey, S., Watts, A.B., Paulatto, M., Kalnins, M.L., Livanos, I., Bejelou, K., Simou, E., and Perros, I., 2014. The emergence and growth of a submarine volcano: the Kameni islands, Santorini (Greece). GeoResJ, 1–2:8–18. **https://doi.org/10.1016/j.grj.2014.02.002**

Okal, E.A., Synolakis, C.E., Uslu, B., Kalligeris, N., and Voukouvalas, E., 2009. The 1956 earthquake and tsunami in Amorgos, Greece. Geophysical Journal International, 178(3):1533–1554. **https://doi.org/10.1111/j.1365-246X.2009.04237.x**

Oulas, A., Polymenakou, P.N., Seshadri, R., Tripp, H.J., Mandalakis, M., Paez-Espino, A.D., Pati, A., Chain, P., Nomikou, P., Carey, S., Kilias, S., Christakis, C., Kotoulas, G., Magoulas, A., Ivanova, N.N., and Kyrpides, N.C., 2016. Metagenomic investigation of the geologically unique Hellenic Volcanic Arc reveals a distinctive ecosystem with unexpected physiology. Environmental Microbiology, 18(4):1122–1136. **https://doi.org/10.1111/1462-2920.13095**

Pallikarakis, A., Triantaphyllou, M.V., Papanikolaou, I., Dimiza, M.D., Reicherter, K., and Migiros, G., 2018. Age constraints and paleoenvironmental interpretation of a borehole sedimentary sequence along the eastern part of the Corinth Isthmus, Greece. Journal of Coastal Research, 34(3):602–617. **https://doi.org/10.2112/JCOASTRES-D-16-00191.1**

Papazachos, C.B., 2019. Deep structure and active tectonics of the South Aegean Volcanic Arc. Elements, 15(3):153–158. **https://doi.org/10.2138/gselements.15.3.153**

Parkes, R.J., Cragg, B.A., and Wellsbury, P., 2000. Recent studies on bacterial populations and processes in subseafloor sediments: a review. Hydrogeology Journal, 8(1):11–28. **https://doi.org/10.1007/PL00010971**

Parks, M.M., Moore, J.D.P., Papanikolaou, X., Biggs, J., Mather, T.A., Pyle, D.M., Raptakis, C., Paradissis, D., Hooper, A., Parsons, B., and Nomikou, P., 2015. From quiescence to unrest: 20years of satellite geodetic measurements at Santorini volcano, Greece. Journal of Geophysical Research: Solid Earth, 120(2):1309–1328. **https://doi.org/10.1002/2014JB011540**

Pe-Piper, G., and Piper, D.J.W., 2005. The South Aegean active volcanic arc: relationships between magmatism and tectonics. In Fytikas, M., and Vougioukalakis, G.E. (Eds.), The South Aegean Active Volcanic Arc: Present Knowledge and Future Perspectives. Developments in Volcanology, 7: 113–133. **https://doi.org/10.1016/S1871-644X(05)80034-8**

Piper, D.J.W., and Perissoratis, C., 2003. Quaternary neotectonics of the South Aegean arc. Marine Geology, 198(3–4):259–288. **https://doi.org/10.1016/S0025-3227(03)00118-X**

Polymenakou, P.N., Nomikou, P., Zafeiropoulos, H., Mandalakis, M., Anastasiou, T.I., Kilias, S., Kyrpides, N.C., Kotoulas, G., and Magoulas, A., 2021. The Santorini volcanic complex as a valuable source of enzymes for bioenergy. Energies, 14(5):1414. **https://doi.org/10.3390/en14051414**

Preine, J., Hübscher, C., Karstens, J., and Nomikou, P., 2022a. Volcano-tectonic evolution of the Christiana-Santorini-Kolumbo rift zone. Tectonics, 41(11):e2022TC007524. **https://doi.org/10.1029/2022TC007524**

Preine, J., Karstens, J., Hübscher, C., Crutchley, G.J., Druitt, T.H., Schmid, F., and Nomikou, P., 2022b. The hidden giant: how a rift pulse triggered a cascade of sector collapses and voluminous secondary mass-transport events in the early evolution of Santorini. Basin Research, 34(4):1465–1485. **https://doi.org/10.1111/bre.12667**

Preine, J., Karstens, J., Hübscher, C., Nomikou, P., Schmid, F., Crutchley, G.J., Druitt, T.H., and Papanikolaou, D., 2022c. Spatio-temporal evolution of the Christiana-Santorini-Kolumbo volcanic field, Aegean Sea. Geology, 50(1):96–100. **https://doi.org/10.1130/G49167.1**

Pyle, D.M., 1990. New estimates for the volume of the Minoan eruption. In Hardy, D.A., Thera and the Aegean World III (Volume 2). London (Thera Foundation), 113–121.

Pyle, D.M., and Elliott, J.R., 2006. Quantitative morphology, recent evolution, and future activity of the Kameni Islands volcano, Santorini, Greece. Geosphere, 2(5):253–268. **https://doi.org/10.1130/GES00028.1**

Rabillard, A., Jolivet, L., Arbaret, L., Bessière, E., Laurent, V., Menant, A., Augier, R., and Beaudoin, A., 2018. Synextensional granitoids and detachment systems within cycladic metamorphic core complexes (Aegean Sea, Greece): toward a regional tectonomagmatic model. Tectonics, 37(8):2328–2362. **https://doi.org/10.1029/2017TC004697**

Rohling, E.J., Marino, G., and Grant, K.M., 2015. Mediterranean climate and oceanography, and the periodic development of anoxic events (sapropels). Earth-Science Reviews, 143:62–97. **https://doi.org/10.1016/j.earscirev.2015.01.008**

Rotella, M.D., Wilson, C.J.N., Barker, S.J., Schipper, C.I., Wright, I.C., and Wysoczanski, R.J., 2015. Dynamics of deep submarine silicic explosive eruptions in the Kermadec arc, as reflected in pumice vesicularity textures. Journal of Volcanology and Geothermal Research, 301:314–332. **https://doi.org/10.1016/j.jvolgeores.2015.05.021**

Royden, L.H., and Papanikolaou, D.J., 2011. Slab segmentation and late Cenozoic disruption of the Hellenic arc. Geochemistry, Geophysics, Geosystems, 12(3):Q03010. **https://doi.org/10.1029/2010GC003280**

Sachpazi, M., Laigle, M., Charalampakis, M., Diaz, J., Kissling, E., Gesret, A., Becel, A., Flueh, E., Miles, P., and Hirn, A., 2016. Segmented Hellenic slab rollback driving Aegean deformation and seismicity. Geophysical Research Letters, 43(2):651–658. **https://doi.org/10.1002/2015GL066818**

Satow, C., Gudmundsson, A., Gertisser, R., Ramsey, C.B., Bazargan, M., Pyle, D.M., Wulf, S., Miles, A.J., and Hardiman, M., 2021. Eruptive activity of the Santorini Volcano controlled by sea-level rise and fall. Nature Geoscience, 14(8):586–592. **https://doi.org/10.1038/s41561-021-00783-4**

Satow, C., Tomlinson, E.L., Grant, K.M., Albert, P.G., Smith, V.C., Manning, C.J., Ottolini, L., Wulf, S., Rohling, E.J., Lowe, J.J., Blockley, S.P.E., and Menzies, M.A., 2015. A new contribution to the Late Quaternary tephrostratigraphy of the Mediterranean: Aegean Sea core LC21. Quaternary Science Reviews, 117:96–112. **https://doi.org/10.1016/j.quascirev.2015.04.005**

Schippers, A., Neretin, L.N., Kallmeyer, J., Ferdelman, T.G., Cragg, B.A., John Parkes, R., and Jørgensen, B.B., 2005. Prokaryotic cells of the deep sub-seafloor biosphere identified as living bacteria. Nature, 433(7028):861–864. **https://doi.org/10.1038/nature03302**

Schmincke, H.U., and Sumita, M., 1998. Volcanic evolution of Gran Canaria reconstructed from apron sediments: synthesis of VICAP project drilling. In Weaver, P.P.E., Schmincke, H.-U., Firth, J.V., and Duffield, W. (Eds.), Proceedings of the Ocean Drilling Program, Scientific Results. 157: College Station, TX (Ocean Drilling Program). **https://doi.org/10.2973/odp.proc.sr.157.135.1998**

Shaw, B., and Jackson, J., 2010. Earthquake mechanisms and active tectonics of the Hellenic subduction zone. Geophysical Journal International, 181(2):966–984. **https://doi.org/10.1111/j.1365-246X.2010.04551.x**

Sternai, P., Caricchi, L., Garcia-Castellanos, D., Jolivet, L., Sheldrake, T.E., and Castelltort, S., 2017. Magmatic pulse driven by sea-level changes associated with the Messinian salinity crisis. Nature Geoscience, 10(10):783–787. **https://doi.org/10.1038/ngeo3032**

Syracuse, E.M., van Keken, P.E., and Abers, G.A., 2010. The global range of subduction zone thermal models. Physics of the Earth and Planetary Interiors, 183(1):73–90. **https://doi.org/10.1016/j.pepi.2010.02.004**

Templeton, A.S., 2011. Geomicrobiology of iron in extreme environments. Elements, 7(2):95–100. **https://doi.org/10.2113/gselements.7.2.95**

Tsampouraki-Kraounaki, K., and Sakellariou, D., 2018. Seismic stratigraphy and geodynamic evolution of Christiana Basin, South Aegean Arc. Marine Geology, 399:135–147. **https://doi.org/10.1016/j.margeo.2018.02.012**

Vougioukalakis, G., Sparks, R.S., Druitt, T., Pyle, D., Papazachos, C., and Fytikas, M., 2016. Volcanic hazard assessment at Santorini Volcano: a review and a synthesis in the light of the 2011–2012 Santorini unrest. Bulletin of the Geological Society of Greece, 50(1):274–283. **https://doi.org/10.12681/bgsg.11728**

Walter, T.R., and Amelung, F., 2007. Volcanic eruptions following M ≥ 9 megathrust earthquakes: implications for the Sumatra-Andaman volcanoes. Geology, 35(6):539–542. **https://doi.org/10.1130/G23429A.1**

Wulf, S., Keller, J., Satow, C., Gertisser, R., Kraml, M., Grant, K.M., Appelt, O., Vakhrameeva, P., Koutsodendris, A., Hardiman, M., Schulz, H., and Pross, J., 2020. Advancing Santorini's tephrostratigraphy: new glass geochemical data and improved marine-terrestrial tephra correlations for the past ~360 kyrs. Earth-Science Reviews, 200:102964. **https://doi.org/10.1016/j.earscirev.2019.102964**